Geological Survey of Sweden

Secondary resources directive

Characterisation of mine tailings in the Bergslagen region using geophysical methods

Mehrdad Bastani, Cecilia Brolin, Virginie Leroux & Lena Persson

www.sgu.se

SGU-rapport 2025:05

Author: Mehrdad Bastani, Cecilia Brolin, Virginie Leroux and Lena Persson
Reviewed by: Daniel Sopher
Head of unit: Mats Wedmark
Editor: Lina Rönnåsen

Cover photo: Measurement with ERT at Bäckegruvan tailing site.
Photographer: Virginie Leroux

April 2025

Geological Survey of Sweden
Box 670, 751 28 Uppsala, Sweden
phone: 018-17 90 00
e-mail: sgu@sgu.se

www.sgu.se

Contents

Abstract

In 2021, the Geological Survey of Sweden (Sveriges geologiska undersökning, SGU) together with the Swedish Environmental Protection Agency received a governmental directive to work to increase the possibilities for sustainable extraction of metals and minerals from secondary resources (N2021/01038). The directive in its entirety was reported to the government in February 2023 (SGU RR 2023:01).

As part of the directive, SGU has documented, sampled, and characterised mining waste (waste rock and tailings) at closed Swedish mines to estimate the quantities of metals and minerals. Secondary resources from mining waste can possibly contribute to the supply of the critical raw materials needed in the ongoing energy transition.

This report focuses on the geophysical investigations made at eight tailings repositories in the Bergslagen mining district. The geophysical methods used include electrical resistivity tomography (ERT), time domain induced polarisation (TDIP), radio-magnetotellurics (RMT), towed transient electromagnetics (tTEM) and ground-penetrating radar (GPR). In addition to the ground-based geophysical measurements, laboratory spectral induced polarisation (SIP) measurements were performed on borehole samples from five of the tailing repositories.

At all investigated sites the resistivity models from the ERT, RMT and/or tTEM measurements, together with borehole information, could be used to determine the extent and depth of the tailings. The ERT measurements with 2 m electrode spacing gave models with the highest resolution in the near surface while the RMT models gave the greatest depth of investigation. The tTEM data were collected in a continuous manner which resulted in an effective and fast data acquisition. The tTEM data were influenced by IP effects and they had to be considered during the inversion process. The inversion result is however dependent on the choice of starting model and for one of the sites (Jan-Matsdammen) the results were unreliable and were not used further in the interpretation.

In cases with low resistivity tailings (like water saturated silt and clay) the base of the tailings was clearly identified with all three methods. In cases with more resistive tailings (like dry and coarser grained tailings) the ERT method showed limited penetration depth most likely due to the poor conditions for current injection.

The resistivity variations within the tailings seem to be primarily explained by changes in the water saturation and grain size. Changes in grain size may in turn often be linked to changes in metal content. A correlation between resistivity and metal content (Fe_2O_3) was found at two of the sites, Hötjärnen and Bäckegruvan. Such a correlation was not observed at the other sites.

The metal content in the tailings was high at all sites and for this reason high IP-responses were expected. However, only at one of the sites, Jan-Matsdammen, the TDIP measurements were of good quality and gave inversion results with a reasonable data fit. There, the increase in chargeability was also well correlated with the increase in the Fe_2O_3 content. At the other sites results were mixed and processing and interpretation more challenging. Several metals were present at all sites, but Fe was by far dominant in weight.

The results from the laboratory SIP-measurements could be correlated with the maximum phase and the grain size. The coarsest grain size (mainly sand) was found in the samples from Jan-Matsdammen. For them the maximum phase occurs at frequencies around 1000-2000 Hz. For the other sites the maximum phase lies above 2000 Hz and could sometimes not be observed in the lab measurements limited at 10 000 Hz. At these sites the grain size was finer (mainly silt and clay). This can explain why it was difficult to observe clear responses in TDIP measurements made at these sites, since we can expect limitations in the frequency content of field measurements.

Sammanfattning

År 2021 fick Sveriges geologiska undersökning (SGU) tillsammans med Naturvårdsverket i regeringsuppdrag att arbeta för ökade möjligheter till hållbar utvinning av metaller och mineral ur sekundära resurser (N2021/01038). Arbetet är tänkt att bidra till omställningen till en mer cirkulär och resurseffektiv ekonomi. Uppdraget i sin helhet redovisades till regeringen i februari 2023 (SGU RR 2023:01).

Som en del av uppdraget har SGU dokumenterat, provtagit och karakteriserat gruvavfall (varphögar och sandmagasin) vid nedlagda svenska gruvor för att bedöma mängden metaller och mineral. Sekundära resurser från gruvavfall kan möjligen bidra till försörjningen av de kritiska råvaror som behövs i den pågående energiomställningen. I en serie rapporter presenteras resultaten från undersökningarna.

Denna rapport fokuserar på hur geofysiska undersökningar kan användas för att uppskatta och karakterisera sekundära resurser i sandmagasin. Rapporten innehåller fördjupade analyser av resultaten från åtta utvalda sandmagasin i Bergslagen. Valet av provplatser baserades på tidigare studier och merparten av avfallet var restprodukter från brytning av järnmalm, men även andra grundämnen som volfram och koppar. Provplatserna finns inom fem gruvområden: Yxsjöberg (en plats), Grängesberg (tre platser), Blötberget (en plats), Stollberg (en plats) och Riddarhyttefältet (två platser).

Syftet med de geofysiska undersökningarna var att genom 3D-modeller ge bättre förståelse för fördelningen av gruvavfallet i sandmagasinen, samt att uppskatta mängden avfall. Delar av resultaten har tidigare beskrivits av Casey m.fl. (2024) och Camitz m.fl. (2024). I denna rapport jämförs och analyseras resultaten mer i detalj. Rapporten beskriver och förklarar även skillnaderna mellan olika geofysiska metoder och ger en bedömning av hur de kan tillämpas.

Inom projektet har olika geofysiska metoder använts på olika typer av sandmagasin, vilket har lett till ett unikt underlag för att utvärdera lämpligheten för olika metoder under olika förutsättningar. De metoder som har testats och utvärderats är

- elektrisk resistivitets tomografi (ERT)
- inducerad polarisation (IP)
- dragen transient elektromagnetisk (tTEM, eng. *towed transient electromagnetic*s)
- radiomagnetotellurik (RMT).

Utöver de geofysiska markmätningarna utfördes laboratoriemätningar SIP (spektralinducerad polarisation) på borrhålsprover från fem av sandmagasinen.

De undersökta sandmagasinen varierar gällande ursprungsmaterial (typ av mineralisering), vattenmättnadsgrad, kornstorlek och inte minst tillgänglighet för olika mätmetoder. På alla undersökta platser kunde sandmagasinens utbredning och djup bestämmas med hjälp av resistivitetsmodeller från ERT-, RMT- och/eller tTEM-mätningarna tillsammans med borrhålsinformation. ERT-mätningarna med ett elektrodavstånd på två meter gav modeller med högst upplösning närmast markytan medan RMT-modellerna gav störst undersökningsdjup. tTEM data insamlades kontinuerligt vilket medförde en effektiv och snabb datainsamling. Insamlad tTEM-data var påverkad av IP-effekter som man måste ta hänsyns till under inversionsprocessen. Inversionsresultatet är dock beroende av valet av startmodell och för en av platserna (Jan-Matsdammen) var inversionsresultaten otillförlitliga och användes inte vidare i tolkningen.

Variationerna i resistivitet inom gruvavfallet kan främst förklaras av variationerna i vattenmättnadsgrad och kornstorlek. Variationer i kornstorlek kan i sin tur ofta vara kopplade till variationer i metallinnehåll. En korrelation mellan resistivitet och metallhalt (Fe2O3) hittades på två av de undersökta sandmagasinen, Hötjärnen och Bäckegruvan.

Metallhalten i avfallet var hög på alla undersökta platser och därför förväntades också en hög IP-respons. Endast på ett av de undersökta magasinen, Jan-Matsdammen, var TDIP-mätningarna av godtagbar kvalitet. Där var ökad laddningsbarhet också korrelerad med en ökad Fe_2O_3-halt. På de andra platserna var resultaten blandade och bearbetning och tolkning av IP-mätningar mer utmanande.

Resultaten från laboratoriemätningarna (SIP) visade en korrelation mellan maximal fas och kornstorlek. Materialet från Jan-Matsdammen hade den grövsta kornstorleken och bestod huvudsakligen av sand. Dessa prover visade en maximal fas vid frekvenser runt 1000–2000 Hz. Materialet från de övriga provtagna platserna visade en maximal fas över 2000 Hz och ibland översteg den 10 000 Hz. Gruvavfallet på dessa platser var betydligt finkornigare och proverna bestod huvudsakligen av silt och lera. Detta kan även förklara varför det var svårt att observera en tydlig och mätbar respons i TDIP-mätningar på grund av begränsningar i frekvensinnehållet i fältmätningarna.

Introduction

In 2021, the Geological Survey of Sweden (Sveriges geologiska undersökning, SGU) together with the Swedish Environmental Protection Agency received a governmental directive to work to increase the possibilities for sustainable extraction of metals and minerals from secondary resources (N2021/01038). The goal of the sampling and geophysical investigations conducted in this study was to provide a general estimate of potential critical raw materials (CRM) and other minerals of economic interest in the mine waste. The work is intended to contribute to the transition to a more circular and resource-efficient economy. The directive in its entirety was reported to the government in February 2023 (SGU RR 2023:01).

As part of the directive, SGU has documented, sampled, and characterised mining waste at closed Swedish mines to estimate the quantities of metals and minerals. The waste material can consist of waste rock (discarded after extraction of ore), tailings (which are the leftovers after mechanical processing of ore) and slag (cinder) produced after melting of the ore. This report is concerned with the use of geophysics to help estimate and characterise the secondary resource left in tailings.

Tailings are a residual product after the ore has been crushed and milled to a suitable grain size at a mineral processing plant (concentrator) and then treated with mechanical, gravimetric and/or chemical processes to recover economically interesting metals and minerals. Tailings are usually deposited in an impoundment or pond near the mineral processing plant. No processing methods can achieve complete recovery of the economic fraction and hence tailings may contain recoverable quantities of economic material. Additionally, minerals or metals which were of little or no economic interest at the time of extraction may have become more valuable due to increased demand induced by the needs of new technologies. New improved extraction methods may also allow for greater recovery of such material, through re-processing of tailings.

To date there are many examples of the use of geophysical methods to study tailings and other mining residues (e.g. Martin et al. 2021, Günther and Martin 2016, Placencia-Gómez et al. 2010, Vanhala et el. 2004). Campbell and Fitterman (2000) for example provide an account of a range of geophysical methods for the investigation of tailings, the physical parameter(s) which are most important, the cause of anomalies and a discussion of best practices for application of these methods. They also note that some of the previous applications were focused on landfills and dump related problem (contaminations), rather than secondary resources. Nguyen et al. (2018) reviewed the contribution of geophysical methods in managing existing landfills for future exploitations and developments. The review emphasised the huge number of historical landfills, their impact on the environment and the potential for extracting significant quantities of valuable material from the waste. In this context they argued the importance of non-invasive geophysical methods for exploration and site characterisation, which are sensitive to the physical properties of subsurface materials (e.g. density, electrical resistivity, magnetic susceptibility). They also described physical properties of waste deposits and how these often differ from the surrounding materials. For example, the electrical resistivity of waste deposits is often significantly different to the surrounding material and hence, geophysical electrical or electromagnetic measurements can be used to characterise the landfill geometry (e.g. size, shape and volume). Furthermore, variations in the internal characteristics of waste mass such as humidity, permeability, composition, water content, etc. can manifest themselves by variation in the electrical properties of the waste material. Isunza et al. (2022) showcased their results of geophysical studies made in a waste site in Belgium. They concluded that geophysical methods are non-invasive technologies to characterise the subsurface and to image lateral and vertical variations in the physical properties. When complemented with ground-truth data, geophysical models can be interpreted quantitatively in terms of material composition (even zonation) and volume estimation. Günther

and Martin (2016) presented the results from a detailed study made on a mining slag heap in Germany using spectral induced polarisation (see the *Methods* section in the report for a more detailed description of the method). By making a synthetic analysis and applying the method to the field data from the waste site they were able to characterise slag heaps and even mining tailings. Together with complementary laboratory measurements they were able to obtain information about the mineral content and grain size based on the parameters from 2D modelling. Martínez et al. (2021) characterised a tailings dam nearby Federico Mine in Spain by utilizing electrical geophysical methods. The geophysical models provided the basis for a detailed analysis of the internal characteristics of the waste deposits. The lateral and vertical variations in the models were linked to different degrees of moisture content, the geometry of the top of the bedrock as well as the tectonics that affected the pouring/dumping holes. Using estimated geophysical parameters (e.g. electrical resistivity and chargeability) they could characterise different zones such as wet and dry waste, alterations, and zones of high metal accumulation in the waste pond that were correlated to large chargeability anomalies.

This work focuses on the geophysical investigations made at selected tailing repositories in the Bergslagen mining district. Parts of the results are published in two other reports in the frame of the same project (Casey et al. 2024 & Camitz et al. 2024). In these reports models of the tailings thickness based on the geophysical measurements and drillings are presented, but the uncertainty of the results was not discussed in detail, nor the induced polarisation. The purpose of the geophysical investigation was to gain better understanding of the spatial distribution of the mine waste in 3D and to estimate the volume of the tailings.

As part of the project SGU has compiled historical data and sample results from these deposits as well as collection of new samples. SGU mineral resources database contains statistics obtained from mine operators and information about how much material was mined and how much ore was produced. Using this data the quantity of waste material after processing can be estimated to some extent. Most of what was processed in dressing plants was then deposited in tailings repositories, but some was used for other purposes (backfilling, road construction etc.). Based on the field observations, analysis of surface samples, existing historical data, and new geophysical investigations, a few locations were chosen for drilling and sampling with boreholes. Geophysical models were then generated and combined with the results from the chemical analyses to make an estimate of the potential quantities of CRM and other strategic raw materials within the mining waste at the selected areas.

The purpose of the present report is to compare and analyse in more detail the geophysical results from the sites which were investigated. The objective is also to describe and explain the differences between different methods and to give an assessment of their applicability. The focus is on the geophysical parameters like resistivity, chargeability, and phase shift and how these parameters can be related to the tailings characteristics like water saturation, grain size and metal content.

The report starts with some specifications about the selected sites describing the locations and type of waste/tailings. A general account on the theory, data acquisition techniques, measured data, processing, and modelling procedures used for the geophysical methods is also provided. Some of the standard physical models used to link the modelled physical properties to geological observations and processes are also explained. Geophysical models along selected profiles in each site are presented together with the observations made in a few boreholes. A discussion about the outcomes and limitations of the methods follows, which addresses the estimated parameters and their relation to characteristics of the waste deposit. An outlook for future work and further data analysis is also provided. The report contains two appendices:

- Appendix A: Martin, T., 2022a: SIP measurements on four sandy tailing samples.
- Appendix B: Martin, T., 2022b: SIP measurements on six sandy tailing samples.

Selected sites

Eight tailings repositories, located in the Bergslagen area in central Sweden were selected for detailed geophysical measurements (Fig. 1). The tailings were selected based on prior studies conducted by Hallberg and Reginiussen (2020; 2018). Most of the tailings are residual products from mining of iron ore but other elements have also been mined such as tungsten and copper. The geophysical methods used include electrical resistivity tomography (ERT), time domain induced polarisation (TDIP), radio-magnetotellurics (RMT), towed transient electromagnetics (tTEM), and ground-penetrating radar (GPR). SGU also conducted drilling and surface sampling at each site. Samples from a few selected sites were sent to Lund University for lab-based measurements of spectral induced polarisation (SIP). The methods chosen are electric and electromagnetic where the estimated/measured properties reflect the electrical properties of the materials present at each site. Table 1 shows a compilation of all geophysical measurements performed on the tailings within this project. The sites are spread over a relatively large geographical area. The individual sites can be grouped into five mining areas: Yxsjöberg (one site), Grängesberg (three sites), Blötberget (one site), Stollberg (one site) and Riddarhyttefältet (two sites) (Fig. 1).

Yxsjöberg

The largest known tungsten deposit in Sweden was located at Yxsjöberg and was mined until 1989. Copper and fluorite were also extracted from the mine. The tailings were deposited at two tailings ponds, Smaltjärnen (between 1938 and 1963) and Morkulltjärnen (from 1969 to 1989) (Hallberg and Reginiussen 2020). Within this project, we selected the latter site to perform our detailed ground-based geophysical investigations, drilling and sampling (Fig. 1). At Smaltjärnen, Luleå Technical University performed both sampling and geophysical measurements (Hällström et al. 2018 and Palo 2021).

Grängesberg

The Grängesberg Kiruna type Fe-oxide-apatite deposit represents the largest ore mineralisation in the Bergslagen region. Over the past 250 years, 156 million tons of ore have been extracted from the mines in this area (Hallberg and Reginiussen 2020). The deposition of tailings material into ponds started at some point between 1953 and 1955 (based on historical aerial photos) and continued until 1989. The deposition started in the Jan-Matsdammen pond and was followed by deposition in Svandammen and Hötjärnen (Fig. 1)

Blötberget

Blötberget is another Fe-oxide-apatite deposit northeast of Grängesberg. Like Grängesberg, Blötberget contains iron-rich ore dominated by magnetite with minor portions of haematite and apatite. From around 1960, until the closure of the mine in 1979, the tailings were deposited east of the mine, close to Norsberget.

Stollberg

Stollberg is a base metal deposit where mining is believed to have started in medieval times with a focus on silver extraction from lead ore. Large scale mining of lead-zinc and iron-manganese ore occurred from 1869 until 1982, after which the mine closed. The Gårdmyren tailings dam hosts the major part of the tailings resulting from the processing between 1949 and 1982.

Riddarhyttefältet

The Riddarhyttefältet area includes several hundred abandoned mines, where the primary commodities being extracted were iron and copper. The mining went on for several hundred years. Two tailings repositories, Källfallet and Bäckegruvan, were selected for detailed geophysical investigation, drilling and sampling as part of this project.

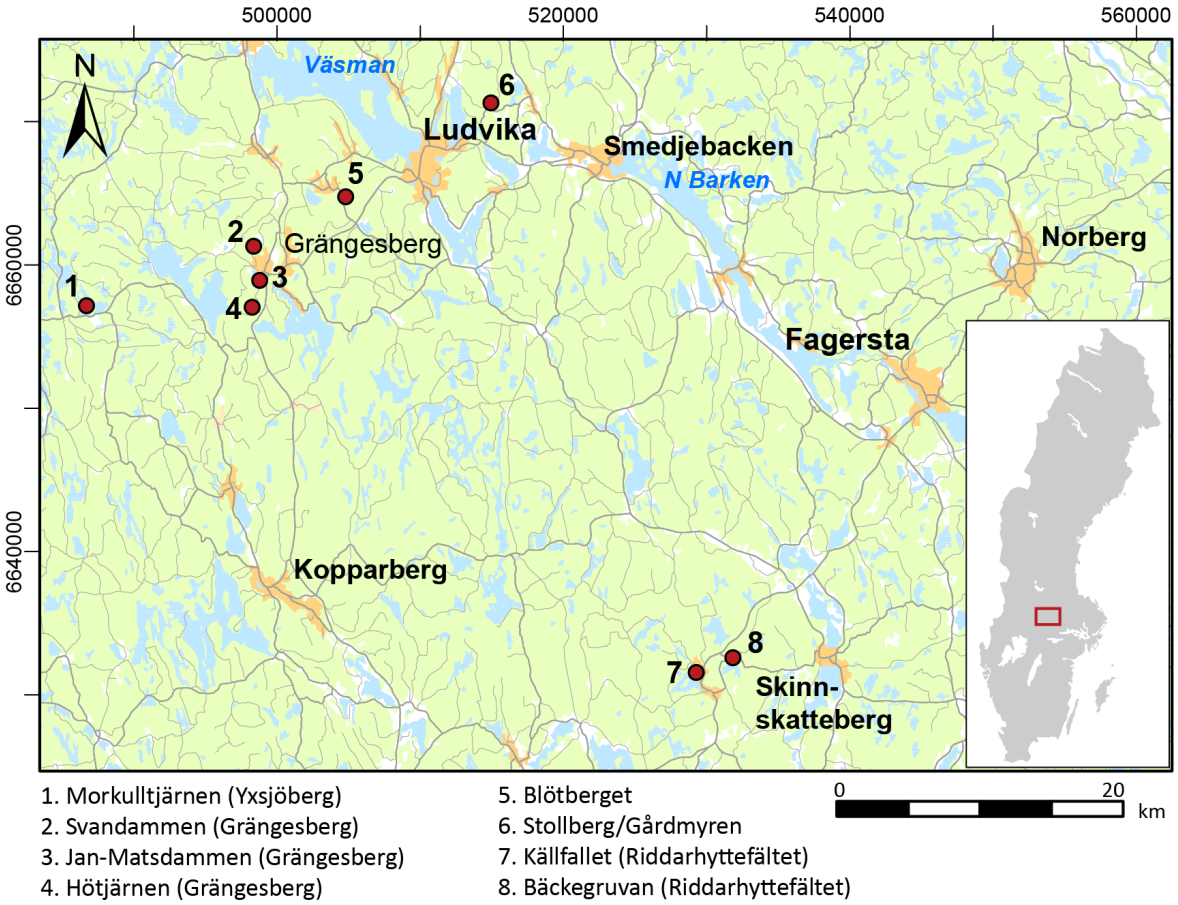

Figure 1. Map showing the location of the tailings repositories in the Bergslagen region which were investigated as part of this project.

Table 1. Description of the geophysical measurements performed on the different tailings deposits as part of this project. The length and type of measurements are described. The depth to the water table corresponds to the time of the measurements and spatial variation exist within each site. The numbering corresponds to that in Figure 1.

Tailings site	**Ore type**	**ERT-IP** number of profiles (total length (m))	**RMT** number of profiles (total length (m))	**tTEM** total length (m)	**GPR** total length (m)	**SIP** number of samples	**Depth to estimated water table (m)**
1. Morkulltjärnen (Yxsjöberg)[1]	W and Cu	3 (1320)	1 (560)	7 400	-	2	< 3
2. Svandammen	Fe-oxide-apatite	3 (570)	-	1 940	-	-	2–5
3. Jan-Mats-dammen	Fe-oxide-apatite	6 (1600)	2 (370)	1 400	-	2	10
4. Hötjärnen	Fe-oxide-apatite	7 (2580)	2 (630)	3 720	-	-	0–2
5. Blötberget	Fe-oxide-apatite	3 (1220)	4 (1400)	-	-	2	>9
6. Stollberg	Pb-Zn and Fe-Mn	5 (1100)	1 (320)	-	2 330[2]	2	>12
7. Källfallet	Fe and Cu	3 (1130)	4 (1200)	1 960	3 220	-	3–6
8. Bäckegruvan	Fe and Cu	10 (3350)	2 (630)	5 400	5 160	2	0–7
Total profile km		**12.9**	**5,1**	**21,8**	**10,7**		

[1] Only referred to as Yxsjöberg in Appendix B.

[2] Measurements made in 2019.

Electrical properties of rocks and unconsolidated sediments

Variation in the electrical properties of rocks and sediments result in varying responses from geoelectrical and electromagnetic geophysical methods. Electrical properties in such materials are observed to vary over several decades, and their study is potentially a powerful way to distinguish between materials and study variations in porosity, water and metal content for example. Hence, geophysical electrical and electromagnetic methods are often utilised by geoscientists to distinguish between different materials in the subsurface and map their geometries. In practice, estimations of the electrical properties using these methods are typically provided by inverse modelling of data collected in the field. But inversion results generally provide estimates over relatively large volumes. In this study we also consider laboratory measurements of the electrical properties on samples. These provide reference data on a relatively small scale but are important for interpreting and validating the results from field geophysical measurements.

Electrical properties are measurable in the presence of an external electric field. Electrical resistivity is a measure of the resistance of a medium to electric current. Its inverse, conductivity measures how well a material conducts current. Electrical permittivity is related to the ability of material to become electrically polarized. Both are included when speaking of complex electrical resistivity or conductivity. Electrical properties are in general dispersive, i.e. they vary with frequency. Maxwell's equations show that in the presence of an electric field two systems of current flow are generated, namely conduction and displacement. Vinegar and Waxman (1984) used the general constitutive equations for a linear, homogeneous, isotropic, and time-invariant medium to explain the behaviour of frequency dependent electrical properties. The constitutive relationships connect the measured fields and electrical properties:

$$\mathbf{J} = \sigma^*(\omega)\mathbf{E} \quad (1)$$

$$\mathbf{D} = \kappa^*(\omega)\varepsilon_0\mathbf{E} \quad (2)$$

where **J** is the current density, **D** the displacement field and **E** the electric field. ω is the angular frequency of the signal , $\sigma^*(\omega)$ is the frequency-varying complex conductivity and $\kappa^*(\omega)$ is the frequency-varying complex dielectric constant.

$\kappa^*(\omega) = \varepsilon(\omega)/\varepsilon_0$, is dimensionless, where ε_0 is the permittivity of free space (8.85×10^{-12} F/m) and $\varepsilon(\omega)$ the dielectric permittivity of the medium.

If one considers that $\{\sigma', \sigma''\}$ and $\{\kappa', \kappa''\}$ are the real and imaginary part of σ^* and κ^*, respectively, one can also rewrite (1) and (2) as:

$$\mathbf{J} = [\sigma'(\omega) + i\sigma''(\omega)]\mathbf{E} \quad (3)$$

$$\mathbf{D} = [\kappa'(\omega) + i\kappa''(\omega)]\varepsilon_0\mathbf{E} \quad (4)$$

The following text summarises some equations which have been derived describing the relation between complex conductivity, permittivity, and resistivity (see Tarasov and Titov, 2013) and references therein):

In practice complex resistivity can also be expressed using its real and imaginary terms $\{\rho', \rho''\}$

$$\rho^*(\omega) = \rho' + i\rho'' \quad (5)$$

Or as $\rho^*(\omega) = |\rho|e^{i\varphi}$

With $|\rho|$ defining its amplitude and φ the phase angle.

$$|\rho| = \sqrt{\rho'^2 + \rho''^2} \quad (6)$$

$$\varphi = Arctan\left(\frac{\rho''}{\rho'}\right) \quad (7)$$

Note that φ is negative in the case of induced polarization.

Some authors prefer to use complex conductivity, since they find it more directly related to conduction mechanisms, but in this work, we have used the complex resistivity, as commonly done in resistivity and IP studies.

The geophysical methods employed here, except for GPR, use relatively low frequencies for which conduction currents dominate over displacement currents. Hence, conductivity is the dominant term for these methods and the resistivity is independent of the frequency. It is only when using the induced polarization method that frequency dispersion is considered. Conversely displacement currents dominate in the GPR method where frequencies of the order of MHz to GHz are used. For GPR the complex permittivity $\varepsilon^*(\omega)$ becomes the dominant term.

From laboratory measurements and theoretical considerations, we know that electrical properties are specifically related to porosity, water content, presence of conductive minerals, clay content and porewater conductivity, following relationships that vary depending on the composition and the inner structure of the material. Therefore, they can be used to infer the structure and types of materials in the subsurface.

Data acquisition using geophysical electromagnetic methods can be more or less time consuming. Measurements made from aircraft or equipment which is towed behind a vehicle are usually relatively fast, but they can require specific field conditions, for example open terrain. Other methods, such as ERT and (galvanic) IP, can be more time-consuming as they require direct contact with the ground and each measurement is made over a specific period. The resolution and depth of investigation that can be attained depends on the resistivity, frequency of the electrical or electromagnetic signal being used, and the configuration of the measurement array (for example the electrode spacing in ERT or the size of the loop in TEM). The lateral spatial resolution also varies among the methods and decreases with increasing depth. The specific conditions in the field, such as the presence of highly conductive sediments at the surface, can also strongly affect the response and depth of investigation of these methods.

Table 2 lists the methods used in this study, the type of measured data, and the estimated physical properties for each of them.

Table 2: Geophysical methods used in this study, the corresponding measured quantities, and the estimated physical parameters.

Geophysical method	Measured quantity/field	Estimated physical quantity/property
Direct Current (DC) Electrical Resistivity	Potential difference, electrical current	Electrical resistivity
Induced Polarization (IP)	Potential difference decay over time, electrical current	Chargeability
Spectral induced polarization (SIP)	Potential difference, electrical current in difference frequency	Spectrum of complex resistivity
Electromagnetics (EM) -Radio-magnetotellurics (RMT) and Transient electromagnetics (TEM)	Electric and/or magnetic fields, currents (induced or injected),	Electrical resistivity, conductance, conductivity
Ground Penetrating Radar (GPR)	Electric field, currents (induced)/arrival times	Permittivity/EM wave velocity

It is important to note that the resistivities of different rocks and sediments can overlap significantly, hence, the identification of subsurface materials based on resistivity alone is not often possible. Figure 2 illustrates the variation in the electrical resistivity of a range of earth materials relevant for this study. As can be seen, in some cases the values overlap over several orders of magnitude. It is therefore important to consider other forms of information (such as borehole data) or to integrate the results from several methods to reduce the uncertainty in the interpretation. Joint inversion (i.e. the inversion of measurements from several methods together) can also be used to improve the accuracy of estimated physical properties of the subsurface.

Except for situations when massive conductive ore, or interconnected metallic grains are present, the primary conduction mechanism within geological materials is electrolytic, i.e. it is due to charge transport by ions in pore fluid. A second mechanism is the interfacial or surface conduction in the electrical double layer (EDL). These mechanisms are studied by several works (e.g. Archie 1942, Archie's saturation equation cited by Ward, 1990, Waxman and Smits 1968, Shevnin et al. 2007 among others). In general, when surface conductivity is significant it is difficult to use the sole (real) resistivity to relate to other parameters and it is recommended to use induced polarization as well to reduce ambiguity in the interpretation (see e.g. Weller et al. 2013, Vinegar and Waxman 1984).

For a rock containing conductive particles/minerals the bulk resistivity may be seemingly unaltered if these are not connected. But the conductivity of the rock may increase dramatically if the conductive material is present in a massive form or as veins. In rock or soils with disseminated mineralisation significant IP responses in terms of chargeability can be expected as well as specific complex resistivity spectra. Such spectra can potentially contain a lot of information about the material's composition and structure and were early recognized as offering a way to distinguish between different kinds of ores (see Pelton et al. 1978 for example). Several physical models at the microscopic scale have been designed to explain IP responses in such materials (one can cite for example Wong (1979), Bücker et al. (2018), Revil et al. (2015)) but none of them can to date explain all effects and each of them may correspond to specific cases. On a more macroscopic level the effective medium theory has been applied (Zhdanov 2018, Bérubé 2024 and Gagnon 2024) in an attempt to describe materials containing several kinds of conducting minerals of different size and shapes.

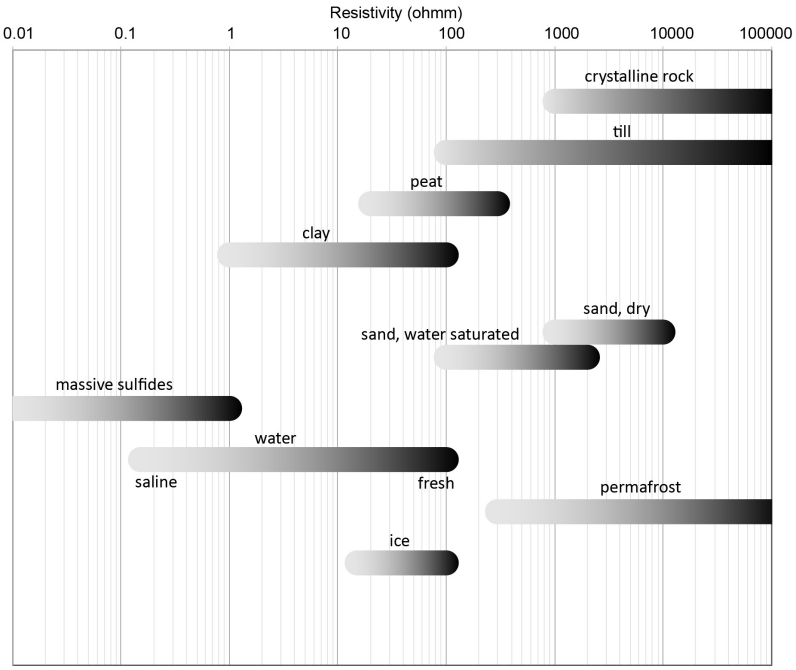

Figure 2. Variation of electrical resistivity for some minerals, rocks and sediments relevant in this study (after Parasnis 1997 and Palacky 1987).

In our interpretation we have considered a few phenomenological models (Pelton's Cole-Cole model, the maximum phase angle (Fiandaca et al. 2018), the Debye decomposition (Nordsiek and Weller 2008).

The resistivity changes with temperature following a relationship analog to that given by Ward (1990) after Keller and Frischknecht (1966):

$$\rho(T) = \frac{\rho_{25}}{1+\alpha(T-25)} \quad (8)$$

With T the temperature in °C, ρ the resistivity and ρ_{25} the resistivity in ohmm at 25 °C. There is no general agreement about the value of the coefficient α since it probably depends on the conduction mechanisms in the specific material considered as discussed in literature (Binley and Slater 2020 and Lévy et al. 2019). Ward (1990) gives an average value of 0.025°C^{-1}. Sumner (1976) and Samouëlian et al. (2005) give 0.0202°C^{-1} in soils. Lévy et al. (2019) computed 0.033°C^{-1} from the values published by Vinegar and Waxman (1984) for shaly sands. For the kind of material considered here, mine tailings, we can probably expect a value in the range 0.02–0.03 °C^{-1} but it is difficult to be more precise without specific data.

For porous geological materials which are partly saturated, it can be observed that the resistivity dramatically increases when the temperature drops below the freezing point. This relatively sharp change in resistivity can sometimes be used to characterise permafrost in field data. When it comes to induced polarization, effects are possibly less strong and more complex, but the method has also been used to map permafrost (e.g. Revil et al. 2019, Maierhofer et al. 2022, Coperey et al. 2019). It is also important to consider temperature differences when comparing laboratory and field when using resistivity-IP methods.

It is convenient to use empirical phenomenological models when working with IP and SIP, since they do not in themselves imply a precise physical explanation which would often be intricate and complex. One of the most widely used and discussed models to describe the low-frequency dispersion of resistivity studied in SIP is the so-called Cole-Cole model as defined by (Pelton et al. 1978). It only uses four parameters to describe the dispersion of the complex electrical resistivity ρ^* at low frequency:

$$\rho^*(\omega) = \rho_0\left[1 - m\left(1 - \frac{1}{1+(i\omega\tau)^c}\right)\right] \quad (9)$$

Where ρ_0 is the DC electrical resistivity, m is the chargeability and τ is the Cole-Cole (Pelton) relaxation time and c is the Cole-Cole (Pelton) exponent or frequency dependency. If c = 1 the model corresponds to a Debye polarization, with an exponential decay in time-domain. However, experimental data (Pelton et al. 1978, Kemna 2000) indicate that the value of c is most often between 0.1 and 0.6. The broadness of the dispersion as illustrated on figure 3 increases with decreasing values of c.

Chargeability is defined by Seigel (1959) in the following way:

$$m = \frac{\rho_0 - \rho_\infty}{\rho_0} \quad (10)$$

where ρ_∞ is the measured resistivity for the highest frequency. The phase of the complex conductivity peaks at the angular frequency (after Tarasov and Titov 2013):

$$\omega_{peak(\varphi)} = \frac{1}{\tau}(1-m)^{\frac{1}{2c}} \quad (11)$$

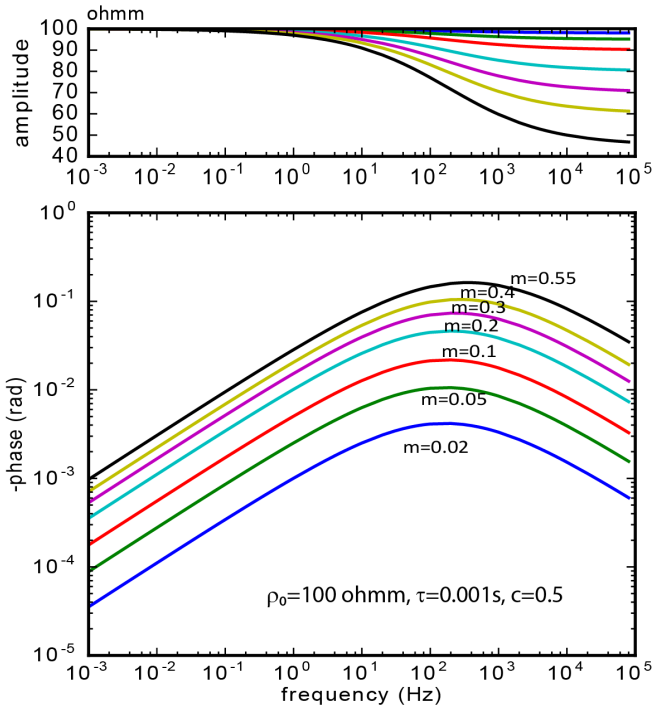

Figure 3. Computed amplitude and phase in the (Pelton) Cole-Cole model depending on the chargeability value **m**.

In the time-domain, a Pelton-type dispersion corresponds to a slower than exponential dispersion. Normally a Pelton-type model can only describe a single-peak frequency spectrum. It is however possible to combine several models to describe more complex spectra.

Although this model is frequently used because of its simplicity another difficulty often pointed out is that its parameters are not independent from each other. This leads (Fiandaca et al. 2018) to the definition of a re-parametrisation:

$$\tau_\varphi = \tau_{pelton}(1-m)^{\frac{c}{2}} \qquad (12)$$

Where φ is the maximum phase angle, τ_φ corresponds to the frequency for which the maximum phase is attained, and c is the exponent which is the same as in the Pelton model. Using the expression in this form, which is known as the maximum phase angle (MPA) approach, Fiandaca et al. (2018) was able to obtain better inversion results than with the classical Cole-Cole model.

Another widely used model is the Debye decomposition proposed by Nordsiek and Weller (2008), after Debye (1929, cited by Tarasov and Titov 2013). In that case the complex resistivity is viewed as the sum of individual Debye models, each with an individual chargeability and relaxation time:

$$\rho^*(\omega) = \rho_o\left[1-\sum_{k=1}^{n} m_k\left(1-\frac{1}{1+i\omega\tau_k}\right)\right] \qquad (13)$$

Each individual Debye component corresponds to an exponential decay, but it is possible to reconstitute a Cole-Cole dispersion with a sum of Debye models.

The Cole-Cole model as defined by Pelton, or the MPA approach, can be applied when materials are expected to show such a dispersion pattern. Laboratory measures, experiments and modelling results have shown that it is notably the case when the size of the conducting minerals follows a log-normal distribution (noted by Revil et al. 2022).

An almost complete account of nearly all aspects of resistivity and (spectral) induced polarization can be found in Binley and Slater (2020).

Methods

In the following we describe the geophysical methods used in this study, focusing on the way they have been specifically applied in this project.

DC resistivity and IP

The IP and the DC resistivity method, which is also referred to as electrical resistivity tomography (ERT), both measure the electrical potential in the earth established in response to the injection of an electric current into the ground.

In both methods an impedance $Z^* = k\rho^*$ is calculated that is generally complex. k is the geometrical factor. In DC resistivity the current is applied under a sufficiently long time so that one can assume a steady state (zero frequency) is reached, which simplifies the computations. The measured impedance is considered real and determines the DC resistivity. The effects of conduction of current by the ions in the pore water, and of conduction at the surface of the grains and inside conducting or semi-conducting minerals cannot be distinguished with DC resistivity.

ERT method

ERT is an established and well-documented technique. It dates to the 1920s when the first vertical electrical soundings were performed. It has been applied in its modern form, with multielectrode systems since the 1990s. ERT is routinely used in many applications, for example geological mapping, mineral prospecting, groundwater studies, geotechnical applications, and environmental studies, such as contamination monitoring etc.

For the ERT measurements one uses a pair of electrodes for current injection (C1, C2), and at least another pair to measure the resulting potential difference (P1, P2) as shown in Figure 4. If several electrodes are deployed along a 2D profile, many different four-electrode geometries or electrode arrays can be utilised (see Szalai and Sarka 2008). In this study we used the so-called gradient array geometry. This geometry enables dense data coverage along a profile and is very practical when using multichannel instruments. It also has versatile imaging capability in a variety of situations (see e. g. Dahlin and Zhou 2004; Dahlin and Zhou 2006).

By measuring the potential difference (ΔV), and the injected current (I) one retrieves the apparent resistivity ρ_a defined as:

$$\rho_a = k\frac{\Delta V}{I} \tag{14}$$

For electrodes at the ground surface, the geometrical factor k is defined as:

$$k = \frac{2\pi}{\left[\frac{1}{C_1P_1} - \frac{1}{C_1P_2} - \frac{1}{C_2P_1} + \frac{1}{C_2P_2}\right]} \tag{15}$$

For larger geometrical factors (larger electrode distances) the measured potential difference and signal to noise ratio typically decrease. In addition, longer cables tend to pick up more noise from the environment. Another factor which can contribute to measurement error is uncertainty in the positioning of the electrodes (for a systematic study see e. g. Zhou and Dahlin 2003).

Measurements with arrays of larger dimensions increase the depth of investigation (DOI) and reflect the properties of a larger volume compared to measurements done with smaller arrays. To obtain an image of the electrical resistivity measurements, data from many different combinations of current and potential electrode pairs are collected and used together for modelling electrical resistivity of ground below survey areas.

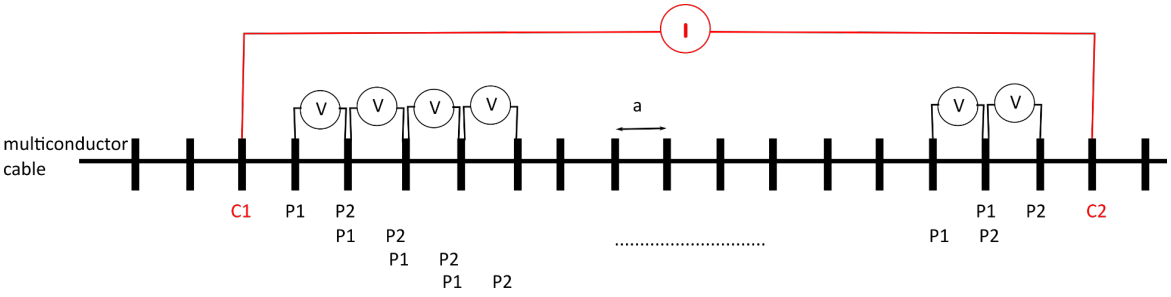

Figure 4. Multielectrode gradient measurement with current electrodes (C1 and C2) and potential electrodes (P1 and P2). Here the distance between P1 and P2 is the unit electrode spacing **a**, but many multiples are used, as well as for the distance between current electrodes.

Time domain IP (TDIP) and SIP

The IP effect has been known since the establishment of the DC resistivity method in the 1920s. Several general accounts of its history have been published (see Seigel et al. 2007, Kemna et al. 2012, Binley and Slater 2020, Revil et al. 2022). The method is widely applied in mineral exploration, hydro-geophysics, environmental studies, and for investigation of organic compounds and materials.

The IP can be measured either in time or frequency domains. In TDIP measurements one typically measures the decaying potential after the current turn-off and computes the apparent chargeability by integration over a series of given time windows (Figure 5A). The apparent chargeability is defined for a given time-window $[t_1, t_2]$ as:

$$M_a = \frac{1}{V_o[t_1 - t_2]} \int_{t_1}^{t_2} V(t)dt \qquad (16)$$

The integral corresponds to the grey area in Figure 5A, and the apparent chargeability gives an average of the normalised potential in the given time-window.

In frequency-domain measurements one typically measures the apparent resistivity for two or more frequencies (below 10 000 Hz). In earlier studies one used to compute the percent frequency effect (PFE). Figure 5B illustrates the measurement for one frequency.

The PFE is defined for two frequencies $f_1 < f_2$ as:

$$PFE = 100 \frac{\rho(f_2) - \rho(f_1)}{\rho(f_1)} \qquad (17)$$

This methodology was not applied in the project, but it is given here for comparison, since chargeability and percent frequency effect are two ways to estimate the amplitude of the polarization, which is the aim with the IP method. As discussed by Lesmes and Frye (2001) and Sumner (1976) both PFE and chargeability can be used equivalently since they are proportional (at least for qualitative interpretation). They are also proportional to the phase angle φ for small phase angles like the ones generally encountered in the earth materials. When electrolytic conduction is the dominant mechanism, the phase angle (or the chargeability) provides a way to estimate the relative amplitude of other charge transfer or storage mechanisms.

Working with SIP means recovering the complex resistivity spectrum from a few mHz up to a few kHz. This enables better discrimination between different materials. Measurements can be done directly at several frequencies or by studying the shape of the decay curve in the time-domain. Each response can be retrieved from the other by Laplace or Fourier transform.

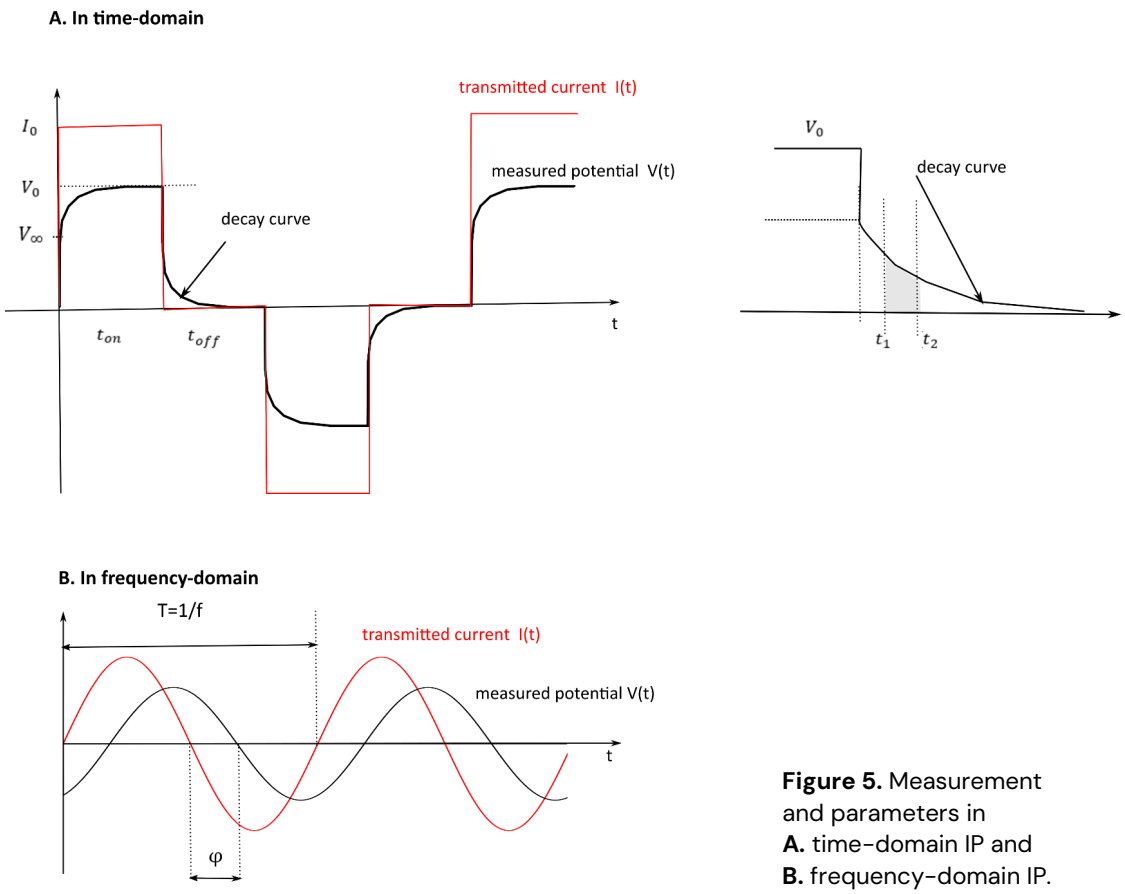

Figure 5. Measurement and parameters in **A.** time-domain IP and **B.** frequency-domain IP.

SIP is commonly measured in laboratory studies. It is more direct and potentially easier to interpret. However, it is challenging and time consuming to study SIP from field measurements. TDIP measurements are faster. Complex resistivity spectra can theoretically be equivalently recovered from TDIP measurements, but it requires that the decay curve is accurately recovered, and the timespan is adequate. However, this technique is for practical reasons usually limited in the higher frequency range. But the relevant frequency range is determined by the objective of the investigation, and it is not always needed to reach high frequencies. Recent comparisons published by Martin et al. (2020) and Maurya et al. (2018) show the practical advantages of using TDIP techniques with multielectrode systems regarding logistics and data quality.

Both TDIP and SIP measurements are generally affected by EM (or inductive) coupling, either external, that is induced by coupling between the cables and the ground or internal between different parts of the measurement system. The disturbance becomes more important for larger electrode distances, long cables, and lower resistivities and can contribute to a significant fraction of the measured signal. Methods and software exist to take these effects into account and correct for it (e.g. Ingeman-Nielsen and Baumgartner 2006; Ghorbani et al. 2009). Nevertheless, it is generally difficult and may require knowledge over the position of the cables, and the existing programs can only consider a full electromagnetic solution in 1D. Therefore, it is usually recommended to design field measurements to minimise the EM coupling. The noticeably affected IP data are usually discarded, since the inversion codes commonly used to-date cannot take the inductive effects into account.

The use of multielectrode systems with long unshielded multiconductor cables may lead to significant capacitive coupling (crosstalk). One way to reduce that problem is to use separate cables for current injection and potential measurements (Dahlin and Leroux 2012). Experience has shown that it is generally not necessary if the contact resistance of the electrodes is kept

below 1000 ohmm. This can however be difficult to achieve in practice. It is also important that the measuring instrument has a very high input impedance, but this condition is generally fulfilled with modern instrumentation.

The kind of electrode used and the contact resistance at the electrode is also important. Traditionally non-polarizable electrodes were used for induced polarizable measurements. But several studies have shown that they did not always bring a significant improvement to the measurement (e.g. Dahlin et al. 2002, Zarif et al. 2017) and today stainless-steel rods are commonly used for measuring IP. They are more durable and easier to handle in the field and they do not require stabilisation. However, some attention should be paid in case saline solutions are used to improve the contact.

Inductive and capacitive coupling and the effect of the electrodes must also be considered in lab measurements. Attention must be paid to the design of the sample holder and to the lab instrumentation, in order not to induce spurious effects.

TDIP field measurements can be done with the same kind of multi-electrode equipment used for ERT by recording the decay of the potential after the current turn-off when using the so-called 50% duty cycle. The 50% duty cycle is a measuring cycle divided in four equally long parts: first positive current on, then current off, negative current on, followed by another current off, and it is illustrated in Figure 5A. Olsson et al. (2015) showed that 100% duty cycle measurements gave equivalent results. In that case the measuring cycle does not include current turn-off but only reversal of polarity which divides the time needed for the measurement by two. The TDIP signal levels are much lower than in the ERT and several significant sources of disturbances exist even after minimising couplings and electrode effects. The processing developed by Olsson et al. (2016), implemented in the AWB software, results in longer decay curves actually available for inversion which cover a wider frequency range when compared to the standard processing made with the field instrument (Terrameter LS).

Assuming that crosstalk and EM-coupling are negligible, each datapoint on the decay curve is still affected by several sources of noise. These different sources of noise can be summarised below (Olsson et al. 2016):

$$V_{measured}(n) = V_{response}(n) + V_{drift}(n) + V_{spikes}(n) + V_{harmonic\ noise}(n) + V_{random}(n) \quad (18)$$

V_{drift} is the background drift resulting from the polarization at the electrode, $V_{harmonic\ noise}$ is a disturbance in the signal due to the alternating current supply, V_{spikes} are another kind of anthropogenic noise, and V_{random} is random noise in the surrounding environment. Accurate recovery of the decay curve requires minimising these different forms of noise. This can be done by recomputing chargeability in IP windows from the recorded full-waveform signal using the procedure developed by Olsson et al. (2016) (Fig. 6).

Assuming that such processing has been applied to the full waveform data, before inverting either the whole decay curves or the apparent chargeability, it is still important to inspect the decay curves and the pseudo-sections of chargeability to remove data that are obviously strongly affected by noise. Early times in the decay curve can be affected by EM-coupling effects induced by the transmitted current and must often be removed. Hence, the first 5 to 10 ms can rarely be used. This effect lasts longer for larger electrode spacings and geometrical factors. Typically, one considers that decay curves in TDIP show a smooth monotonic decay of the potential, as exemplified in Figures 3 and 6. But negative apparent chargeability and decay curves with negative parts are still possible and constitute valuable information that should not be discarded. (Sumner 1976, Dahlin & Loke 2015, Fiandaca et al. 2022). Inspection and post-processing of decay curves measured in the field is nevertheless a difficult and lengthy process and to-date it must still be made by an operator.

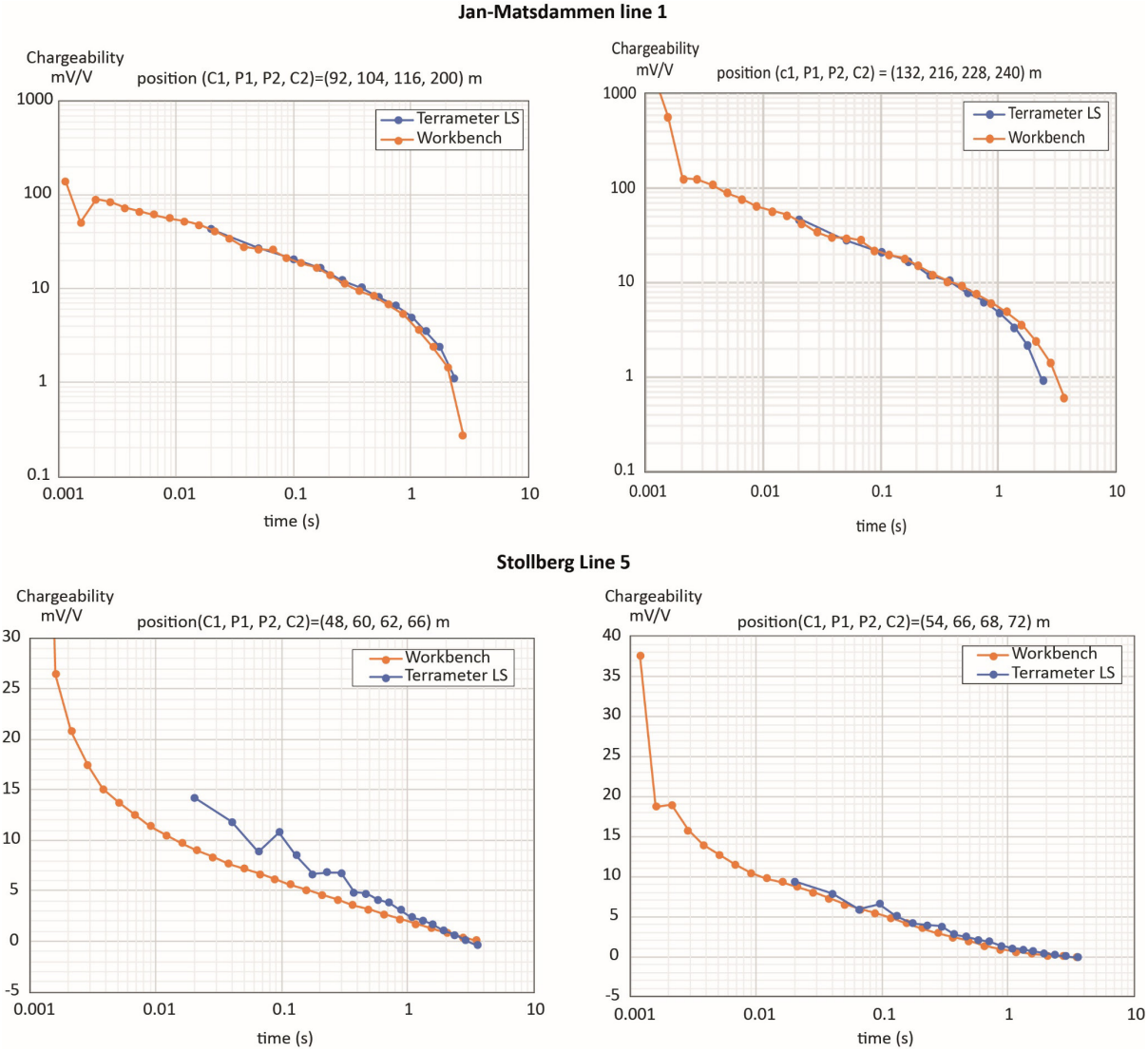

Figure 6. Chargeability from two locations along line 1 in Jan-Matsdammen and two locations along line 5 in Stollberg. The blue decay curves are retrieved by the instrument Terrameter LS2 and the equivalent red curves are obtained from processing developed by Ohlsson et al. (2016) in Aarhus workbench.

In the field, a long-enough recording time must be set to allow complete charge buildup and decay of the IP effect, thereby ensuring adequate recovery of the low-frequency part of the signal. At the same time, one seeks to keep it as short as possible to reduce the time spent in the field. A choice of IP recording windows for averaging and recording chargeability in the instrument also needs to be made. For better control, and to allow re-computation of decay curves it is recommended to save the fully recorded signal with at least a few kHz sampling rate. This enables inspection, more accurate processing and potentially increase of the usable decay time or bandwidth (Olsson et al. 2016). Figure 6 shows a few examples of the signal processed with two different processing settings.

ERT and TDIP data acquisition in this project

The instrument used to measure ERT and TDIP was an ABEM Terrameter LS2. The measurements were made using the gradient array with a 2 m electrode spacing for most profiles in most cases but a 5 m spacing was used on a few lines. The maximum available power in the instrument (600 W) was selected on almost all profiles. This meant that the average current used

was around 200 mA. In Bäckegruvan up to 1.5 A could be used. Generally, we tried to use no less than 20 mA.

The instrument estimates the contact resistances for all electrodes before starting the actual measurement at every station. In order to keep these resistances below 1000 ohm, special attention was given to the electrodes; they were hammered deep and had to be watered at several sites, sometimes using salt water. The measurements done in 2022 were particularly demanding because of frozen soil at Stollberg and Blötberget. This requirement could however be achieved at almost all sites for almost all measurements, the highest contact resistances measured being of a few kilo-ohms. The position of each end of cable was generally measured using a handheld GPS with a mean precision around 2 m depending on field conditions. At Bäckegruvan a more precise differential GPS was used with a general precision under 0.3 m. Elevations were computed after the acquisition using a digital elevation model with at least 2 m horizontal resolution.

The measured data contain the full wave responses sampled at 3750 Hz for the measurements made in 2021 and 7500 Hz for the measurements from 2022. Following Olsson et al. (2015) we used a square wave with no off-time (100% duty cycle) and with a half period of four seconds. This choice was thought to make it possible to work sufficiently fast in the field while preserving a large enough frequency content. We have saved the full response for all data in order to be able to apply a more effective processing to the TDIP field data than what can be done in the instrument and possibly increase the frequency content as described in Olsson et al. (2016). Two to three measuring cycles were generally recorded in the field.

At the beginning of the project a test was made in the field at Hötjärnen using separate current and electrode cables following Dahlin and Leroux (2012) and using a protocol file provided by Torleif Dahlin. The results showed no significant difference with those obtained using only one cable at the same location when looking at the chargeability computed by the instrument. It was concluded that the capacitive coupling was not a large source of error at this locality and would probably not be at the others. Consequently, all measurements were acquired with only one cable at all the other tailing deposits, which resulted in a considerable simplification of field logistics.

Inversion of ERT data

The aim of inversion is to find a resistivity model of the ground that can explain the measurements. The most used methods are based on the least-squares optimisation that aims at minimising the sum of the squares of discrepancies between measured and calculated data. This is done iteratively. One starts with a model of the resistivity that consists in a mesh of individual cells with pre-defined values for the inversion parameters describing the part of the underground we want to image. It is systematically modified at each iteration until a sufficiently good fit is obtained. Because of problems with singularity when solving for 2D or 3D geometries, one must use regularisation constraints. It generally consists in allowing only a certain amount of variation in space, both laterally and with depth, in adjusting the forward modelling grid to the expected resolution and depth of investigation and by applying a roughness matrix. One also generally limits the allowed change between models, and the quality of the desired data fit can be adjusted to the estimated noise level. Taking topography into account is also desirable. One well-known inversion program is Res2DInv. We have used it only a little for comparison and evaluation. It is always important to check the results in terms of data fit and plausibility, and possibly to re-adjust the parameters and re-run the inversion in case the results are not satisfying.

The results shown in this report were obtained by inversion of ERT data using the Aarhus Workbench (AWB) software (Auken et al. 2005 & 2009) developed by Aarhus GeoSoftware. The AWB software used the finite difference method in the forward modelling. Prior to the inversion the user sets the number and thickness of the layers in the model and has the possibility to choose vertical and horizontal constraints which control the variation allowed between adjacent

model cells. Depending on the estimated noise the user can also specify a standard deviation which describes the error in the data.

Ways to estimate the quality and significance of the inversion results are provided, like a computation of the depth of investigation (Christiansen et al. 2012). It is important to remember that the solution of the inverse problem in ERT profiling is not unique and that the models obtained with these methods have a minimum structure, are often smooth, can be influenced by the starting model and that resistivity contrasts are often not fully recovered. It is always important to compare the inversion results with borehole data when available.

The ERT data were inverted using 2D LCI modelling in Aarhus workbench. A smooth inversion technique was used with 20 to 30 layers with logarithmically increasing thickness down to between 40 and 60 m depth depending on the site. Different vertical and lateral constraints were applied, also depending on the site. Uniform starting models with automatically computed resistivity were used.

Processing and inversion of TDIP data

All profiles were imported into individual site projects using the software Aarhus workbench, where they could be inspected so that what was considered as bad data could be removed. The so-called Lunds advanced processing method was used for the import of TDIP data, with an initial delay time of 0.001 s and the computation (by integration) of eight gates per decade with logarithmically increasing durations. For the processing we have followed standard recommendations. This means that in most cases we have removed either entire decay curves or parts of decay curves which do not exhibit a smooth monotonic decay. This was important to obtain a stable inversion result. We have proceeded in this way to save time and as a first approximation. It is inevitable that valuable parts of the signal might have been removed.

The AWB software inverts the TDIP data taking into account the shape of the decay curve and the transmitted current waveform (Fiandaca et al. 2013, 2018). The response for several frequencies is computed using frequency dependent complex resistivity in the frequency domain and the time-domain response (decay curve) is then computed via Fourier transform. Most of the forward modeling is carried out in the frequency domain, but the inversion parameters are computed for the time-domain, i.e. for the decay curves. Optimisation is used to reduce the computation time and stabilise the inversion. As for the resistivity inversion vertical and horizontal constrains on the inversion parameters are used to regularise their variations in the horizontal and vertical directions. Several alternatives exist for the computation of induced polarization effects. We have used the maximum phase angle approach (MPA). It is described in Fiandaca et al. (2018) and corresponds to a re-parameterization of the so-called Cole-Cole model as defined by Pelton. In the MPA inversion scheme the inversion parameters are the direct-current resistivity (ρ_o), the maximum phase angle (φ_{max}), the relaxation time (τ_φ) corresponding to the maximum phase angle and the frequency exponent c. These parameters can be reasonably well resolved if the time constant lies within the frequency content of the signal considered and if the exponent c is sufficiently large to define a clear phase maximum (Madsen et al. 2017). Here one is limited by the sampling rate and usable time-windows of the decay curve. Specifically, the decay curve needs to start early if one is interested in high frequencies and last long enough for lower frequencies. The sampling rate is especially critical at early times where potential variations are rapid. In general, the resistivity models obtained with or without considering the IP are slightly different.

We have inverted induced polarization decay curves using the MPA method and a smooth inversion scheme. The discretization was similar to the one used for the ERT inversions. The horizontal and vertical constraints varied between different sites where default values were typically used.

Towed Transient Electromagnetic (tTEM)

TEM is an electromagnetic method used to detect and image subsurface features which are electrically conductive such as clays, massive sulphides, graphitic mineralisation, groundwater, etc. In TEM measurements, typically, a relatively strong direct current (DC) is maintained in an ungrounded loop, referred to as the transmitter. The current is switched off causing sudden changes in the magnetic flux which in turn induces a secondary electric field in the underlying ground below the transmitter. An additional receiver loop then measures the time varying secondary magnetic field (Fig. 7) that is generated by the induced eddy currents (see Nabighian & Macnae 1991). A transmitter with a high magnetic moment (i.e. the product of current, number of turns and surface area) offers a stronger signal to noise ratio (S/N) and consequently a greater depth penetration. The choice of the Tx-Rx configuration depends on the geological target as well as the field conditions (topography, access roads, etc). However, there are a number of established transmitter (Tx) and receiver (Rx) configurations which are commonly used. Nabighian & Macnae (1991), give a detailed account on the resolution and sensitivity of different Tx-Rx configurations that have been applied to a number of different subsurface targets. TEM measurements can be conducted on land (Spies and Parker 1984; Goldman and Fitterman 1987; Auken et al. 2019), in the air (Nabighian & Macnae 1991; Sørensen and Auken,2004; Eadie et al. 2018) and in a marine environment (Ziolkowski and Wright 2007; Tezkan et al. 2008).

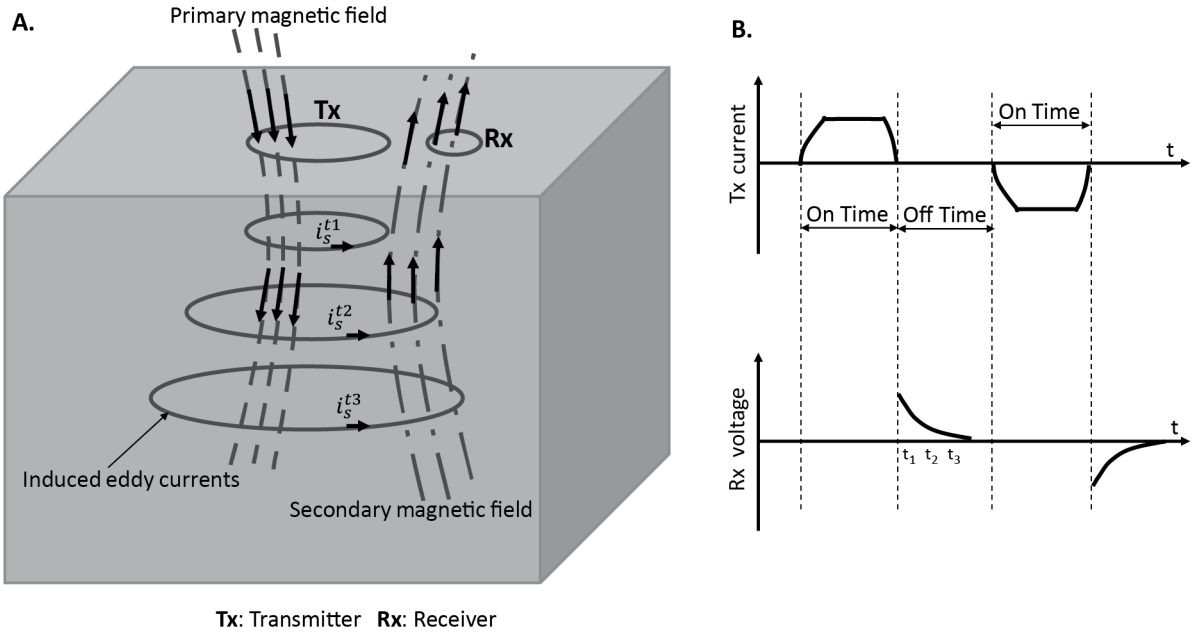

Figure 7. A. Schematic showing the primary magnetic field generated by the transmitter coil at different time windows and the secondary magnetic field generated by induced eddy currents in the subsurface. **B.** The current in the transmitter loop (Tx) is switched off after being active for a period of time. A voltage caused by the time changing secondary magnetic field, associated with eddy currents in the subsurface is then measured over time in the receiver loop. The same procedure is repeated several times to enhance the S/N.

The towed-TEM (tTEM) system used in this study was developed at Arhus University by the HydroGeophysics Group (HGG) between 2016 and 2018. Auken et al. (2019) give a detailed account of the system specifications which are briefly explained here. During development the HGG has tested and refined the system configuration over time. The dimensions of the Tx and Rx as well as the offsets between the Tx, Rx, and ATV for the system used in this study are shown in in Figure 8A. tTEM is designed for highly efficient data acquisition and detailed 3D-mapping of subsurface down to a depth of about 70 m. The Tx and Rx coils, mounted on sleds, offer the possibility to easily acquire data over moderate terrain, such as agricultural land, unpaved roads and gravel areas. Figure 8B shows the tTEM system in action where the Tx and Rx are towed behind an all-terrain vehicle (ATV).

The data acquisition procedure is very similar to the SkyTEM system as detailed by Auken et al. (2009). The measurements are conducted sequentially in two transmitter modes, namely low moment (LM), and high moment (HM). Each measurement moment typically takes 0.5 seconds and includes hundreds of individual transient measurements. The GPS antenna is mounted on the transmitter frame (Fig. 8A). The tTEM system in this configuration can operate at speeds of up to 20 km/h depending on terrain and surface conditions.

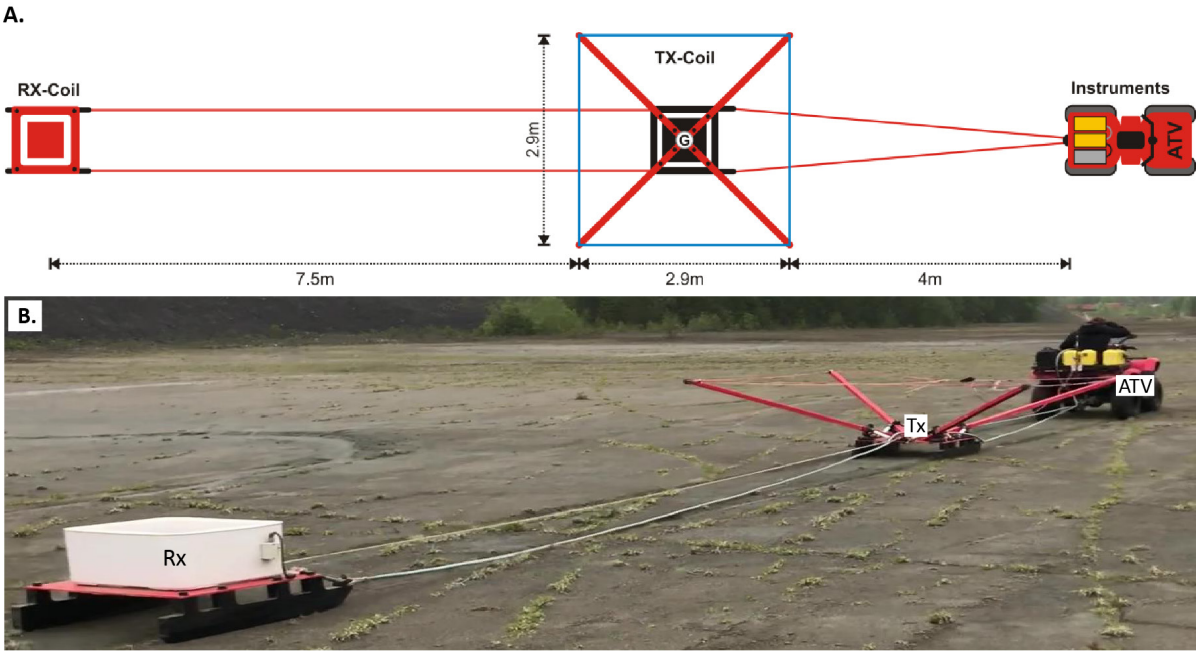

Figure 8. A. A schematic showing the configuration of the system taken from the report sent by the HGG (HydroGeophysics Group 2022). **B.** tTEM system in the field at the Bäckegruvan site in Sweden. Photo: Mehrdad Bastani.

tTEM data processing and inversion

Auken et al. (2019) give a detailed account on the system calibration and processing of acquired tTEM data. The data are processed using a very similar technique to that applied to the SkyTEM data with tools provided in the Aarhus Workbench (AWB) software package (Auken et al. 2009). The raw dataset contains various files (transient data from the receiver, GPS positions, transmitter currents, system geometry, etc.) that are imported into AWB. In the pre-processing stage the noise is suppressed by reversing the polarity of the alternating pulses and stacking (Fig. 7B). This is done within a certain number of time gates that are linearly spaced in logarithmic time. Narrower time windows are used at earlier times, where the signal strength is relatively high and the decrease steep to maximise the resolution. While at later times, longer time windows are utilised to boost the signal to noise (S/N) ratio. The strongest noise sources are powerlines (lower frequencies) and powerful VLF transmitters (higher frequency noise). The change of elevation of towed Rx above the ground (due to rough terrain) in the presence of the Earth magnetic field also induces noise that interferes with the TEM signal. Such noise, typically in the 0–20 Hz band, depends on the ATV's velocity and is in the order of 5–20 $\mu V/m^2$ (Auken et al. 2019). This noise is strongly reduced by suspending the Rx mechanically, applying a lowpass filter to the data and stacking the data (summing repeated measurements). The raw data are first processed automatically (Fig. 9A and C) to remove various types of effects (coupling, low S/N, line turns). In the next stage the raw data are further processed by spatial averaging where a certain number of gated transients are stacked and averaged over a given distance which is usually 10 m (although in practice the distance will vary as a function of the survey parameters, e. g. ATV's speed).

When performing the spatial averaging of the transient data, a filter called a trapezoid filter is used (for details see Auken et al. 2009). The trapezoid filter is narrower at early times to avoid over-smoothing of near-surface geology and is wider at late times to increase the S/N ratio needed to obtain a greater depth penetration. The averaged data are further processed manually to remove noisy or coupled data (Fig. 9B and D) which is a time-consuming process.

Inversion of the processed data is usually conducted in two steps. First using lateral constrained 1D inversion (LCI) along each profile (Auken et al. 2005). Data with higher misfit can then be removed to prepare for the more robust quasi 3D inversion, the so-called spatially constrained inversion (SCI) developed by Viezzoli et al. (2009). Figure 10 shows the resistivities from the LCI inversion along a profile in the Bäckegruvan area. The light-coloured parts of the model at depth mark the parts of the model which lie below the depth of investigation (DOI) of the tTEM signal. Below the DOI the estimated resistivities have larger uncertainty. The data misfit, superimposed on the section as a brown line with dots in Figure 10, is the root mean square misfit (RMS) at each measurement point given by

$$RMS = \sqrt{\frac{\sum_1^N \frac{\left(d_i^m - d_i^e\right)^2}{\sigma_i^2}}{N}} \qquad (19)$$

where d_i^m, d_i^e, σ_i^d, and N, are the measured data, estimated data, data error for the ith gate and the total number of data points (or gates), respectively. During the processing of the tTEM data the GPS position information was also processed and smoothed in order to assign a location for the spatially averaged data and subsequent resistivity model.

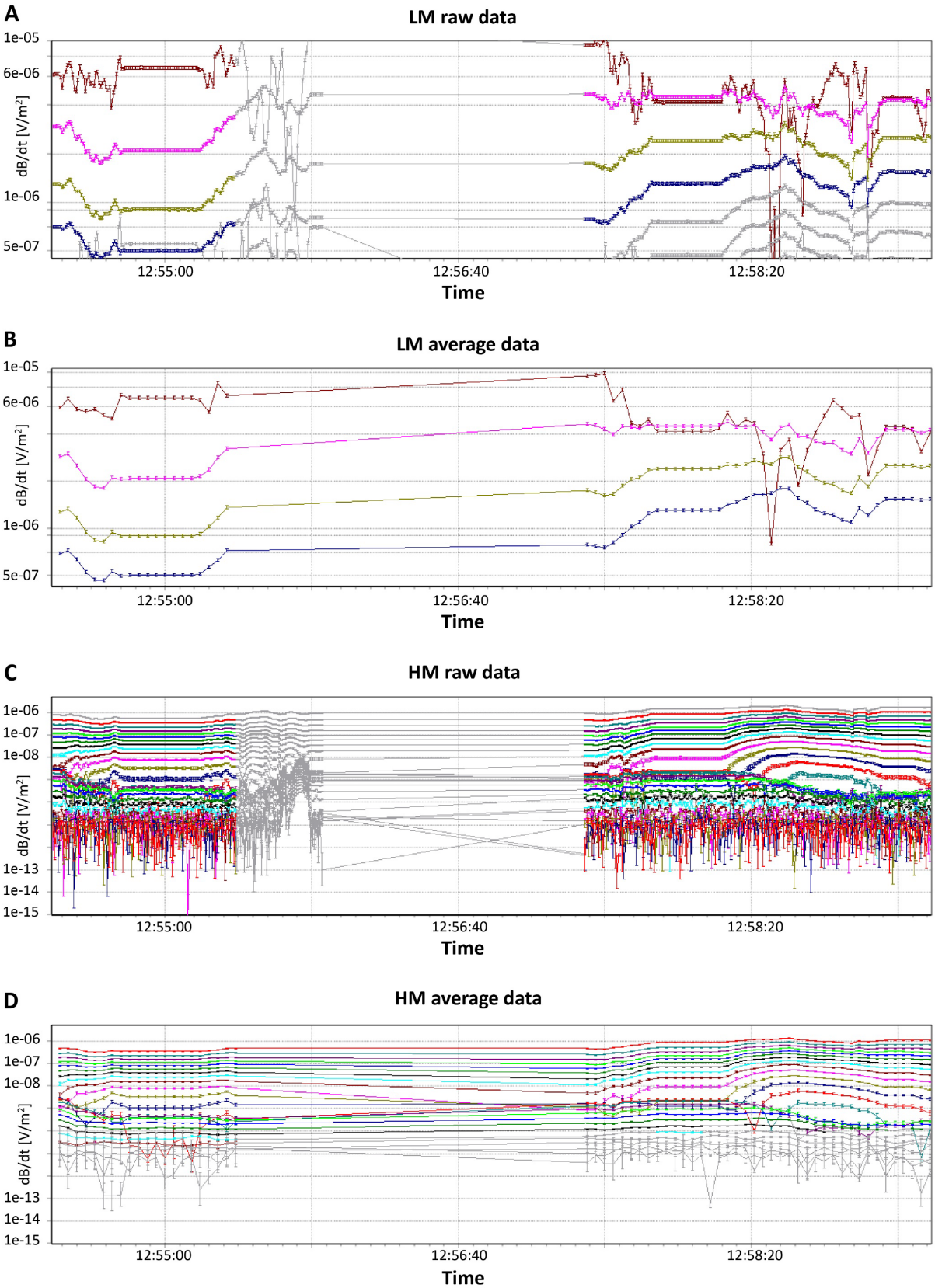

Figure 9. An example of tTEM data collected in the field at Bäckegruvan site. **A.** Gated raw LM data. **B.** Averaged and manually processed LM data. **C.** Gated raw HM data. **D.** Averaged and manually processed HM data.

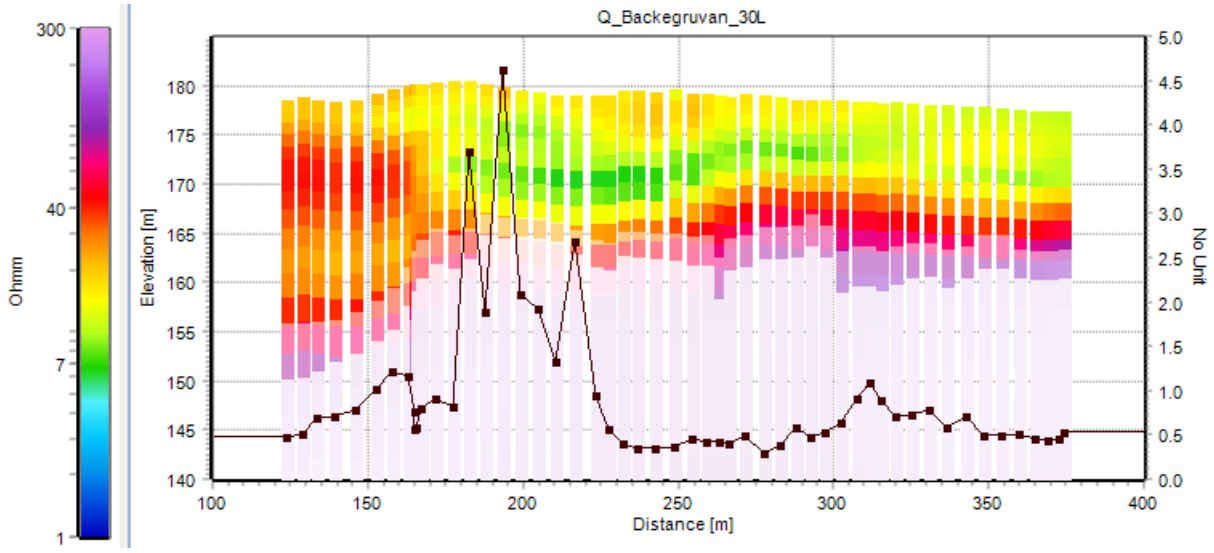

Figure 10. An example resistivity-depth section from the inversion of tTEM data collected at Bäckegruvan site. The results are from the LCI inversion made by HGG at Aarhus University. The light shaded area shows the parts of the resistivity models below the DOI. The brown line and dots, superimposed on the resistivity models depict the data misfit as the RMS for each resistivity model, see the right-hand side of the figure for the RMS scale.

IP effects in TEM data

In areas with high concentrations of disseminated conductive minerals and/or metals, strong IP effects with negative decay are often observed in TEM data (Kratzer and Macnae 2012; Macnae 2016; Viezzoli et al. 2013 & 2016). In such areas the inversion of TEM data is strongly affected by the IP phenomena and the data cannot be fitted properly or in some cases the inversion may not converge at all.

Almost all tTEM data collected in this study were found to be influenced by IP effects (Fig. 11). Hence, the data could not be fitted with the standard smooth model setup (routinely applied to tTEM data elsewhere). Hence, we utilised an inversion scheme referred to as the Maximum Phase Angel (MPA) where the IP effects are considered. This scheme, where both positive and negative data are considered, resulted in an improved data fit.

MPA inversions add two major difficulties to the process. Firstly, the inversion contains four times the model parameters and is thus more ill-posed than the resistivity-only inversion. Secondly, the inversion result is strongly dependent on the choice of starting model, requiring significant manual user-input to recover appropriate models of the resistivity and IP parameters (Madsen et al. 2023). The MPA model setup are shown in Table 3. All processing and inversion of the tTEM data was done by Aarhus Hydrogeophysics Groups (HGG).

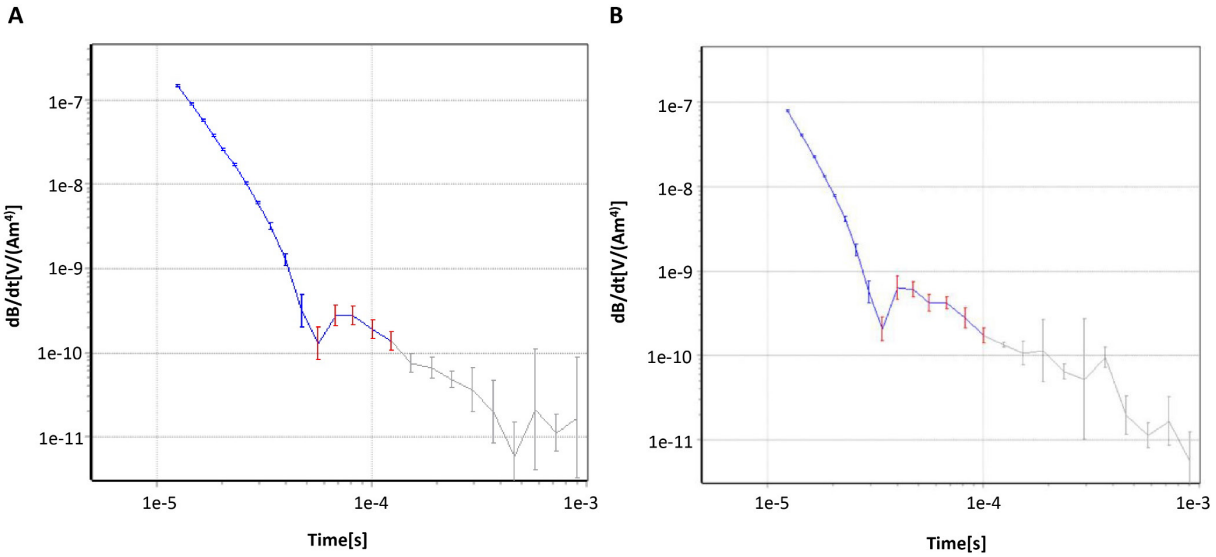

Figure 11. Example of varying IP effects in data. Blue gates indicate positive data, and red gates indicate negative data. **A.** IP decay from Bäckgruvan. The sign change is seen at 57 microseconds in this sounding. **B.** IP decay from Bäckgruvan. The sign change is seen at 33 microseconds in this sounding.

Table 3. MPA model setup. From the report by HydroGeophysics Group (2022).

Parameter	Value
Number of layers	30
Starting resistivities (ohmm)	100
Starting phi (mrad)	30
Starting t (s)	10–4
Starting C (no unit)	0.8
Thickness of first layer (m)	1.0
Depth to last layer (m)	120
Thickness distribution of layers	Logarithmically increasing with depth

RMT

The radio magnetotelluric (RMT) method is an electromagnetic method which covers a broader frequency range than the widely used very low frequency (VLF) method. The EM signal sources for the RMT are the distant VLF and radio transmitters (Tezkan et al. 2000; Bastani et al. 2015) typically operating in the frequency ranges 10–300 kHz, but can in some cases reach frequencies as high as 1 MHz. Müller and his group in Centre d'Hydrogéologie, Université de Neuchâtel first introduced the RMT method. They carried out scalar RMT using the RMT-R instrument in the frequency range 12–240 kHz to study a porous aquifer in the Cornol area, Switzerland (Turberg et al. 1994). Tezkan el al. (1996 and 2000) and Persson (2001) have utilised the same instrument for various applications to conduct near-surface geophysical investigations. Pedersen et al. (2006) used the RMT data collected at different locations in Europe (Sweden, Spain, the Netherlands, Hungary) to study the distribution of radio transmitters. Their analysis revealed that a reasonable number of radio transmitters with an acceptable S/N ratio in the RMT band existed at all sites. Like the tTEM method the primary EM signals from the radio transmitters induces secondary EM fields in the ground. These can be measured and used to model near-surface structures down to a maximum depth of about 300 meters. The depth penetration of the RMT signal increases

with increasing electrical resistivity of the ground and decreasing transmitter frequency. The data acquisition system used for the measurements in this project is the EnviroMT system developed at Uppsala University (Bastani 2001). The measurement setup is shown in Figure 12. The three components of the magnetic field (in three perpendicular directions) and two horizontal components of the electric field are registered simultaneously. The measured components are then processed using the techniques detailed in Bastani and Pedersen (2001) to estimate the frequency dependent EM transfer functions of the earth, namely the impedance tensor (**Z**) and the tipper vector (**T**). In the frequency domain **Z** (in Ohm) and **T** (dimensionless) are defined as:

$$\begin{bmatrix} E_x(f) \\ E_y(f) \end{bmatrix} = \mathbf{Z}(f) \begin{bmatrix} H_x(f) \\ H_y(f) \end{bmatrix}, \mathbf{Z}(f) = \begin{bmatrix} Z_{xx}(f) & Z_{xy}(f) \\ Z_{yx}(f) & Z_{yy}(f) \end{bmatrix} \quad (20)$$

$$[H_z(f)] = \mathbf{T}(f) \begin{bmatrix} H_x(f) \\ H_y(f) \end{bmatrix}, \mathbf{T}(f) = [A(f)B(f)] \quad (21)$$

where E (in V/m) and H (in A/m) are the electric and magnetic fields, respectively and the subscripts x, y and z represent the directions in which they are measured. Traditionally x, y, and z refer to geomagnetic reference coordinate system with positive directions towards north, east, and downwards, respectively. f (in Hz) is the frequency of the band where the transfer functions are estimated. The impedance tensor is frequency dependent and can be used to analyse the dimensionality. For a 1D earth model the diagonal elements (Z_{xx},& Z_{yy}) are zero and $Z_{xy} = -Z_{yx}$. The apparent electrical resistivity and phase of the impedance are then given by:

$$\rho_a(f) = \frac{|Z(f)|^2}{2\pi f \mu_0} \quad \& \quad \phi(f) = arg[Z(f)] \quad (22)$$

μ_0 (in H/m) is the magnetic permeability of a vacuum. In a 2D case, with data collected along a profile perpendicular to the geological strike, the diagonal elements are zero and the apparent resistivity is directionally dependent. The determinant of the impedance tensor is given by:

$$Z_{\text{det}}(f) = [Z_{xx}(f)Z_{yy}(f) - Z_{xy}(f)Z_{yx}(f)]^{1/2} \quad (23)$$

The determinant of the impedance tensor is rotationally invariant. Pedersen and Engels (2005) show that the determinant data can be used in 2D modelling in the case that 3D effects are not significant. Later Bastani et al. (2011) showed an application of the 2D inversion of determinant RMT and controlled source RMT data in Greece to model possible faults within the bedrock.

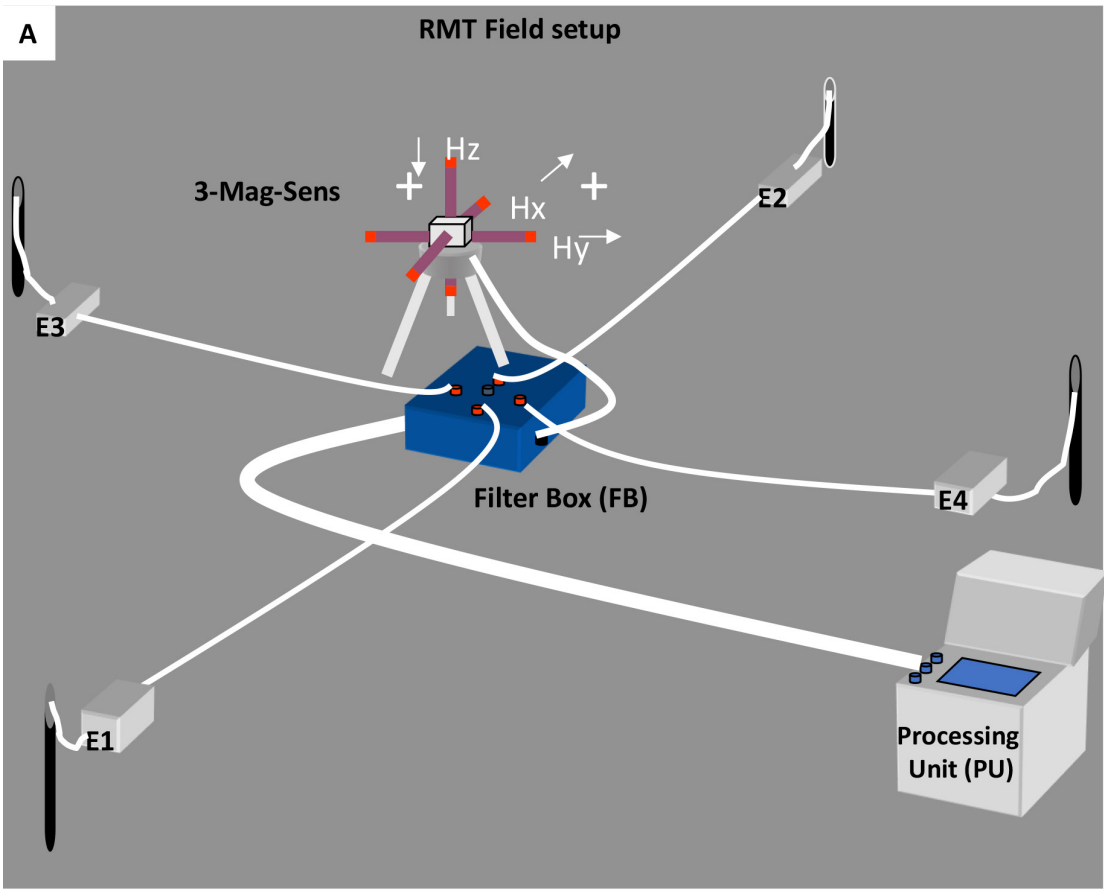

Figure 12. A. RMT setup in the field with two pairs of electrodes (E1-E2 & E3-E4) measuring the electric field and three induction coils measuring the magnetic field in three directions. The data are then filtered in the filter box (FB) and transferred to the processing unit (PU). **B.** The EnviroMT system in the field at Bäckegruvan site. Photo: Mehrdad Bastani.

RMT data processing and inversion

The RMT data are processed with different techniques to estimate the EM transfer functions (Z and T). A detailed account of the processing techniques used in the EnviroMT system (used in this study) can be found in Bastani (2001). An example of the processed RMT data at station 5 along profile 1 in Bäckegruvan is shown in Figure 13. The resistivity and phase are calculated in bands which are one-octave wide, within the frequency range of 10–250 kHz.

A few publications have demonstrated the application of tensor RMT measurements to investigate the resistivity structure of the subsurface at different near surface applications (e.g., Pedersen et el. 2006; Persson et al. 2011; Bastani et al. 2013; Shan et al. 2014). The system has also been used for 3D modelling of resistivity. For example, Bastani et al. (2012) carried out 3D RMT data acquisition at a site contaminated with hydrocarbons in Italy. They compared the resistivity models from 2D joint inversions of ERT and RMT data with the models from 3D inversion of RMT data and concluded that the 3D resistivity model better resolved the geometry of aquifer than the 2D results. Figure 14 shows the resistivity model from 2D inversion of determinant RMT data along profile L1 in Bäckegruvan. The inversion program used is the REBOCC program, developed by Siripunvaraporn and Egbert (2002). The white line in the model shows the DOI estimated using the method proposed by Spies (1989). However, in this case we specify the DOI as one skin depth which is a conservative estimate of the DOI rather than 1.5 times the skin depth, as suggested by Spies (1989). The model shows a more conductive layer at the top and a more resistive interval at depth which may represent the crystalline bedrock. The data fit is a good measure of inversion accuracy and provides a good tool to reject noise-affected parts of the data. An example of data fit along the line 1 is shown in Figure 15 where the estimated (model response) and measured resistivities (top frames) and phases (middle frame) are compared, and the differences normalised to the error values are presented in the bottom frame.

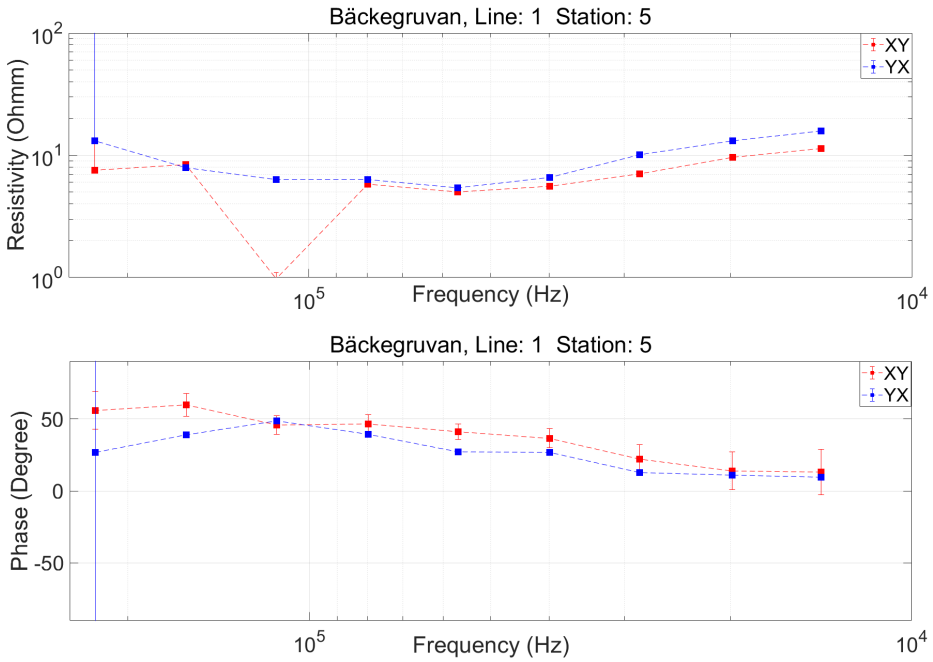

Figure 13. An example of RMT data collected by the EnviroMT system at station 5 along line 1 in Bäckegruvan. The top frame contains the apparent resistivities at 9 sub-bands taken within a frequency range of one-octave. The data are processed using the technique explained in Bastani (2001). The phase of impedance are shown in bottom frame. The red represents the calculated values where current flow (electric field) is in the X direction (or perpendicular to the profile) and the blue represents the calculation where the current flow (electric field) is parallel to the profile direction.

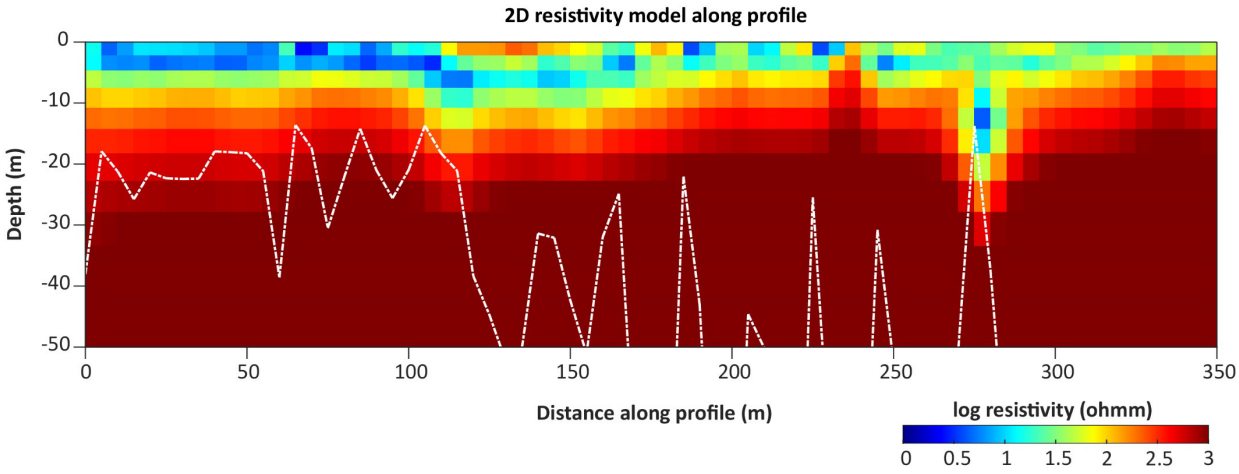

Figure 14. Resistivity model from 2D inversion of determinant RMT data along profile L1 in Bäckegruvan. The white dashed line shows DOI based on the method proposed by Spies (1989).

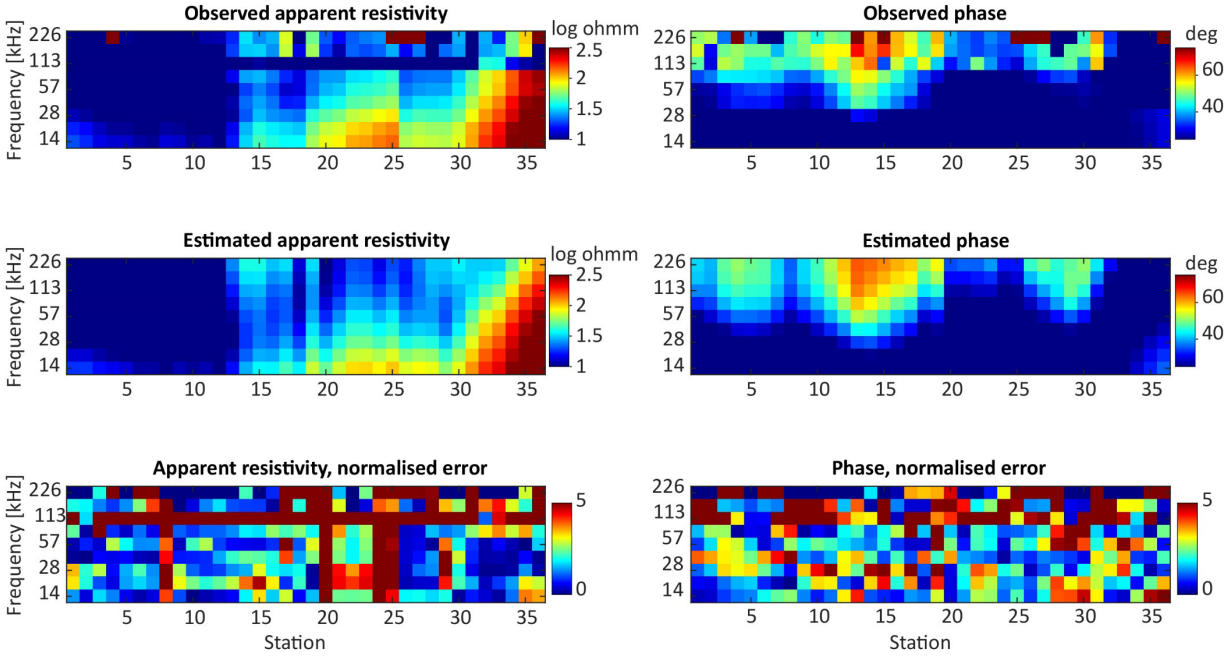

Figure 15. Comparison between the observed resistivity and phase (top panels) and estimated (modelled) determinant RMT data (middle panels) from 2D inversion (see Figure 14 for model). The normalised errors (data misfit) are shown in the bottom panels.

Ground penetrating radar (GPR)

GPR uses high frequency electromagnetic waves that may be reflected at boundaries where the electrical properties change. It is specifically sensitive to changes in the dielectric permittivity, largely dependent on the water content. The result is presented as a radargram where different layers can be identified.

We measured radar profiles with a constant offset using 70 and 300 MHz antennas of the Crossover series produced by ImpulseRadar that are usually pulled behind a car but can also be pulled by an operator (Fig. 16.) Positions were measured using a differential GPS for a number of reference points. These GPS positions were later used to interpolate the positions of all the GPS profiles. A digital elevation model with 2 m resolution was used for the topography.

Only simple processing was made using the ReflexW (Sandmeier 1998–2024) and Oasis montaj software. The processing applied consisted of background removal, time-zero correction and computation of approximate depth using an assumed constant velocity. The value of the velocity at Källfallet was chosen based on what is known of the near-surface material and adjusted using results from the other geophysical measurements.

GPR data was acquired only at the Bäckegruvan and Källfallet sites (Fig. 16). We also had access to data measured at Stollberg in 2019, which had been processed in a similar way (see Table 1).

Figure 16. The SGU's GPR system used at the Källfallet site. An operator can pull the system and operate the data acquisition. Photo: Mehrdad Bastani.

SIP laboratory measurements on tailings samples

The SIP (spectral induced polarisation) response was measured in the lab at Lund University on 10 samples taken from five of the eight tailings deposits that were investigated. The results are documented in reports presented in Appendix A and B. At each tailings site two samples from two different depths were taken from the same borehole. Table 4 summarises the specifications of the samples.

The measurement technique used is the same as the one described in Hupfer et al. 2016. The complex resistivity was measured for 70 frequencies logarithmically distributed between 1 mHz and 10 kHz with an Ontash and Ermac Portable Spectral Induced Polarisation field and laboratory unit. A four-point sample holder with non-polarizable electrodes was used to hold the samples (Hupfer et al. 2016).

After measurement, the curves were fitted to a Cole-Cole (Pelton) model and to a Debye decomposition, using the program SIPSpectrum class in pyGIMLi (pyGIMLi Development Team 2024).

The grain size distribution was investigated by sieving the material into five granulometric classes. A comparison between the laboratory measurements and grain size distribution is made at the end of the result section.

Table 4. Samples collected for SIP measurements.

Sample name	Sample ID	Geochemical sample ID	Locality	Bore-hole	Depth (m)	Year	Water content
Bb1	PCY220017A	PCY220017A	Blötberget	BH2	6–7	2022	Saturated
Bb2	PCY220021A	PCY220021A	Blötberget	BH2	10–11	2022	Saturated
Y1	PCY220125A	PCY220125A	Yxsjöberg	BH1	2–3	2022	Saturated
Y2	PCY220131A	PCY220131A	Yxsjöberg	BH1	8–9	2022	Saturated
S1	PCY220184A	PCY220184A	Stollberg	BH2	4–5	2022	Unsaturated
S2	PCY220195A	PCY220195A	Stollberg	BH2	15–16	2022	Saturated
G1	PCY210293GF	PCY210278A, PCY210278B	Jan-Matsdammen	BH1	1–2	2021	Unsaturated
G2	PCY210294GF	PCY210282	Jan-Matsdammen	BH1	5–6	2021	Unsaturated
B1	PCY210252GF	PCY210252GA	Bäckegruvan	BH2	4–5	2021	Saturated
B2	PCY210256GF	PCY210256GA, PCY210256GB	Bäckegruvan	BH2	8–9	2021	Saturated

Results

This section details results from investigations at eight tailing repositories using the different methods described in the previous section. The geophysical methods utilised are mainly sensitive to electrical resistivity. These include ERT, TDIP, tTEM, and RMT. In addition to this GPR measurement have been conducted at two sites. Laboratory based SIP measurements were also conducted on material from five of the sites and provided reference data of the electrical resistivity and IP parameters. Because all the induced polarisation measurements conducted in the field within this project were in the time domain the term TDIP (Time domain Induced Polarisation) is subsequently shortened to IP (Induced Polarisation) for the remainder of the report. The following five sections present examples of the resistivity models from the different geophysical methods. The data from different methods are compared and discussed with respect to each other as well as other data which is available from each site. Each section focuses on a survey area which may include one or more tailings repositories.

Yxsjöberg

In this area Morkulltjärnen tailings repository was selected, for the geophysical investigations. The methods used were ERT, IP, RMT, tTEM and sampling for SIP measurements in the lab (see Table 1).

Morkulltjärnen

Morkulltjärnen tailings dam is in the western part of the Bergslagen area (see Fig. 1). The tailings here are residual products from the Yxsjöberg tungsten mine and were deposited between 1969 and 1989. They were deposited over an area of approximately 250 000 m^2. The dam has a gentle northerly downslope and grows increasingly swampier in the lower areas (Fig. 17).

Two ERT-IP profiles were measured during 2021. One 500 m long profile in the east–west direction with a 5 meters-electrode spacing and another one 360 m long in the north–south with a 2 meters-electrode spacing (ERT1 and ERT2 in Fig. 17). Unfortunately, the data were very noisy due to a damaged cable connector but despite this a large part of the resistivity data could still be used to produce a reliable resistivity model. However, the IP data from this line were too distorted, and hence, no attempt was made to invert them. A large portion of the east–west profile (440 m) was remeasured in 2022 with a 2 meters-electrode spacing to obtain a better near surface resolution, with the aim of also acquiring IP data (ERT 3 in Fig. 17).

Figure 17 presents the location of the geophysical measurements acquired at Morkulltjärnen. The tTEM covered most of the tailings area except for the north-western part that was very wet and not accessible with the ATV. Five boreholes were drilled in the area (Fig. 17). At BH1, two samples, one at depth 2–3 m and the other at 8–9 m were collected for SIP measurements (see Table 4).

Figure 18 shows the apparent resistivity and apparent chargeability (IP gate 16 between 0.08 and 0.1 s) along profile ERT 3 after removal of noisy data. The apparent resistivity data are of very good quality and only a few data points were removed (Fig. 18A). Conversely, for the chargeability data, a larger part of the data points had to be removed due to high noise levels especially at larger electrode offsets (Fig. 18B).

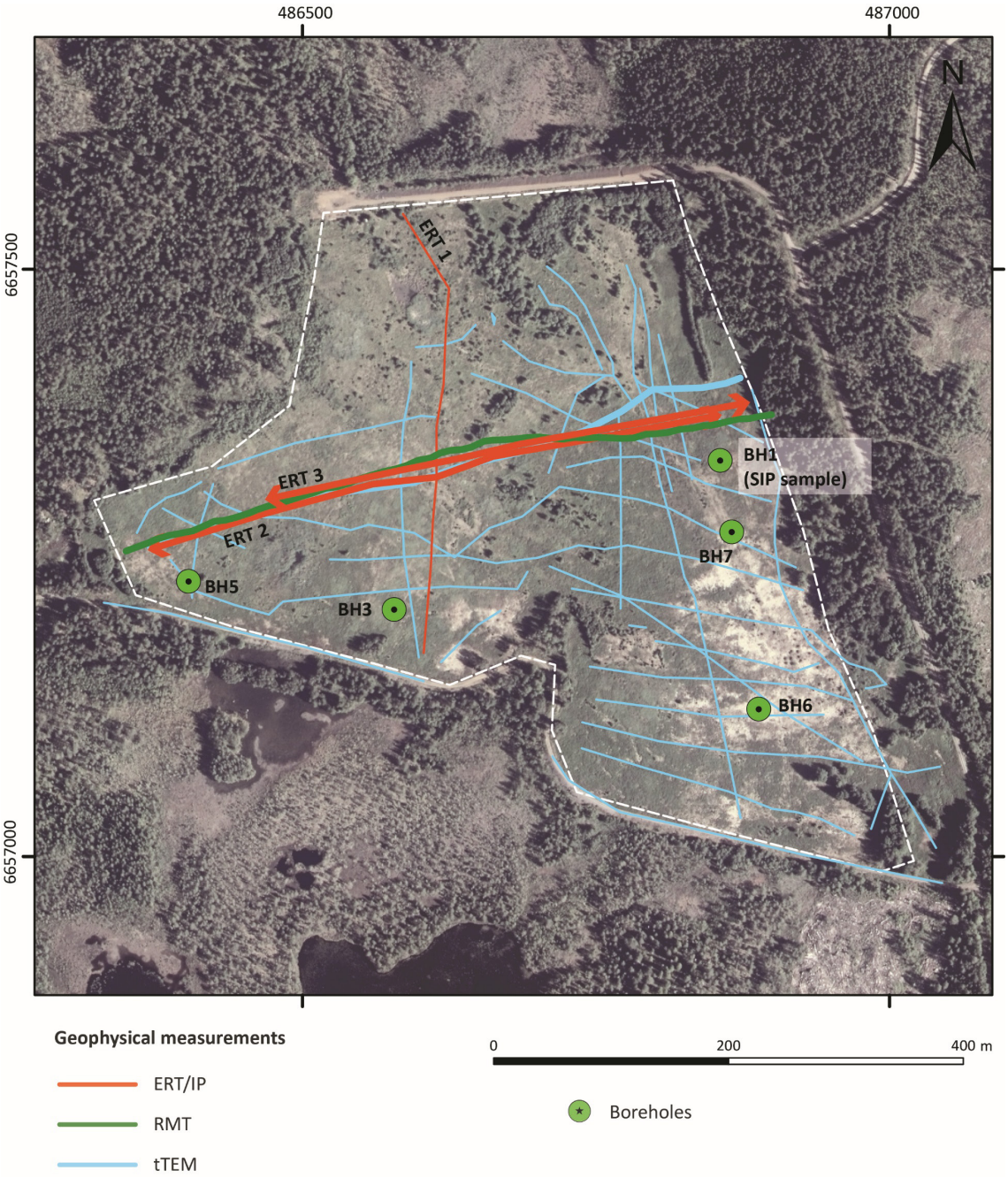

Figure 17. Orthophoto showing Morkulltjärnen tailings dam. The dashed white lines represent the boundary of the tailings. Ground geophysical measurements (lines in different colours) and boreholes (green symbols) are shown. The thicker lines show the location of the profiles shown in this report.

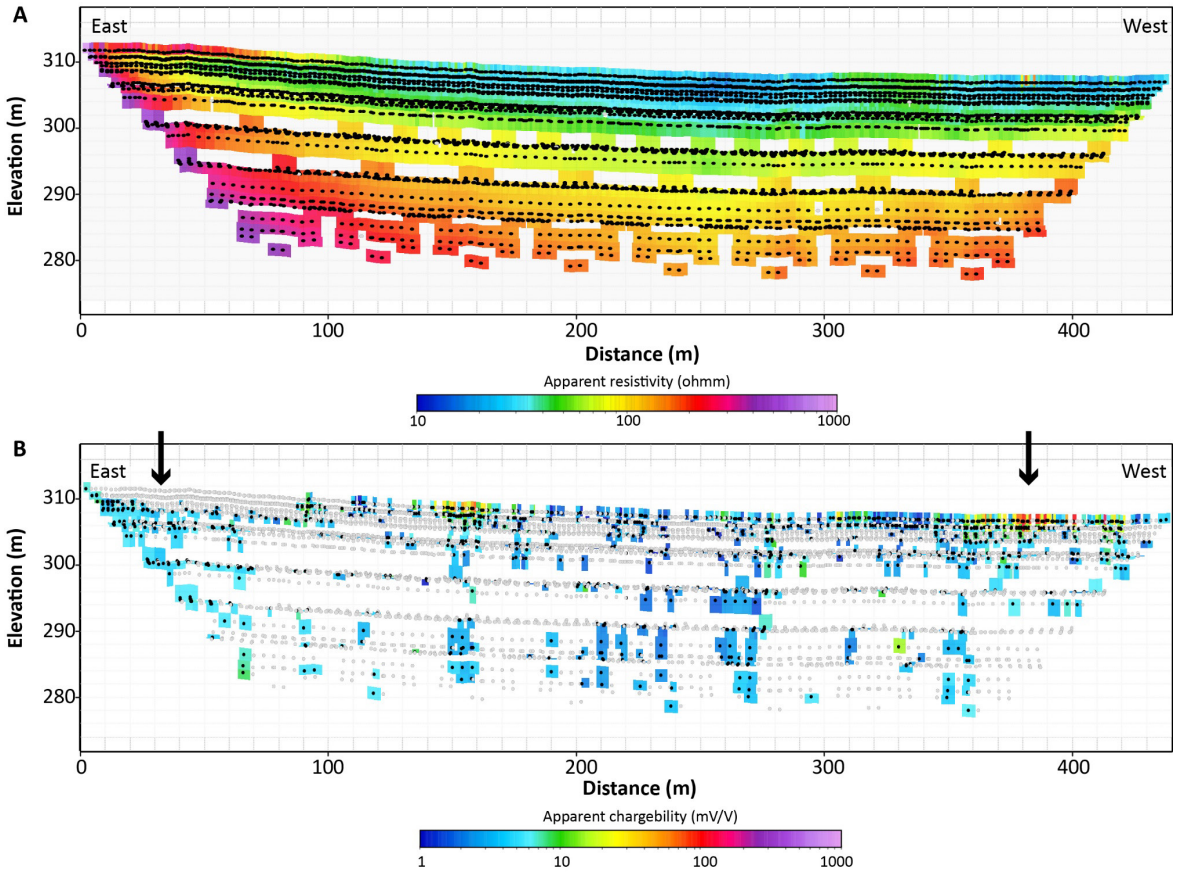

Figure 18. Profile ERT 3 after removal of noisy data. **A.** Apparent resistivity pseudosection, **B.** Apparent chargebility pseudosection in milliVolts/Volts (mV/V) for IP window 16 (0.08–0.1 s). The two arrows at 30 m and 380 m distance mark the location for the IP-curves shown in Figure 20.

The maximum phase angle (MPA) method was used in the 2D inversion of ERT and IP data (see Fiandaca et al. 2018). Figure 19 shows the resistivity models along profile ERT 3. The resistivity model (Fig. 19A) shows low resistivities at the top interpreted to correspond to wet sandy tailings and higher resistivities at the bottom that may correspond to lake sediment and bedrock. This interpretation agrees with the nearby boreholes (Fig. 17). The resistivity of the tailings materials varies between 10 and 30 ohmm and the thickness of the tailings is largest in the central part of the profile (c. 10 m). The thin (1–3 m) high resistive (> 500 ohmm) layer at the top surface, present in the eastern part of the profile, marks the dry sand. Other resistivity variations seen within the tailings may be caused by variation in water saturation, mineralogy and/or grain size.

The phase model (Fig. 19B) shows generally low values (< 5 mrad) except for near surface section where higher phase angles (approximately 30–70 mrad) are observed at some parts along the profile, coinciding with higher apparent chargeability in Figure 18B. Note that the depth of investigation (DOI) is very limited in the phase model due to the very limited number of input data at larger offsets (lower signal to noise ratios).

In Figure 20 two examples of the decay curves along profile ERT 3 (indicated with arrows in Fig. 18B and 19B) are shown. In the eastern part at a distance of 30 m some of the IP decay curves seem rather smooth but a large part of the data contains negative value (Fig. 20A). In figure 18B it shows that almost all IP data from the top surface were removed along the first 100 m of the profile. Figure 20B shows the few remaining data (dots) at a distance of approximately 30 m after removal of decay curves that are assumed not to correspond to IP, together with the modelled response (lines).

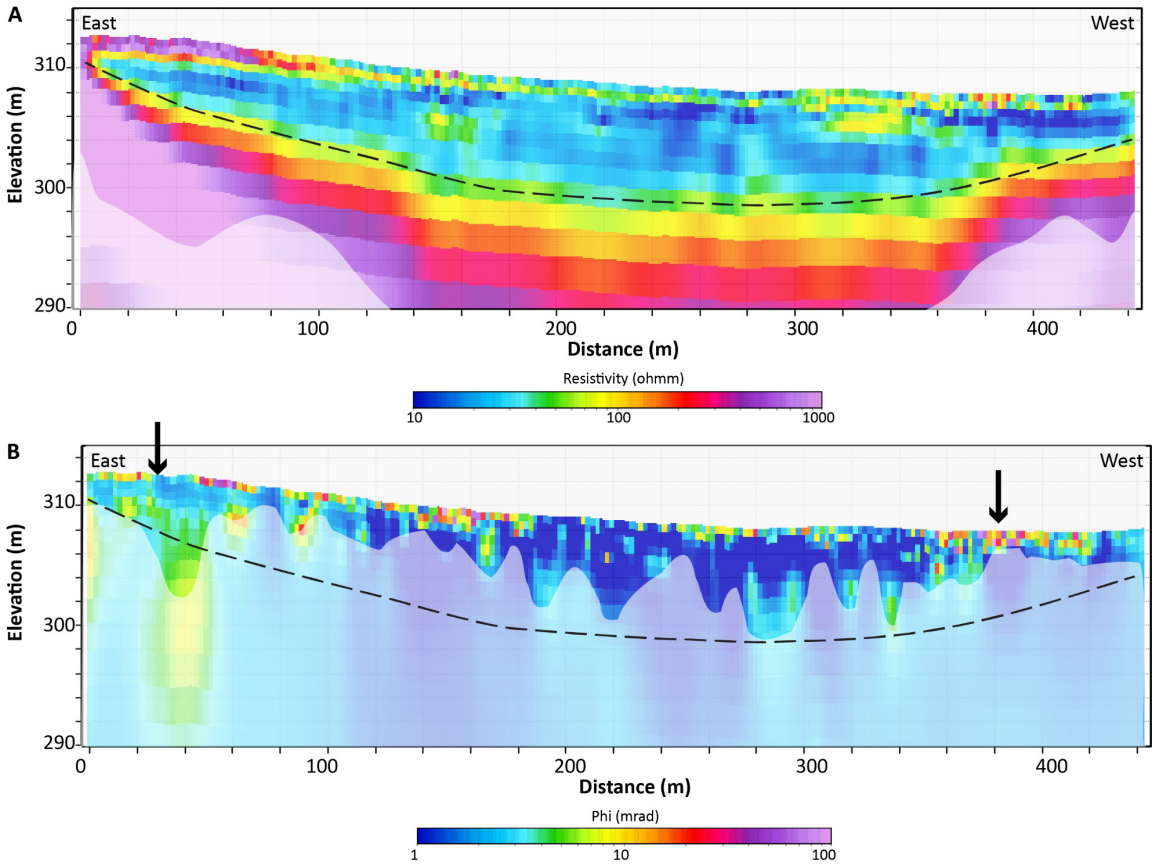

Figure 19. Resistivity and phase model from 2D inversion of ERT and IP data using the MPA method along profile ERT 3. **A.** Resistivity model. **B.** Phase model (maximum phase). The two arrows at 30 m and 380 m distance mark the location for the IP decay curves shown in Figure 20. The dashed line shows the interpreted bottom of the tailings. The white transparent area marks the depth of investigation (DOI).

At a distance of approximately 380 m the IP decay curves are mostly positive and show higher chargeability at the near surface (see Fig. 20C and 18B). Figure 20D shows the remaining data (dots) and the modelled response (lines) after 2D inversion. The data fit is poor here. Given the rather poor data fit and the fact that most part of the IP data have been removed along the profile it is difficult to draw any conclusions regarding the modelled IP parameters and characteristics of the tailings.

Figure 21 shows the resistivity models from the inversion of ERT, RMT and tTEM data along the east–west profile (ERT 3), (see Fig. 17 for locations), in Morkulltjärnen. Note that the line direction is from west to east in this figure and is opposite to that in Figures 18 and 19. The resistivity model from the ERT measurements is a composite of profile ERT 2 and ERT 3 (see locations in Fig. 17), where the first 120 m is from ERT 2 measured with a 5 m-electrode spacing and the remaining part is from ERT 3 with a 2 m-electrode spacing. For comparison the nearest boreholes to the profiles are also shown on each resistivity model (see Fig. 17 for locations).

All three models show the same resistivity pattern with an up to 10 m thick low resistivity top layer corresponding to the tailings followed by a higher resistivity layer at depth corresponding to the lake sediments and the bedrock. The ERT model has the best resolution in the uppermost 5 m of the profile, compared to the RMT and tTEM models (Figs. 21B and 21C). This can be explained by the dense electrode spacing (2 m). Both ERT and RMT can resolve the high resistivity (> 1000 ohmm) in the bedrock. The tTEM model shows the lowest resolution amongst the three methods both in the near surface and at greater depth. Despite that, it is still possible to delineate the bottom of the tailings from the tTEM model in Figure 21C.

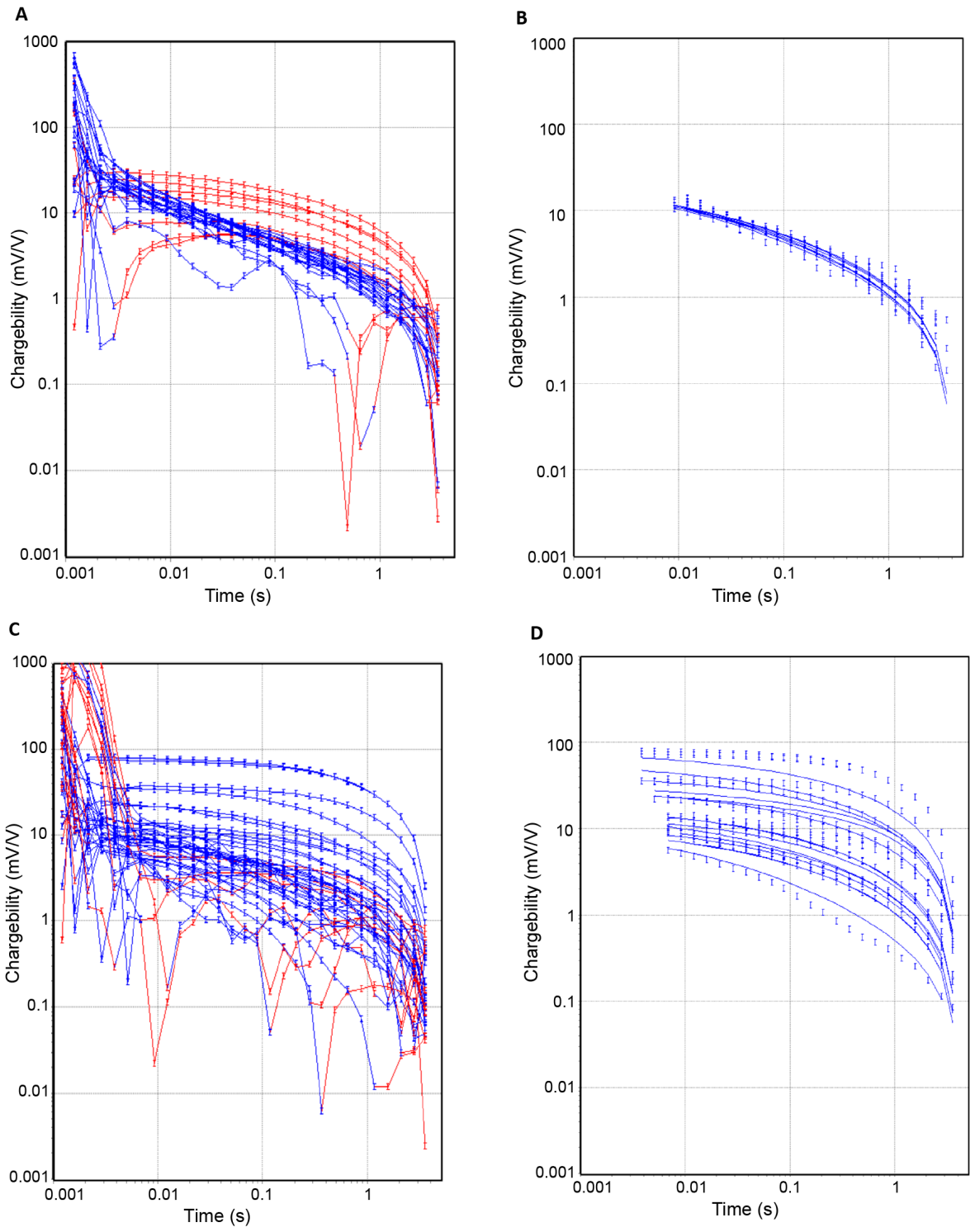

Figure 20. Example of IP decay curves at approximately 30 m and 380 m along Profile ERT 3. Blue curves correspond to a positive sign and red to a negative sign. **A**. Measured IP decays as a function of time at a distance of 30 m. **B**. Remaining IP data (dots) after removal of noisy data and the data response (lines) from the 2D inversion using the MPA method, at a distance of approximately 30 m. **C.** Measured IP decays at a distance of 380 m. **D.** Remaining IP data (dots) after removal of noisy data and data response (lines) from the 2D inversion using the MPA method at distance of approximately 380 m.

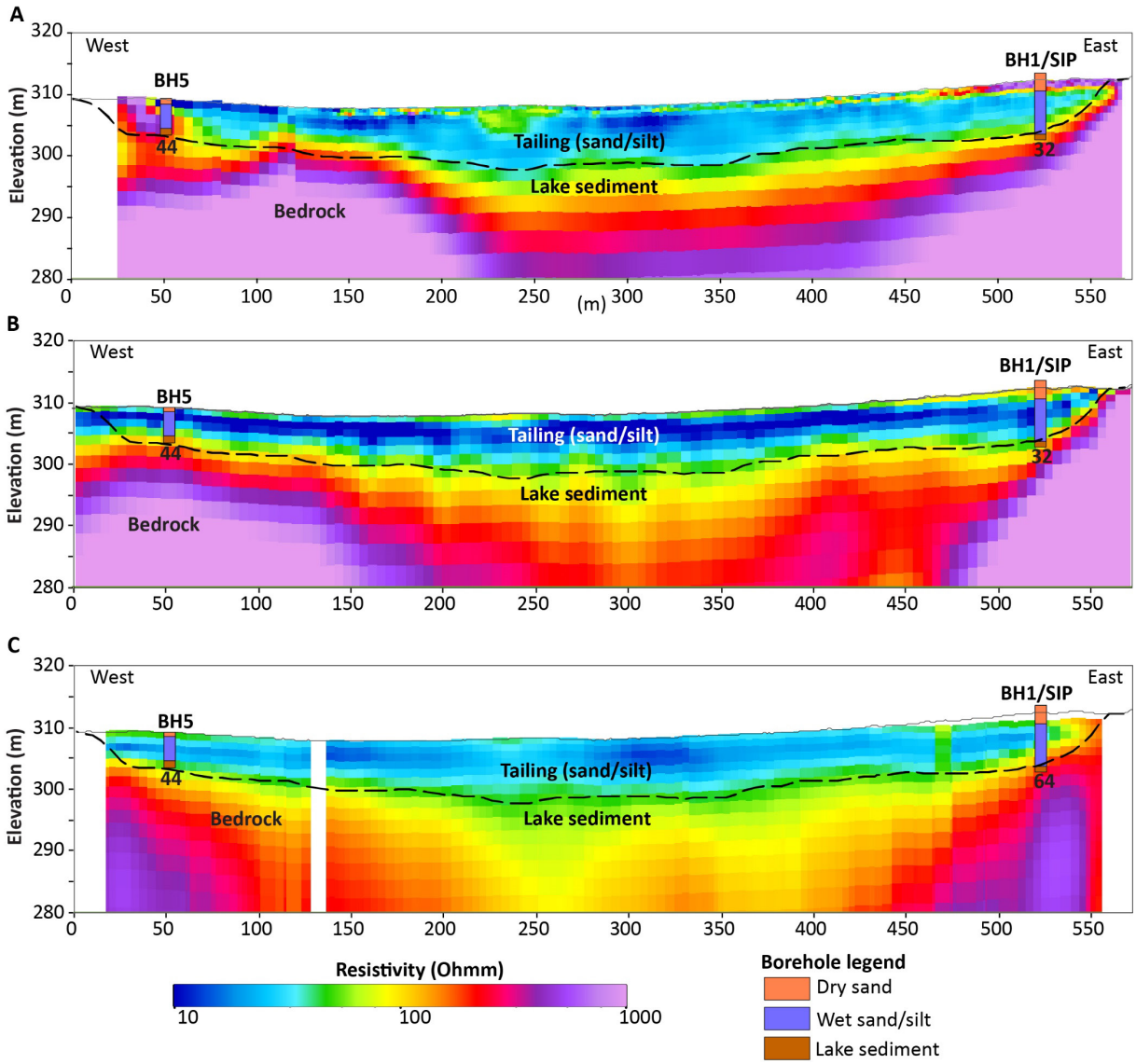

Figure 21. Resistivity models along an east–western profile obtained from three different geophysical methods **A**. ERT, **B**. RMT and **C**. tTEM. The two nearest boreholes are projected on the profiles and their offset in meters (perpendicular to the profile) is shown as a number below. The black dashed line represents the bottom of the tailings interpreted from geophysical models and drillings. See Figure 17 for the location of the profiles.

The nearest boreholes are at a distance of 30 to 60 m from the profiles, and they show good correlation with the resistivity models (Fig. 21). BH5 shows 5 m-thick tailings (1 m dry sand followed by 4 m wet sand and silt) and BH1 shows 10 m tailings (3 m dry sand followed by 7 m wet sand and silt). During drilling it was observed that the tailings were coarse and weathered above the groundwater, showing a strong rusty brown colour and below the groundwater level the material was typically silty sand and light grey in colour (Casey et al. 2024). The change in the grain size is also evident from the sieving results at BH1 (which is discussed later in detail) where the sample from 2–3 m depth seemed coarser compared to the sample at 8–9 m depth.

Figure 22 illustrates a more detailed comparison between the resistivity models at a location close to BH1. All three methods resolve the high resistive dry sand above the groundwater level observed in the borehole. The transition from dry sandy tailings to the low resistive wet tailings is more clearly seen in the ERT and RMT model compared to the tTEM. The transition from low resistive wet tailings to the lake sediments and bedrock with high resistivity is rather smooth for

all methods, as can be expected due to the poorer resolution with depth (and the smoothing regularisation used). Here, information from the borehole is crucial to make a more accurate interpretation of the bottom of the tailings.

The RMT model shows the lowest resistivity (15 to 20 ohmm) for the wet tailings (sand and silt) below groundwater level. This result is in close agreement with the SIP laboratory measurements (see Appendix B) done on the samples collected at 2–3 m (15 ohmm) and 8–9 m (22 ohmm) depth (Fig. 22). The lab measurements of the resistivity were also corrected for the temperature effects using equation (8) to simulate field conditions. The temperature was estimated to be 18°C for the laboratory measurements and between 3 to 5°C for the field measurements. This results in an approximate value of 24 ohmm for the 2–3 m sample and 33 ohmm for the 8–9 m sample.

Chemical analyses of the borehole samples showed high metal content in the tailings with 20% Fe-oxide, 900 ppm tungsten and 500 ppm copper as an average. The high metal contents may contribute to the low resistivity observed in the tailings, but it has not been possible to link any variations in the resistivity to the changes in metal content.

One could expect that the high metal content in the tailings would affect the IP measurements. For the deeper sample S2, the SIP laboratory measurements show a relatively high maximum phase of 90 mrad and chargeability of 260 mV/V (see Fig. 58, Table 5 and Appendix B). However, the maximum phase occurs at a high frequency range (6 kHz) not covered by the TDIP data. The low quality of the IP-data collected in the field at this site may be caused by inductive effects (EM-coupling). These effects are more significant on conductive ground, and for larger electrode distances.

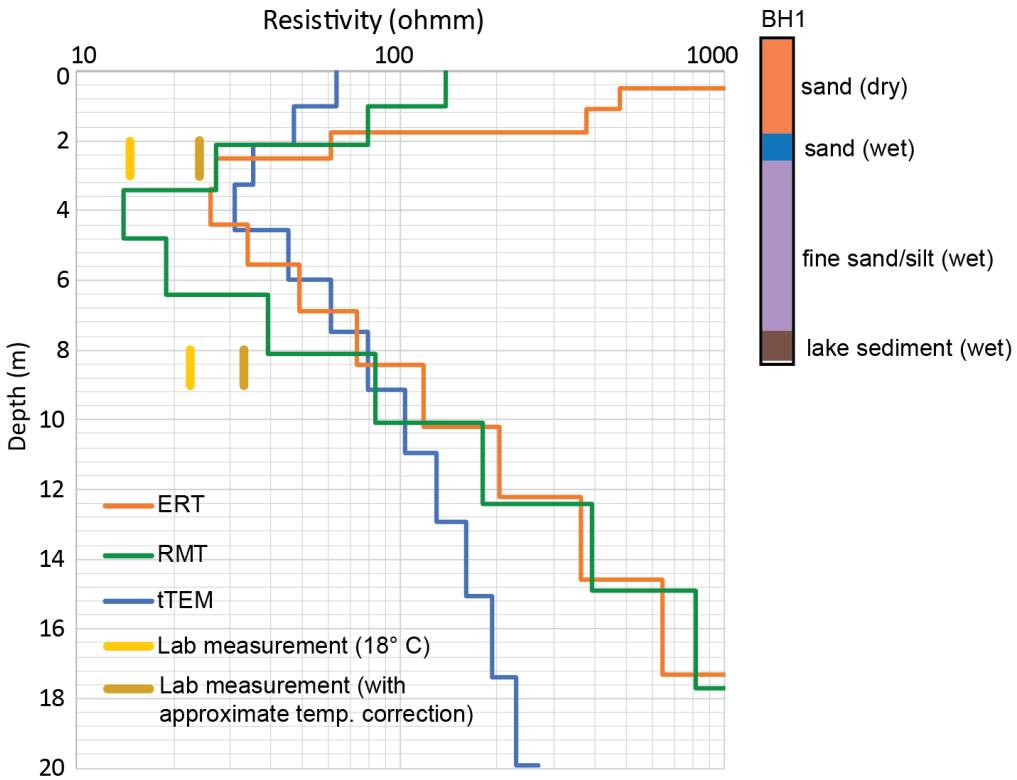

Figure 22. Comparison of ERT, RMT, tTEM inversion results close to borehole BH1 (approximately 30 m along the profile). The results from laboratory measurements on the samples are shown for both uncorrected as well as values which have been corrected for the temperature difference. The geological description of the borehole was observed during drilling. The level (height) of the borehole is adjusted for the difference in elevation (1 m) between the borehole and the geophysical profile.

Grängesberg

There are three tailings' repositories in Grängesberg; Svandammen, Jan-Matsdammen and Hötjärnen (Fig. 23) which all have been studied within this project. The tailings originate from the Kiruna type Fe-oxide-apatite (IOA) deposit in Grängesberg that represents the largest ore mineralisation in Bergslagen. Magnetite is the dominant Fe-oxide mineral, although minor amounts of hematite occur. Large scale mining started in the late 19th century at two fields in Grängesberg. Tailings were originally deposited in the Jan-Matsdammen but in the late 1960s deposition of tailings shifted to two new areas, namely Svandammen and Hötjärnen.

tTEM measurements were conducted in all three repositories in Grängesberg. Due to the significant IP-effect in the data that was collected the MPA inversion scheme was used to invert the data. The resistivity models obtained at all three sites showed unreliable results that were to some extent contradictory with those from the ERT measurements and as a consequence they were not used in the further interpretation of the three tailings. As mentioned earlier, the MPA inversion routine is strongly dependent on the starting model. There is currently ongoing research at the HGG at Aarhus university to develop better inversion routines to model this type of data in a more reliable way.

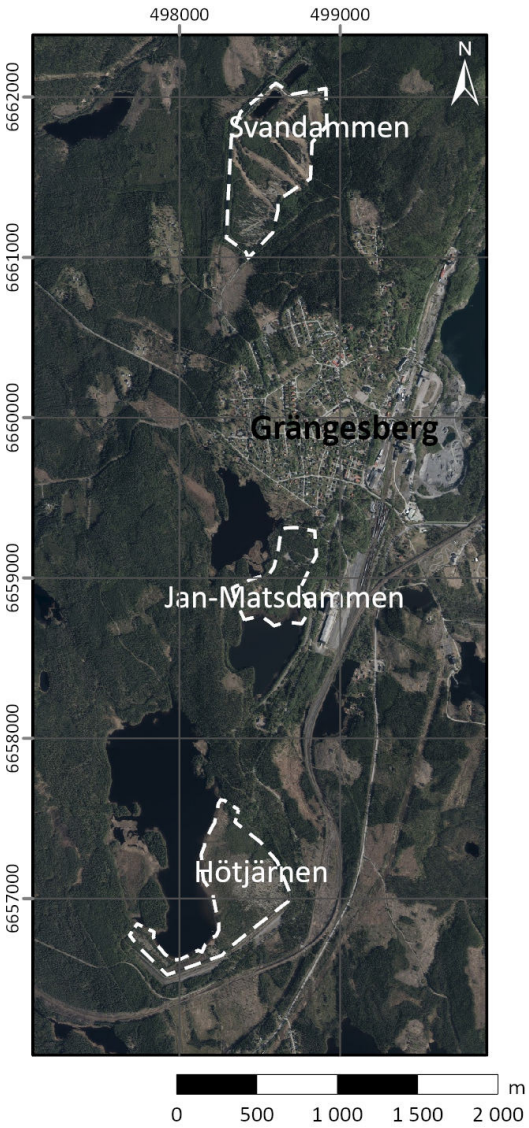

Figure 23. Location of the three tailings repositories in Grängesberg.

Svandammen

Svandammen is the northernmost of the three tailings repositories in Grängesberg (Fig. 1) and a large part of the area is, at present (2022), used as a golf course. The selected area for the geophysical measurements and drilling was located outside of the golf course. This included two ERT-IP profiles (each approximately 290 m long) and a total of 2.5 km of tTEM measurements conducted in 2021 that covered a considerable part of the area. Figure 24 shows the location of the measurements and the boreholes in the area, as well as the location of a buried high voltage electrical cable. The cable is a potential source of the noise in the area.

Both ERT-IP profiles were measured in 2021 with a 2 m electrode spacing. Profile GB_8 shows high quality data for both ERT and IP whereas profile GB_9 has much poorer data quality. This is likely due to a problem in the field with one of the cable contacts (a similar problem occurred at Morkulltjärnen). Another issue for this profile was the vicinity to the buried high voltage cable to the east. Despite the difference in the data quality, the resistivity models along both profiles show a similar and consistent pattern (Fig. 25). In general, they show a high resistive layer at the top (3–4 m thick) underlain by a low resistive layer. Four boreholes were drilled in 2022. Two of them were sampled every meter, and the other two were only drilled to reach the bottom of the sand. The boreholes reveal that the top high resistivity layer coincides with dry silty-sand and the low resistive layer with the wet sand, silt and clay.

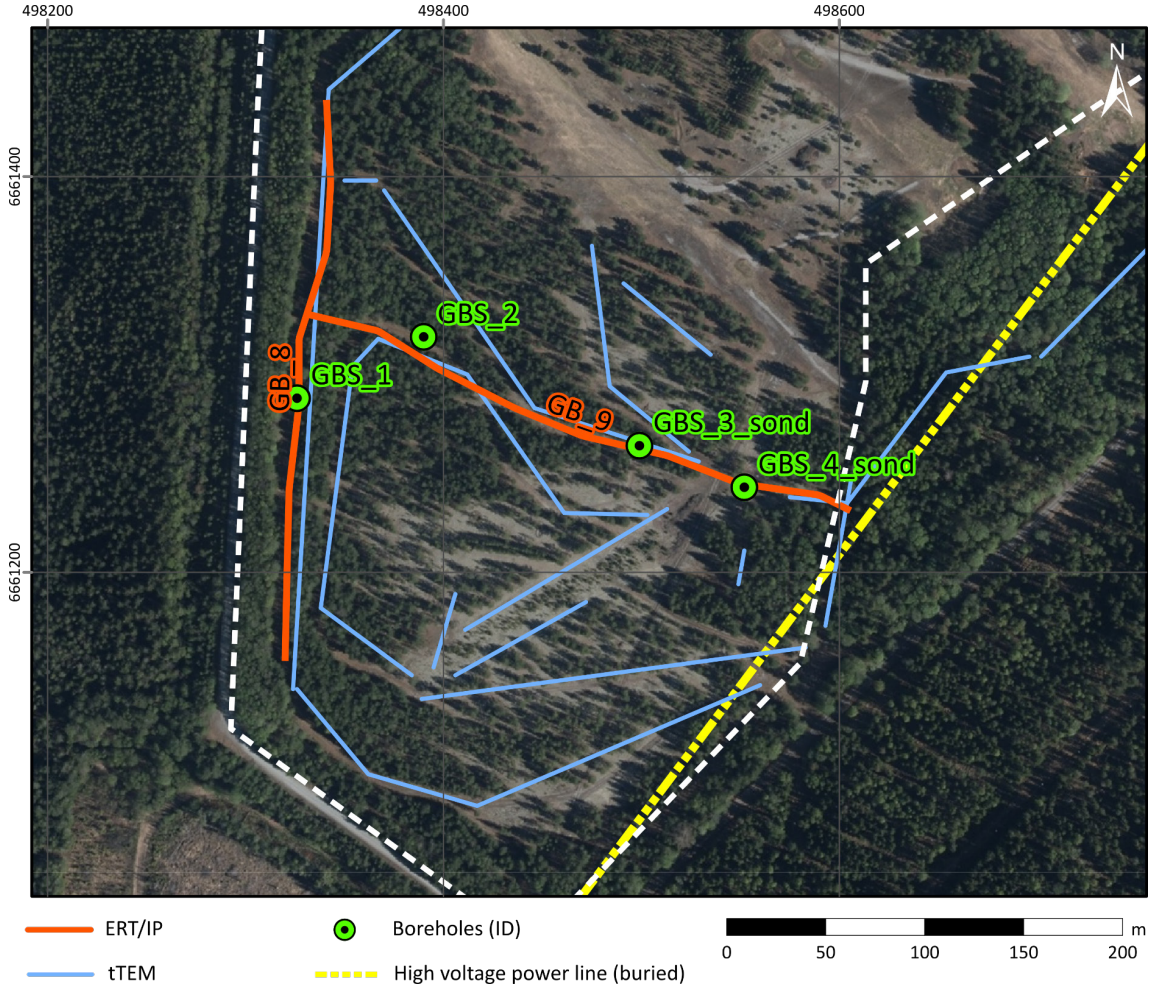

Figure 24. Southern part of the Svandammen tailings repository with location of the geophysical measurements and boreholes.

The IP inversion for profile GB_8 using the MPA method shows low residuals and consistent results (Fig. 26). Here the model shows a relatively high phase (10–20 mrad) within approximately the uppermost three to four meters (Fig. 26). This layer coincides with the high resistive layer seen in the resistivity models (see Fig. 25A) and is dominated by dry silty sand. There is no SIP measurement from the borehole samples and no laboratory reference resistivity or IP data exist. One should note that the measurements covered a small part of the tailing and may not represent the electrical resistivity of the entire material in the tailings.

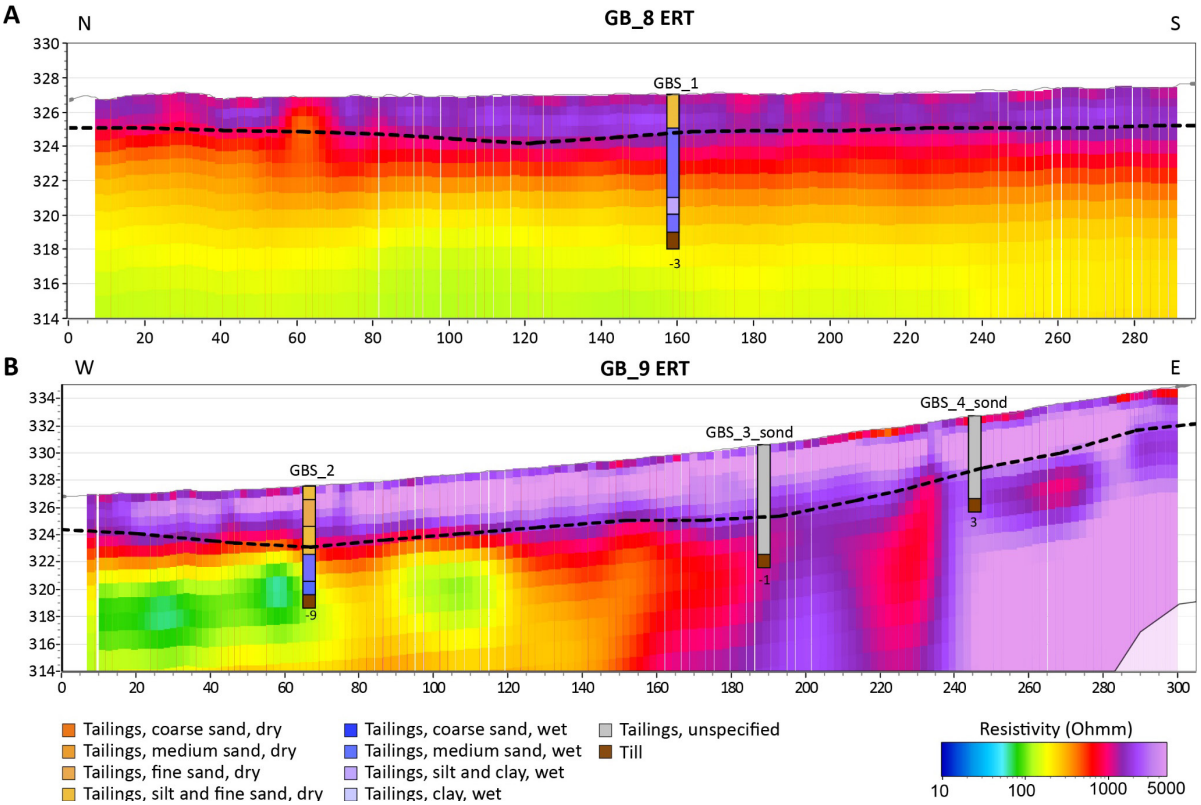

Figure 25. Resistivity model sections for profiles GB_8 and GB_9. The dashed black line shows the interpreted limit between dry and wet sediments.

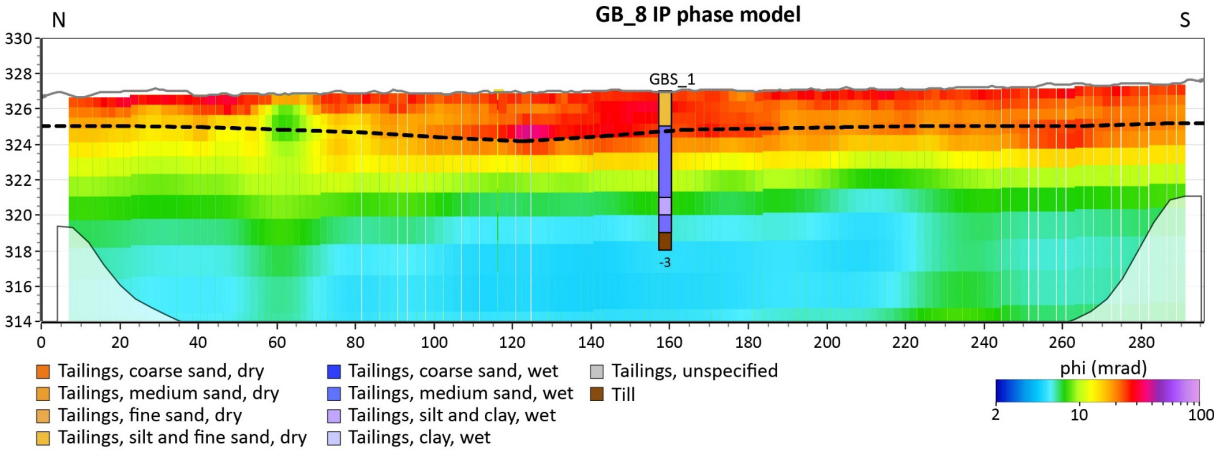

Figure 26. Phase model section from IP measurements. The dashed black line shows the interpreted limit between dry and wet sediments, interpreted from the ERT measurements.

Jan-Matsdammen

Figure 27 shows the location of the different geophysical measurements and the boreholes at Jan-Matsdammen. In total six ERT-IP profiles were measured in 2021. Electrode spacing along two profiles (JMD2 and JMD5) was 5 m whereas 2 m spacing was used for the remaining profiles. tTEM measurements could only be done along gravel paths due to the dense vegetation. The total length for these measurements was 1.5 km. There were also two RMT profiles, collected along two previously measured ERT-IP profiles. Moreover, two boreholes with sediment sampling at every meter were made for geochemical analysis. Additionally, samples were taken for SIP laboratory measurements at two different depth intervals (1–2 m and 5–6 m) from one borehole, which was adjacent to another borehole where sampling was performed. During 2022, Grängesberg Exploration Holding AB, extracted some tailings materials to run some studies and tests (GRANGEX 2023). Additional borehole information could be obtained from this report to complement the new data collected in this study. Note that the boreholes from Grängesberg Exploration Holding AB's investigation will be referred to subsequently in this report as GRANGEX-boreholes and they are shown as blue symbols in Figure 27. There's also geochemical analysis, sieving information and density measurements of samples from these boreholes. This information has been of great value in the interpretation of the geophysical measurements within this project. Note that there are more boreholes drilled by the Grängesberg Exploration Holding AB than are shown in this report, here we only show and discuss boreholes which have geochemical analysis results and are publicly available.

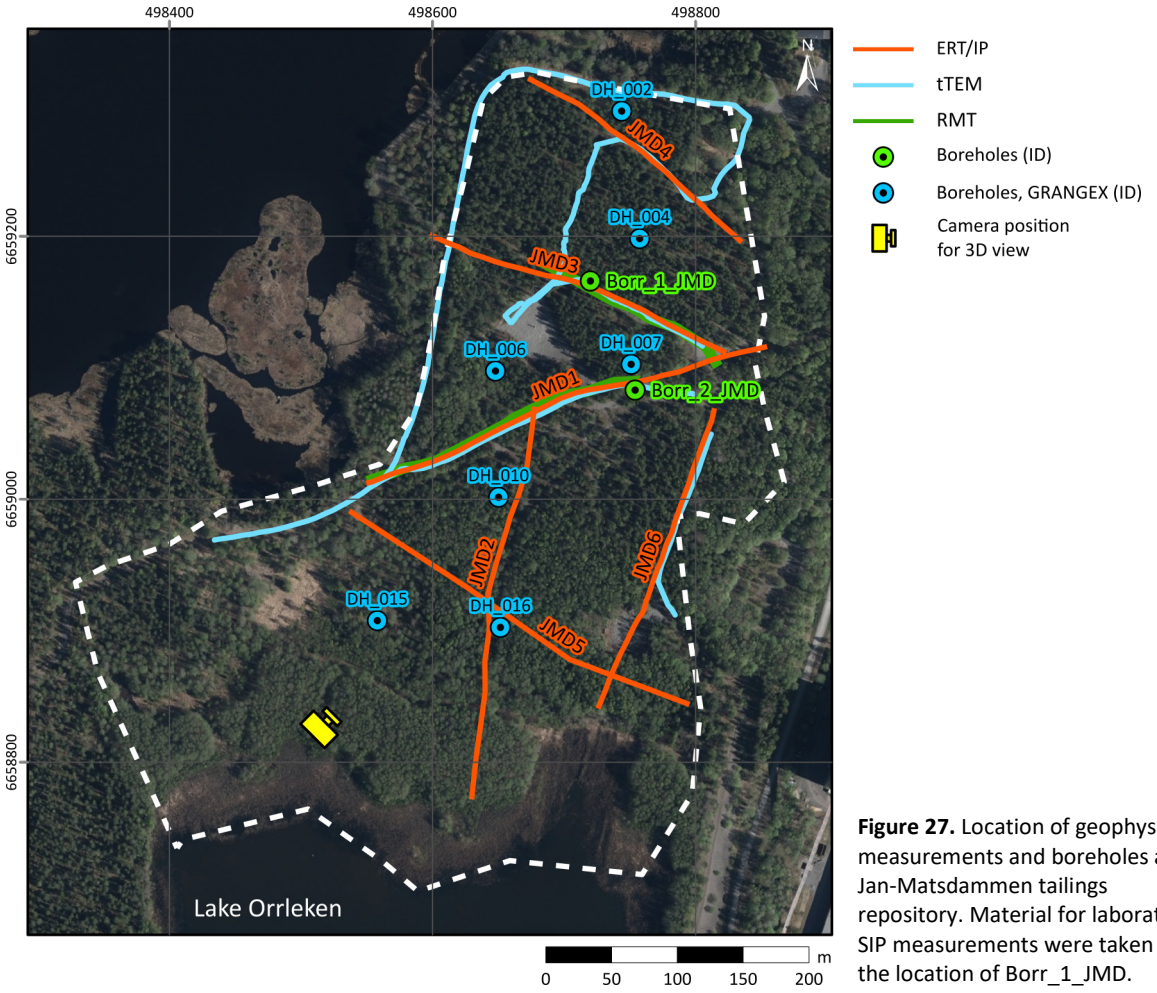

Figure 27. Location of geophysical measurements and boreholes at the Jan-Matsdammen tailings repository. Material for laboratory SIP measurements were taken at the location of Borr_1_JMD.

On initial inspection of the RMT data, it was clear that that the noise levels were too high. This is largely due to the proximity of a railway to the Jan-Matsdammen area. Hence the RMT data had to be disregarded. The ERT-data for all profiles show high quality and the inversions have low residuals and very consistent results. Figure 28 shows the data and inversion results for profile JMD3. Figure 28A and 28B show the resistivity data and pseudosections, respectively. Figures 28C and 28D depict the resistivity model and data residual, respectively.

All the ERT resistivity models demonstrate a similar resistivity pattern, with minor differences across the area (Figs. 28 and 29). A high resistivity layer is observed close to the surface on all profiles, which is approximately 10 m thick and thinning out towards south. Some internal variations in the resistivity exists in this top layer. Below this resistive layer lies a low resistive layer which itself has lower resistivities towards the southern part of the area (Figs. 28 and 29) and lake Orrleken. The interpretation, supported also by several drillings, is that this layer is composed of water saturated sediment, with increased water content moving towards the south lake.

The IP-data in this area also show high quality for all profiles except for JMD2 and JMD5 which were measured with a 5 m electrode spacing. The results from the IP measurements indicate some interesting results. At the Jan-Matsdammen the IP-responses are high, and noise level is rather low, specially along profiles measured with 2 m electrode spacing. Figure 30A shows an example of IP data from profile JMD3 and IP-gate 16 between 0.08 s and 0.1 s and a typical IP decay curve in Figure 30B. Figure 30C, 30D and 30E depict the phase pseudosection, the phase model from 2D MPA inversion, and the normalised data residuals, respectively. The laboratory measurements reveals that the material follows a Cole-Cole model with a maximum phase of 90 mrad (see Fig. 58 and Appendix A). One should note that during processing all negative IP-decay curves have been removed.

The main method used in the inversion of the IP data was the MPA, however the other available methods within AWB were tested and also some trials were made with the "traditional" inversion, namely Res2Dinv program. From testing different settings for the MPA inversion, a tight lateral smoothing constrains, and a medium vertical smoothing constrain for all parameters (resistivity, phase, time constant and c) was found to be most reasonable in this area. The constrains are also reasonable considering the target, i.e. assuming small variations in the horizontal direction (higher lateral constraint) but larger variation in the vertical direction (lower vertical constraint). The tailings were deposited as water saturated sediments and the strata can be approximated to an alluvial fan with changing discharge location. Horizontal layers are also observed in the boreholes.

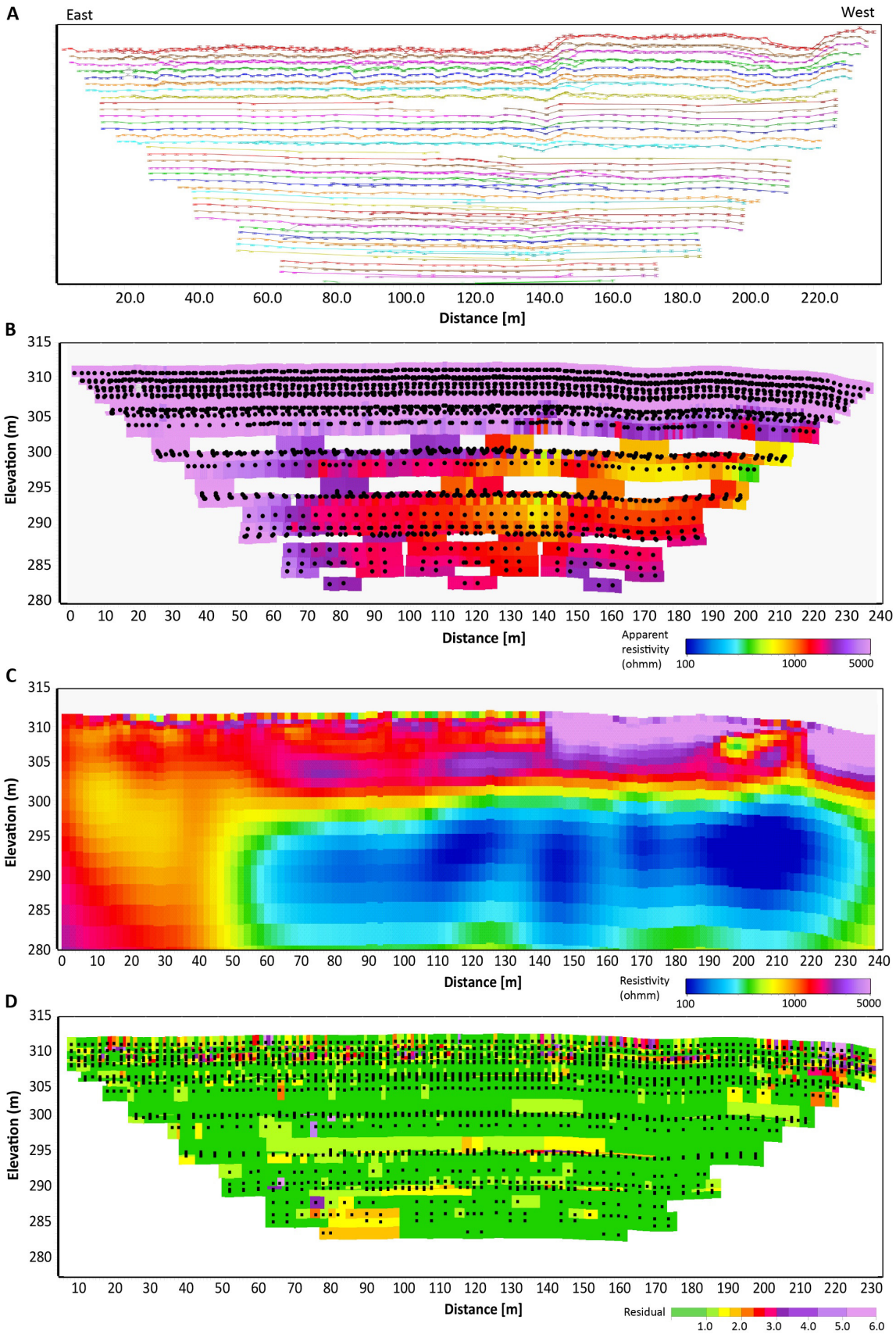

Figure 28. ERT data and resistivity models from 2D inversion along profile JMD3. Note that east is to the left in the figure. **A.** Data with error bars. The y-axis is scaled to show all data and has no unit. **B.** Apparent resistivity, with pseudo depth at the y-axis. The dots represent focus points for the measurements. **C.** Resistivity model (inverted only for resistivity). **D.** Residual section for the model in C.

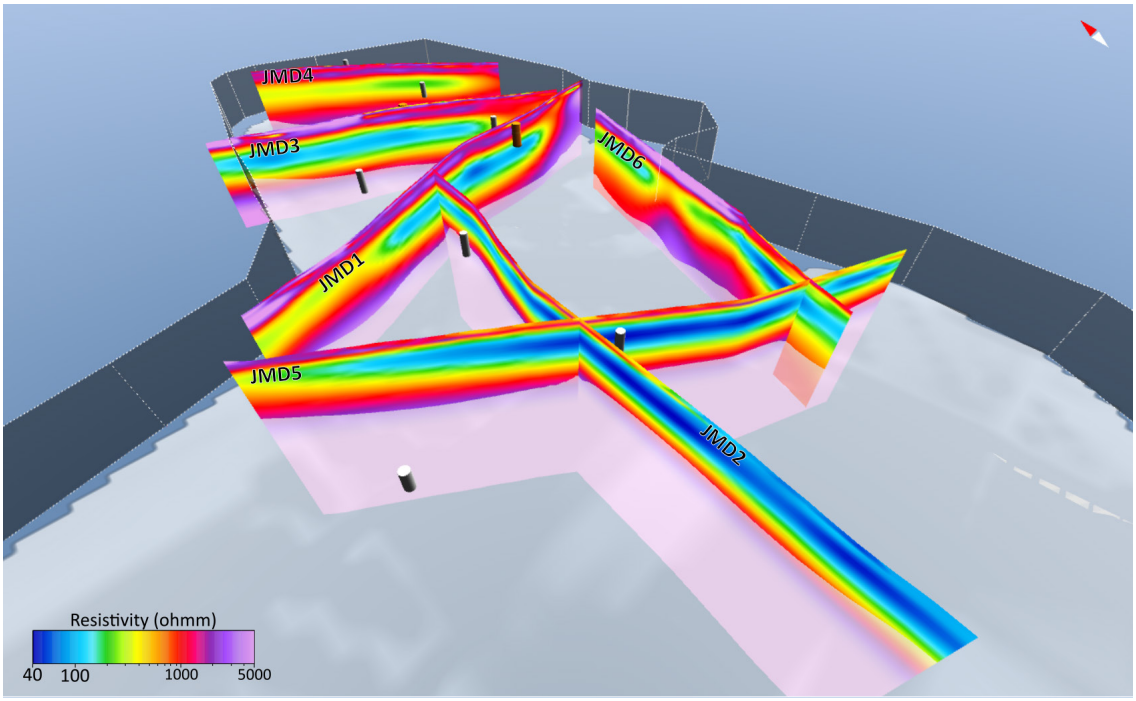

Figure 29. 3D view showing vertical sections of the ERT resistivity models for all the profiles in the Jan-Matsdammen. The light grey shaded layer represents the DOI. View from south-west. The camera position is shown in Fig. 27.

Figure 31 contains the modelled phase along all profiles. For the models along profiles JMD4, JMD3 and JMD1 (Fig. 31A to 31C) a high phase value (>50 mrad) is observed predominantly in the eastern parts of the profiles which dips towards the west. For profile JMD6 (Fig. 31D) this "high-phase" layer is more homogenous and is present as a layer between approximately 298 m to 306 m elevation. There are three boreholes (DH_004, DH_007 and Borr_2_JMD) within this "high-phase" area and all show a significant increase in the Fe-content at depth and at the level of high phase in the inverted models (Fig. 31). The Fe content is measured using different techniques on samples from different boreholes. For the GRANGEX boreholes the Fe-content is measured using the XRF-technique whereas the samples collected by SGU within this project are geochemically analysed. As the methods to describe Fe content with depth differ between boreholes and are not directly comparable, we have focused on a qualitative interpretation of the Fe curves, rather than focusing on the absolute values. Figure 32 is a more detailed comparison between the measured Fe content and the closest phase model at the location of three boreholes. The figure reveals a very strong correlation between the variation of Fe content and the modelled maximum IP phase.

Study of historical orthophotos shows that the discharge points have been in the eastern part of the tailing repository and that a lot of material was deposited during the 1950s and 1960s. The shape of two alluvial fans can also be identified (Fig. 33). A "high phase" area is observed in the eastern part of the repository at about four meters below the ground which depicts a shape like an alluvial fan, which is interpreted to correspond to the material deposited earlier in the operation of the site, seen in historical orthophotos. The historical production information show that the material deposited earlier may have had higher concentrations of the commodity being produced (at this site magnetite) since the extraction techniques have improved over time. Thus, this material is interpreted to have a higher Fe-content compared to the surroundings (an interpretation supported by three boreholes). The IP-measurements at Jan-Matsdammen indicate that this type of measurement technique may have great potential to identify high-grade Fe (magnetite) content in tailings sand. However, more investigations are required to assess what the dependency of IP response and high-grade Fe actually is.

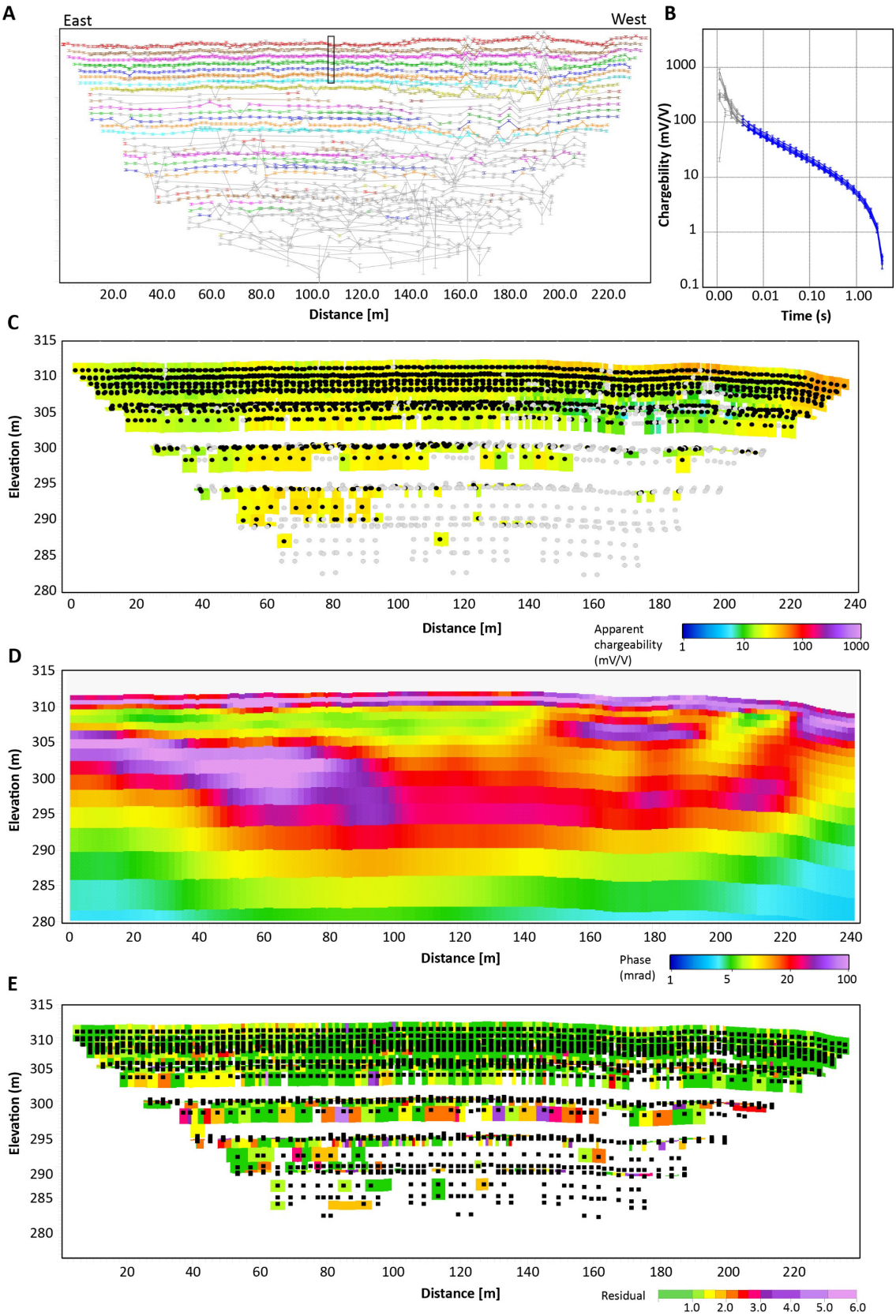

Figure 30. Data and inverted apparent phase model for profile JMD 3. **A.** IP data at gate 16 (between 0.08 s and 0.1 s). The y-axis is scaled to show all data and has no unit, and the box marks the location and points selected. The colored data points are used in the inversion whereas the grey are omitted. **B.** Decay data for IP window 16 with error bars. **C.** Apparent chargeability, with pseudo depth as the y-axis. The dots represent focus points for the measurements. **D.** Phase model (note that tauphi (τ_φ) and c exist but are not shown) obtained using the MPA inversion method. **E.** Residual section for the model in D.

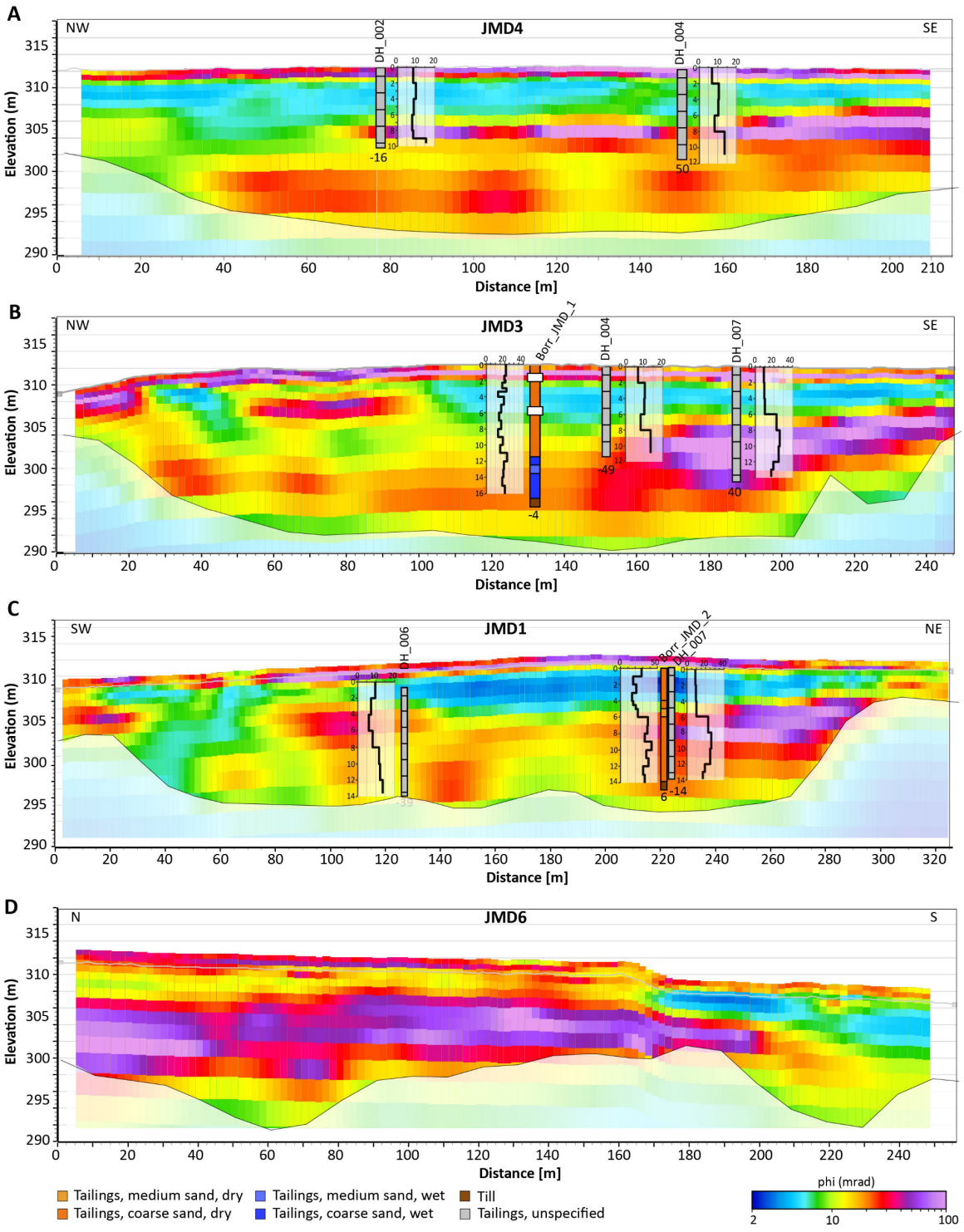

Figure 31. Sections for profiles showing the phase model. The location of the profiles is shown in Figure 27. The boreholes are projected perpendicularly onto the sections where their offset (in meters) is shown as a number below the curve. A negative number means that the borehole is located to the north of the profile and a positive number means that it is located to the south. The Fe-content with depth is presented adjacent to the boreholes obtained from geochemical analysis. For the Grangesberg exploration drillings, with the label "DH", the Fe content is measured using the XRF technique and is given in percent Fe. In the SGU-drillings (Borr_JMD_1 and 2) the measured quantity is Fe_2O_3 and is given in percent. Note that the x-axis for the Fe curves differs between boreholes based on the technique used to analyse the samples.

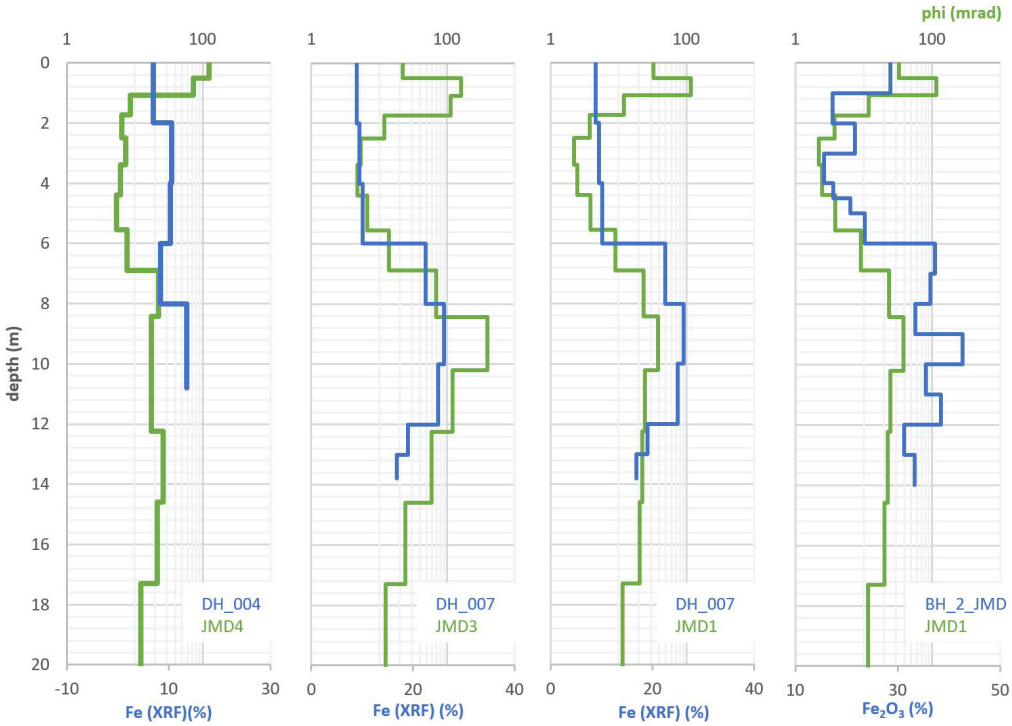

Figure 32. Shows curves of Fe-content as a function of depth (blue) for four different boreholes (see legend for borehole number). For each borehole the closest phase-model (green) is also shown as a function of depth.

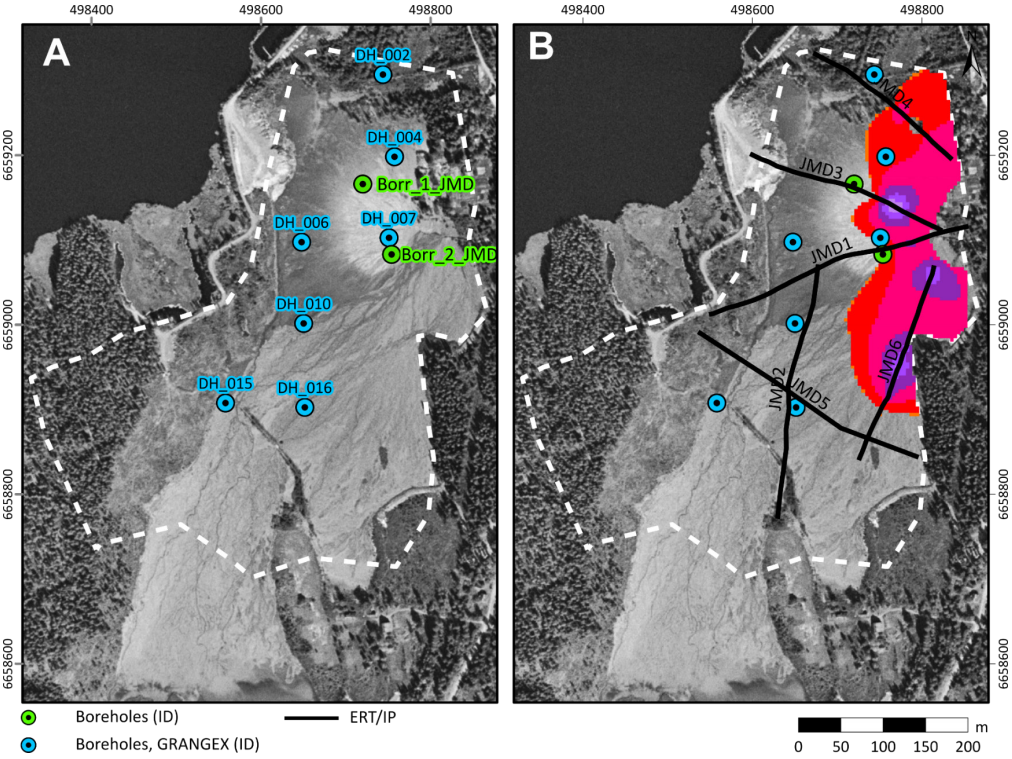

Figure 33. A. Historical orthophoto with reference year 1960. **B**. The same photo where material with a high IP-effect is highlighted. The colored area represents a slice at 302 m.a.s.l. through a 3D grid generated by interpolating the phi values. The slice is masked to only show values above 27 mrad (note that the color legend scale is the same as shown in Figure 31). This material is interpreted to have higher iron content and to be deposited as a fan adjacent to the discharge point.

The models of time constant, τ_φ (tauphi) obtained for all of the inverted profiles (using the MPA inversion) are shown in Figure 34. It is established that time constant variations can be correlated to the grain size changes (see Tarasov and Titov, 2013 and references therein). The available grain size analysis for the boreholes along the profile are also shown in Figure 34. For the GRANGEX boreholes, sieveing analysis have been performed and the results are presented as d_{80} which is the size in μm where 80% of the material has passed through the siev. For the SGU-drillings sieving analysis have only been performed on the SIP-samples and no "depth-profile" can be obtained.

A qualitative analysis was however performed in the field while drilling, and the grain size have been noted for every meter. In order to quanitfy these observations they have been classified into grain-sizes according to the SGF 1984 scale. A logaritmic average value have then been calculated for the observations. For example: at a depth of 4–5 m it was noted that fine to medium sand was present. This has then been translated into a representative grain size of 0.2 to 2 mm. The logarithmic average was calculated and a value of 0.62 mm was used to quantify the grain size at this depth interval. This is how the values plotted for the SGU drillings shown in Figure 34 were obtained. This is a very generalized way to characterise the grain size distribution and may not represent the true distribution. It is however the only way, at this point, to obtain information of possible trends in the grain size distribution from the SGU boreholes. The GRANGEX sieving method is more accurate at estimating grain sizes but there is still potential for errors. If, for example, a sample mainly contains clay particles but includes some fraction of medium sand, the 80% passing size may give a medium sand value, which may not represent the grain size fraction in the sample.

Figure 35 presents a more detailed comparison between the grain size and modelled tauphi where one can see a good correlation between the models and grain size curves for several boreholes. For example, in boreholes DH_002, DH_004, and DH007, there is a rather strong correlation between the two curves, where increasing tauphi corresponds to larger grain size. However, in general from the results in Figure 34 and 35 one can not make a firm conclusion on a strong correlation between the two parameters. This may be partially due to the different scales involved and also the implicit smoothing within the inversion process. Hence, it is possible that the inversions and borehole results may differ significantly. It is also important to note that the inversion process estimates the parameters over a much larger volume than that used for the grain size classifications.

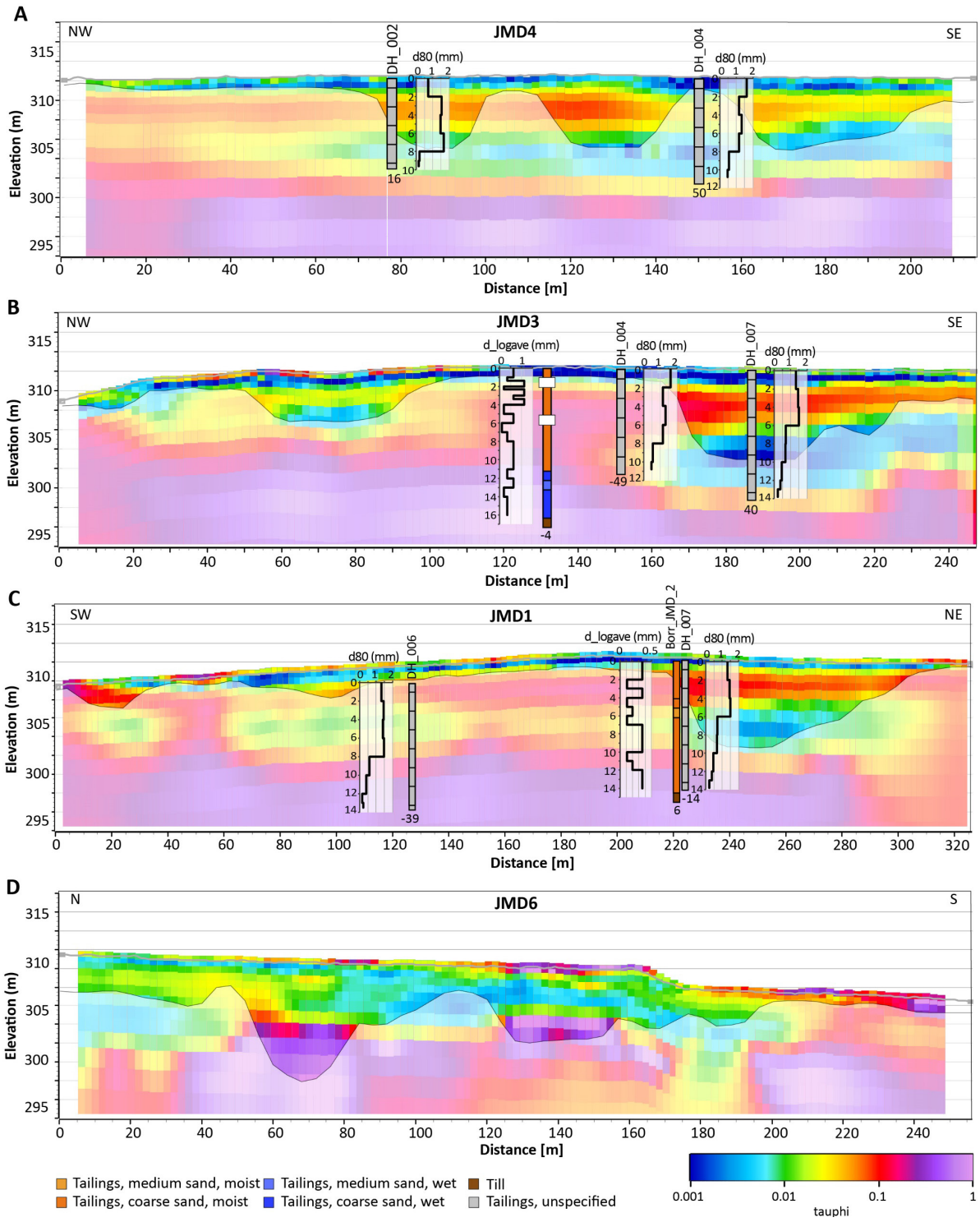

Figure 34. Sections for profiles showing the time constant model (tauphi). The location of the profiles is shown in Figure 33B. The boreholes are projected perpendicularly onto the sections where their offset (in meters) is shown as a number below the curve. A negative number means that the borehole is located to the north of the profile and a positive number means that it is located to the south. Next to the boreholes are curves which describe an estimate or measurement of the grain size with depth. See text for description.

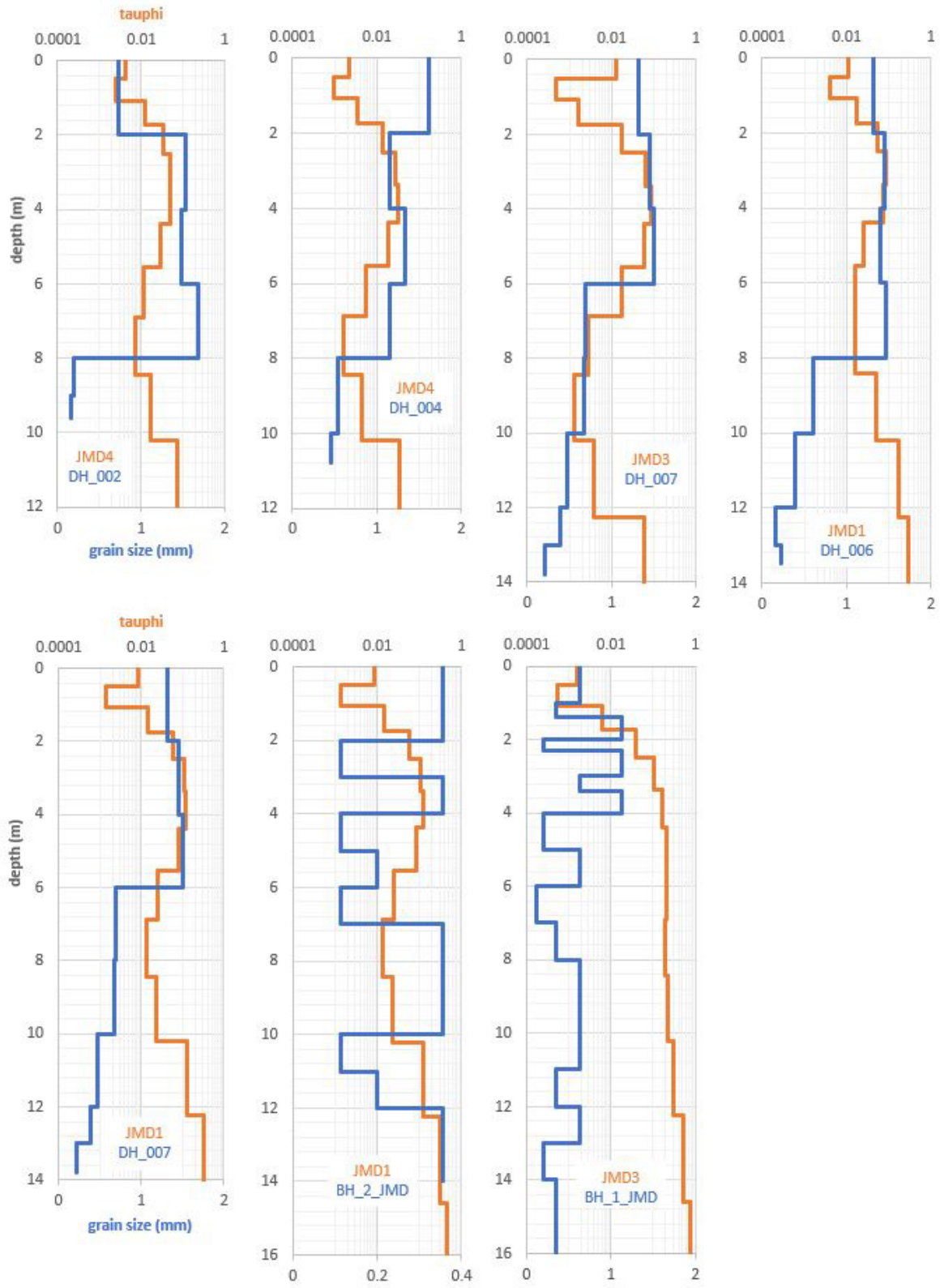

Figure 35. Grain size curves as a function of depth for a range of boreholes (blue). See the blue text in the legend for the borehole name. For each borehole the nearest time constant-model (tauphi) curve is shown (orange).

A comparison of the laboratory measured and calculated parameters of resistivity, phase and time constant is shown in Figure 36. In addition, the Cole-Cole exponent and the modelled responses are also shown in Figure 36. The resistivity values have been corrected for temperature according to equation (8) with a temperature of 16°C for both samples, this yields only a minor correction compared to the 18°C value assumed as the laboratory temperature. The measurement at Jan-Matsdammen were conducted in early June and it is assumed that the uppermost layers of the ground follow the average temperature for that month, which is 16°C. There is no straightforward way to compare a very controlled direct measure of a sample's physical properties to field measurements and the associated inverted models. However, it is still interesting to present the different data and to discuss and study the similarities and differences. The resistivity values show an accepted correlation for the sample taken at 1–2 meters depth (G1) whereas for the deeper sample (G2) the difference is rather large. In this case the trend in the lab measurements is somewhat opposite to the resistivity model, where the laboratory measurements show a lower resistivity at depth and the model generally shows a higher resistivity. It is therefore important to note the difference in scales and also the limitations in the inversion method. The samples taken at Jan-Matsdammen are the only samples in the project where we can compare with the inverted models of the IP-parameters with the results from laboratory SIP-measurements. In a similar way to the resistivity comparison, the lab and modelled IP-parameters show a fairly good fit for the shallowest sample (G1) whereas for the deeper sample (G2) they differ considerably (Fig. 36). It should be noted that for the tauphi and C, the DOI is very shallow at the location of the samples (borehole Borr_JMD_1 in Fig. 34). This indicates much lower sensitivity in the inversion at depth. At this stage due to the shallow DOI and low number of sample points, it is not possible to draw any strong conclusions. More laboratory measurements are required to further investigate the relationship between the model and lab parameters across the study area.

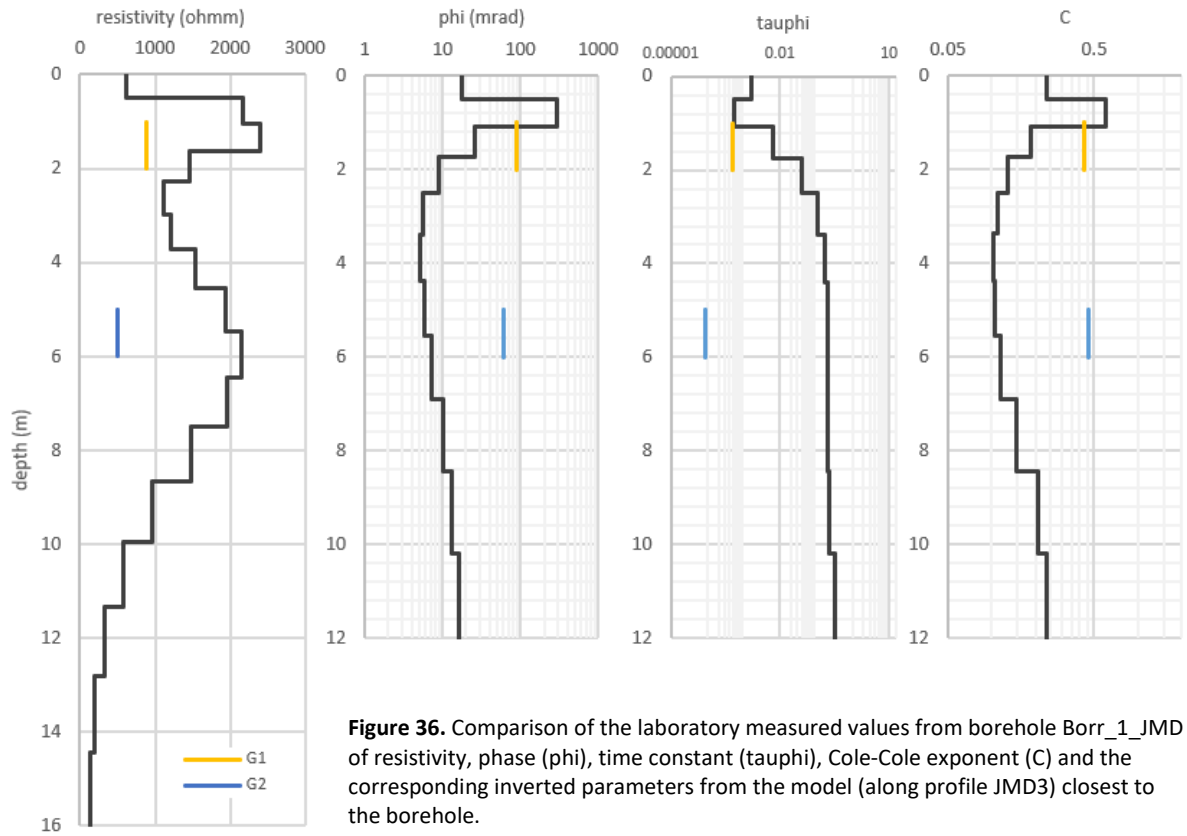

Figure 36. Comparison of the laboratory measured values from borehole Borr_1_JMD of resistivity, phase (phi), time constant (tauphi), Cole-Cole exponent (C) and the corresponding inverted parameters from the model (along profile JMD3) closest to the borehole.

Hötjärnen

At Hötjärnen geophysical measurements also include ERT-IP, tTEM and RMT. Most of the ground geophysical measurements were performed in 2021 and two boreholes were completed the same year. Complementary ground geophysical measurements were performed in 2022. Figure 37 shows the location of the geophysical profiles and boreholes. In total seven ERT-IP profiles were acquired, where two profiles (profile 4 and profile 5) were measured with 5 m electrode spacing and the remainder with 2 m spacing. tTEM measurements were concentrated in the southeastern corner of the tailings repository where it was easier to access and drive the ATV. The tTEM measurements have good coverage in this part of the tailings deposit with a total of 4 km of profile data. Two RMT profiles were measured with 10 m station spacing in the same directions as the two previously measured ERT-IP profiles. One of the two boreholes conducted (HT_BH1), was sampled every meter until the base of the tailings. The other borehole (HT_BH2) reached the base of the tailings but due to time constraints was only sampled in the upper 10 m. There are no laboratory SIP measurements from the samples collected from Hötjärnen.

The ERT and RMT measurement are, in general, high quality with a low level of noise. Figure 38 shows the resistivity models from the 2D inversion of ERT and RMT data along profile 3 and 4. The RMT measurements were conducted along the eastern part of profile 3 and along almost the whole length of profile 4.

The resistivity model along ERT profile 3, measured with 2 m electrode spacing images several interesting resistivity patterns (Fig. 38A). Nearest to the surface is a 2-meter-thick high resistivity layer, which thins out towards the west, in the vicinity of the dam (Fig. 37). This is interpreted as dry tailings deposits located above the water table and the water saturation is interpreted to increase closer to the dam. In the east of the profile, the underlying bedrock appears as a high resistive feature which dips towards the southwest. Further to the west, the bedrock is interpreted to be too deep to be resolved in the data. The base of the tailings sand is interpreted to follow the base of the low resistivity layer (grey line in Figure 38A). Within the water saturated tailings there are variations in resistivity, with alternating high and low resistivity layers. Profile 3 exemplifies the general resistivity pattern observed along most of the ERT profiles in Hötjärnen which all are shown in a 3D view in Figure 39.

The RMT profile (Fig 38B) covers only the eastern part of the ERT profile 3 (approximately 250 m from the eastern end). The interpreted base of the tailings is clearly outlined in the resistivity model but the thin, shallow high resistive layer corresponding to dry sand closest to the surface is not resolved well in the RMT model.

ERT profile 4, measured with 5 m electrode spacing, (Fig. 38C) shows a similar pattern as profile 3. The resistivity model shows 5 layers with alternating high and low resistivity and the models agrees where the two profiles cross. It is also evident that the resolution is lower compared to profile 3 in the uppermost 5 m due to the larger electrode separation. The resistivity model from the RMT measurements (Fig 38D) shows a similar resistivity pattern as the ERT model, with the exception of the uppermost high resistive layer that is not resolved. Compared to the ERT model the RMT model outlines the bedrock surface better due to the greater penetration depth. The RMT model also identifies the high resistivity layer at about 280 m.a.s.l. along profile 4 which is seen in the ERT resistivity model (Fig. 38C and 38D).

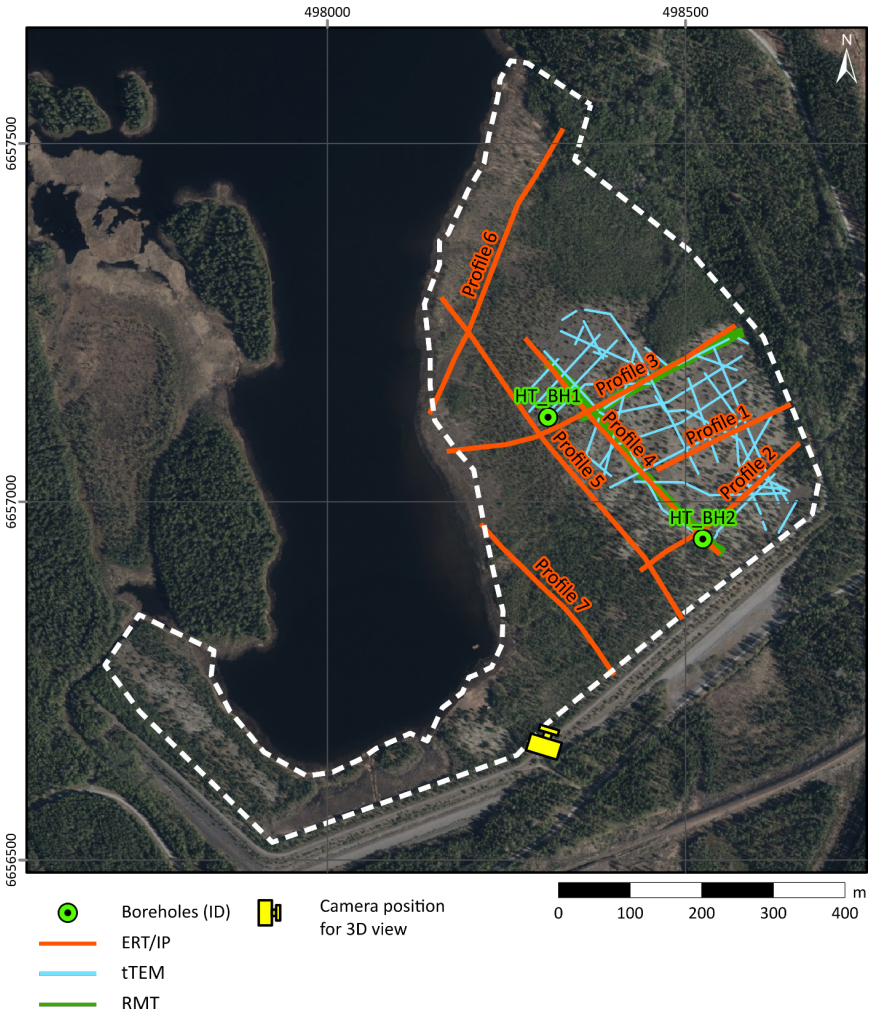

Figure 37. Hötjärnen tailings repository with the location of the different types of geophysical measurements performed and the location of boreholes. The dashed white line represents the boundary of the tailings deposit.

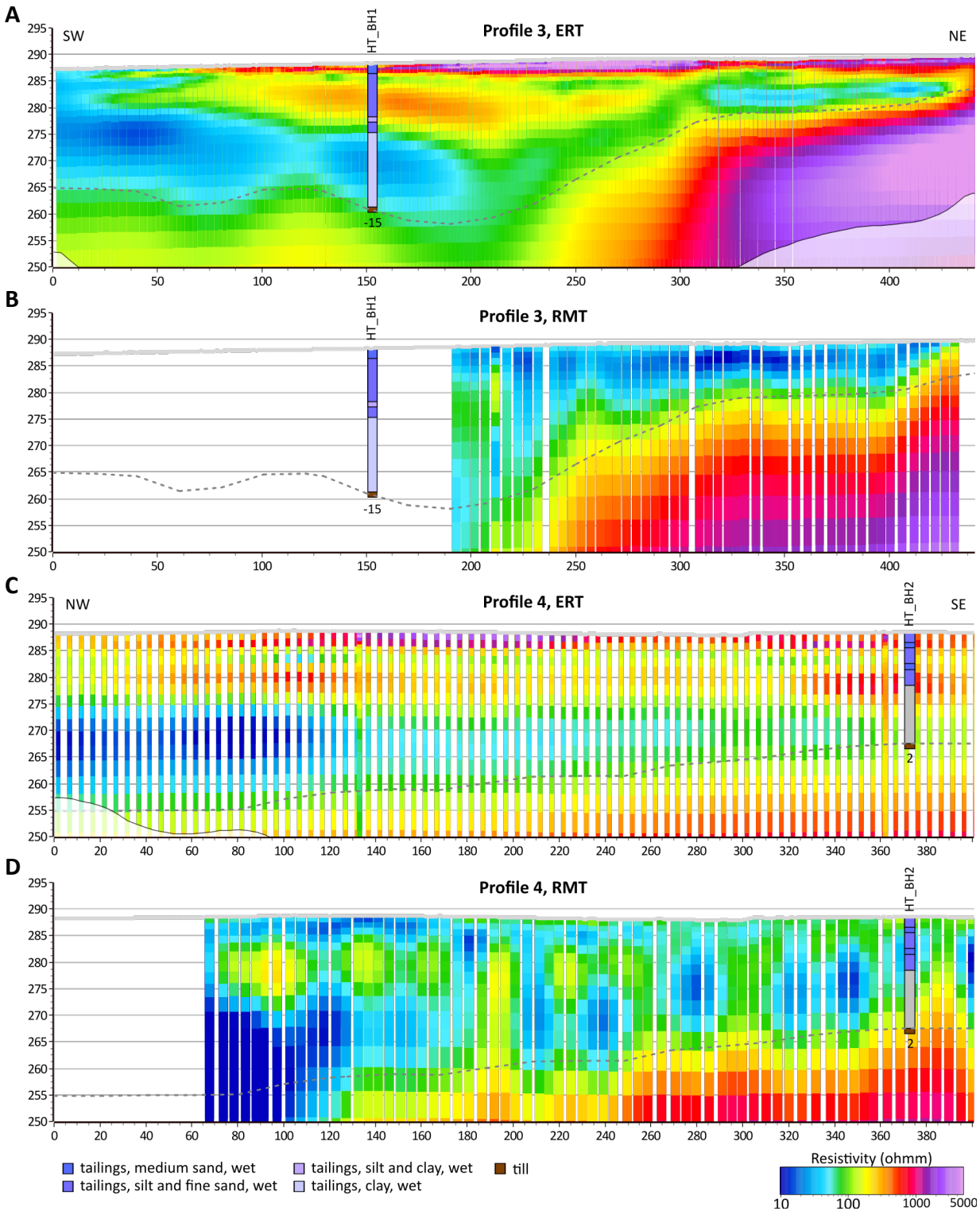

Figure 38. Profile 3 and 4 with inverted resistivity models from ERT (A and C) and RMT (B and D). The dashed grey line shows the interpreted base of the tailings.

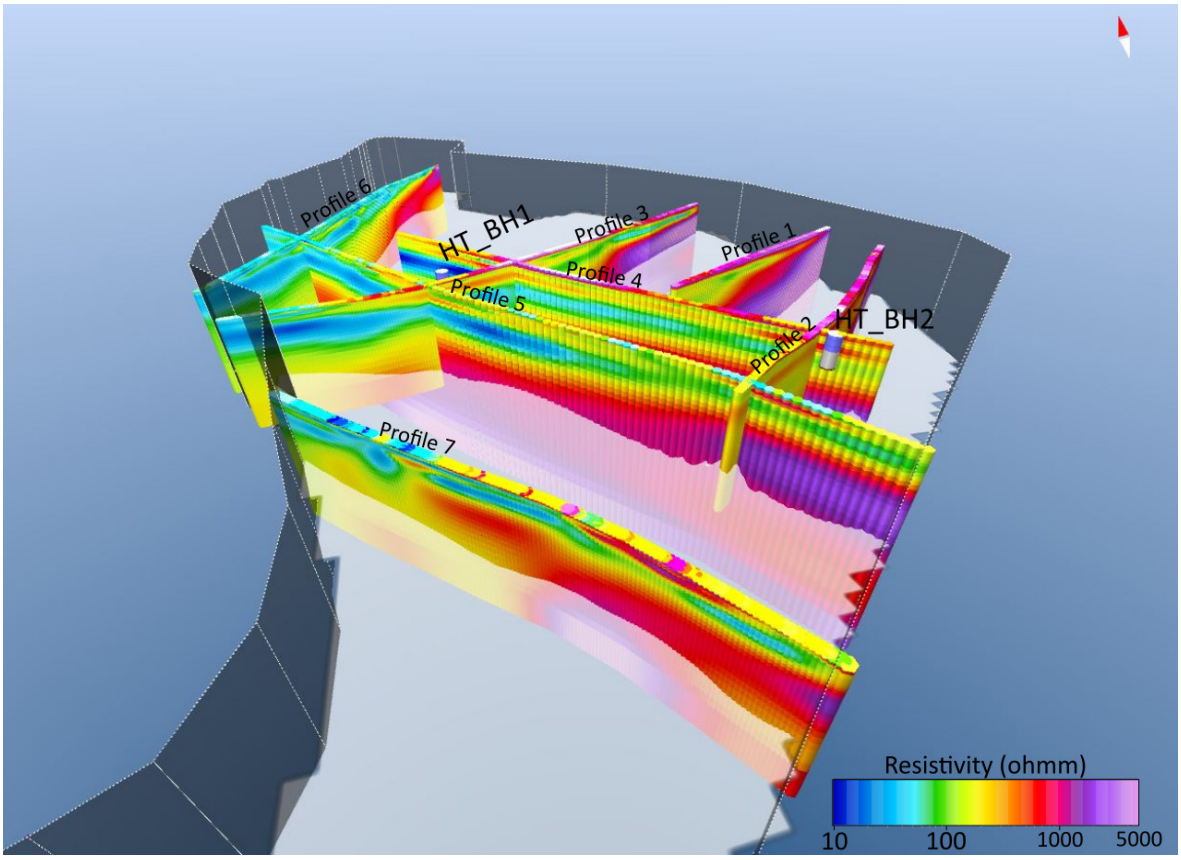

Figure 39. 3D view showing ERT resistivity models for all profiles at Hötjärnen. The white shaded layer represents the DOI. The camera position is shown in Fig. 37.

The borehole HT_BH1 is the deepest borehole in the Grängesberg tailings deposits, extending to a depth of 27 m. Based on the historical orthophoto the location of the borehole is near the center of the pond that existed prior to deposition of the tailings. At 14–15 m, BH1_HT showed a distinct shift in the properties of the tailings (Fig. 40). The sediments changed from a typically grey, mica rich, medium- to fine-grained sand, to a very fine-grained layer dominated by silt and clay. A transition is also evident in the resistivity models were the resistivity changes from around 300 ohmm to 50 ohmm. A change is also evident in the concentration of several elements from the geochemical analysis. The clay rich layer shows up as a lower resistivity area which can be outlined in the profile (Fig. 40). A very prominent increase in the REE and P_2O_5 occurs at the same level as the shift in grain size occurs. The Fe content (mainly magnetite) is very high at a depth of about 5 m (Fig. 40 and 41) and then decreases gradually with depth. This may indicate that high Fe-content, in this deposit, is related to coarser grain sizes, whereas higher levels of REE may be associated with the finer clay-rich material. We cannot make a general conclusion from only one sampled borehole, however, if such a relationship exists, then the clay-rich sequence (relatively REE rich) could be detected and imaged using the ERT-measurements. Another observation is that the thin layer with the highest Fe concentration coincides with the thin layer with low resistivity (approximately 100 ohmm) at an elevation 285 m (Fig. 40).

The IP-data show variable quality at Hötjärnen. The data along profiles (4 and 5) measured with 5 m electrode spacing are noisier. IP data along profiles 1 and 2 have quite high quality but the profiles are short. Profile 3 shows good responses close to the surface, however the deeper data are filtered out after processing. Profile 6 and 7 have variable noise levels along the profile and with depth, making the reliability of the inverted model difficult to address.

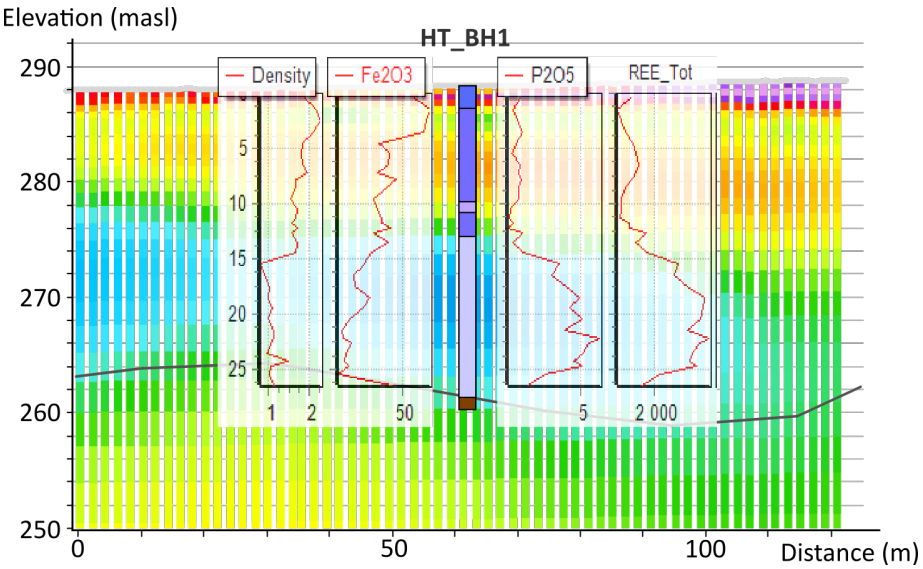

Figure 40. Part of ERT model along profile 3 with results from density measurements and geochemical analysis of Fe_2O_3, P_2O_5 and REE total (the y-axis shows depth while the x-axis shows density in g/cm^3, percentage for the Fe_2O_3, P_2O_5 curves and ppm for the REE tot axis).

Figure 41. Tailings sand collected from the surface at Hötjärnen repository, the high content of magnetite is apparent when holding a magnet close to the material.

Blötberget

Ground geophysical measurements were conducted at the eastern Blötberget (Norsberget) tailings repository in spring 2022 (see Fig. 1 for area location). ERT-IP and RMT data were acquired along profiles shown in Figure 42. Three boreholes were drilled within the tailings deposit, the locations of which are shown in Figure 42. Samples for SIP measurements were collected at 6–7 and 10–11-meters depth from borehole Bbg_2 (Fig. 42).

On commencement of drilling, it was apparent that the tailings sequence was very dry in Bbg_1 and Bbg_3, which also may have caused the drill to get stuck due to high friction. As a result, sampling was not performed within these boreholes. At Bbg_2 the material had a higher water content and sampling could be performed throughout the interval with tailings. The groundwater level was noted at 9 meters depth.

Despite performing fieldwork in late spring (May) many parts of the ground were still frozen with an approximately 10 cm thick ice layer, which proved challenging for the acquisition. To conduct ERT-IP measurements a good electrode contact with low resistance is vital. For this reason, the electrodes were hammered through the ice layer and saltwater was added to gain a better contact. As a result, the contact resistance was kept under 1000 ohm for most of the electrodes during the measurements. The collected RMT data are of good quality in the area and these measurements were not affected by the frozen ground.

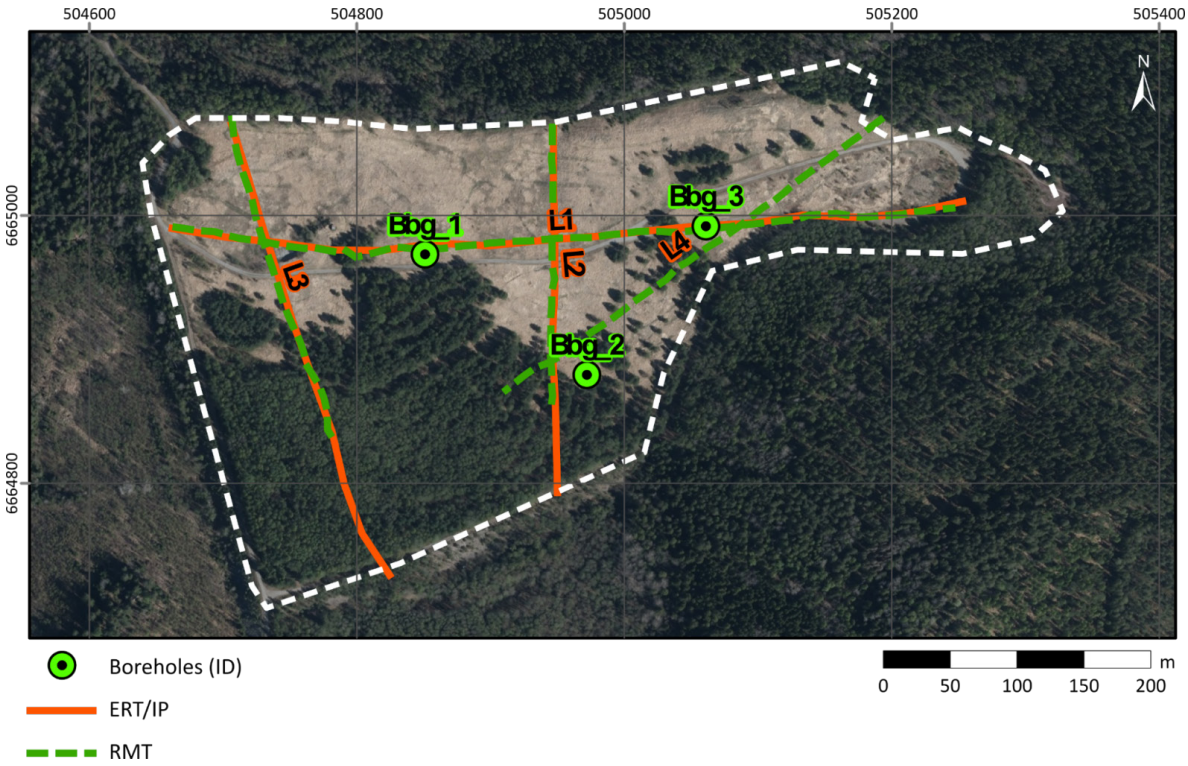

Figure 42. Location of geophysical profiles, boreholes and sampling points at the Blötberget mine tailing site. The dashed white lines represent the boundary of the tailings.

Figure 43 shows the resistivity models from inversion of ERT and RMT data along profile L1 and L2. The RMT models along both profiles (Fig. 43B and D) show three layers; a highly resistive (500–1000 ohmm) layer at the top followed by a layer with lower resistivity (50–200 ohmm) and at the bottom another highly resistive layer (1000–5000). These layers correspond most probably to dry sand, moist/wet sand, and finally bedrock. The RMT models show a reasonably good correlation with the observations made in the boreholes, especially along profile 2 (Fig. 43D). The wet tailings appear in the model as low resistivity and the till shows relatively higher resistivities in the model.

The resistivity model from ERT data show a different result compared to the RMT model (Fig. 43A and C). The highly resistive (2000–5000 ohmm) upper layer with a thickness of up to 15 m in the ERT profiles L1 and L2 may be caused by the thin ice layer plus the dry sand, however this relatively large thickness seems to be an overestimate. Below this layer the models indicate very low resolution, and the depth penetration is probably very limited. The bottom of the tailings cannot be identified from the ERT-models.

Figure 44 illustrates a more detailed comparison between the resistivity measured on the SIP samples and the resistivity models from ERT and RMT at the location close to Bbg_2. During drilling the sand was considered to be moist from the surface down to the base of the hole. The diagram shows clearly that the resistivity model from the RMT measurements correlates very well with the resistivities measured on the SIP samples.

As a result of the better correlation with the sample data and apparently more geologically reasonable inversion result, only the RMT models were used to interpret the base of the tailings (Fig. 43 and 44).

The IP data collected from this area was of high quality with smooth decay curves but unfortunately due to time limitations in the project, processing of these data was not performed. However, it should be noted that there is a risk that these measurements were influenced by the frozen ground layer, which can make interpretation difficult. The SIP laboratory measurements show a high phase of about 90 mrad for the deeper (10–11 m) sample. The phase maximum is however beyond the maximum frequency of 10 000 Hz (see Fig. 58, and Appendix B).

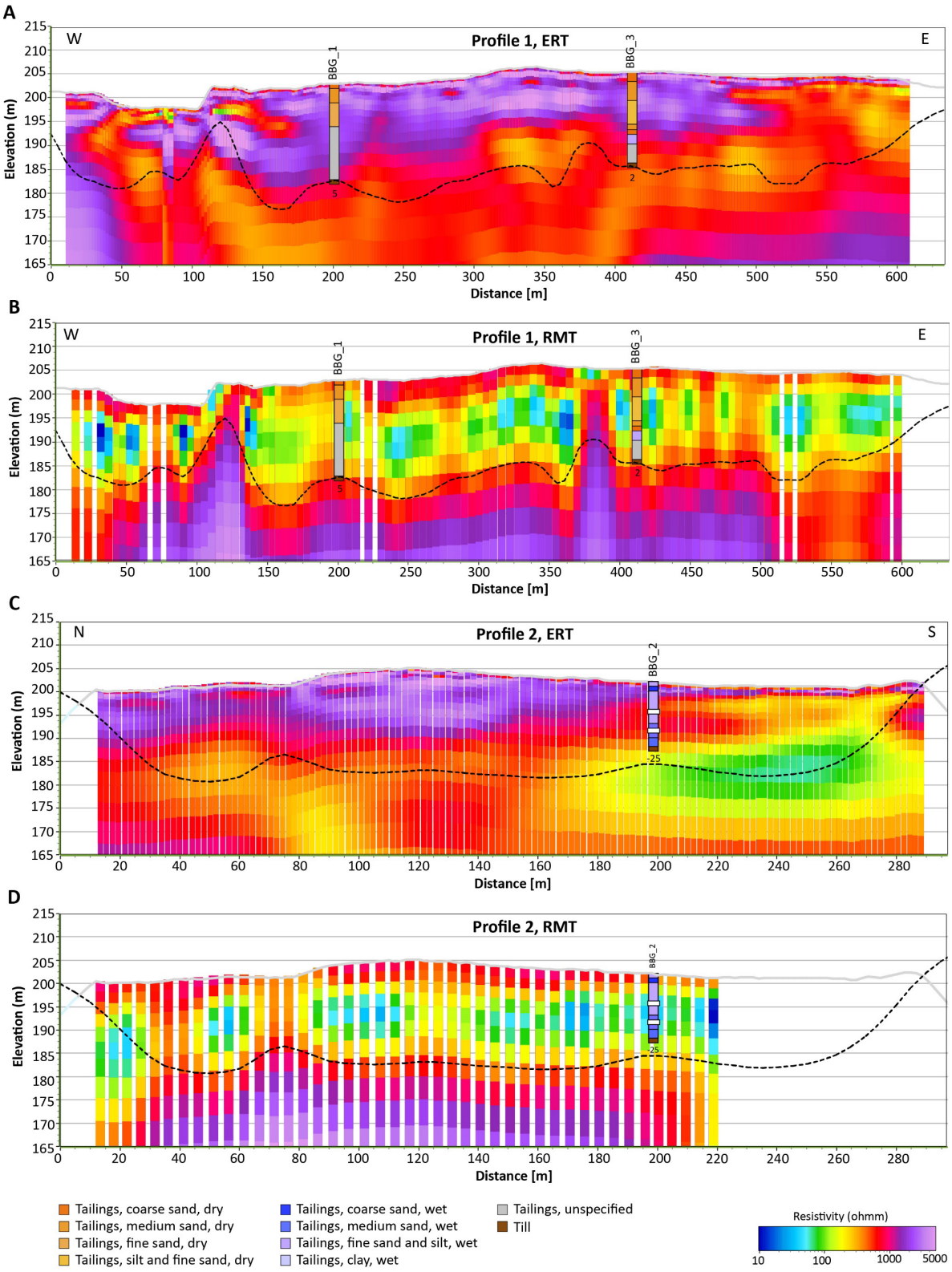

Figure 43. Resistivity models from the inversion of ERT and RMT data along profiles L1 and L2. The geological observations made from the boreholes is also shown. The black dashed line is the interpreted base of the tailings, the interpretation is only based on the RMT models (B and D) and the boreholes.

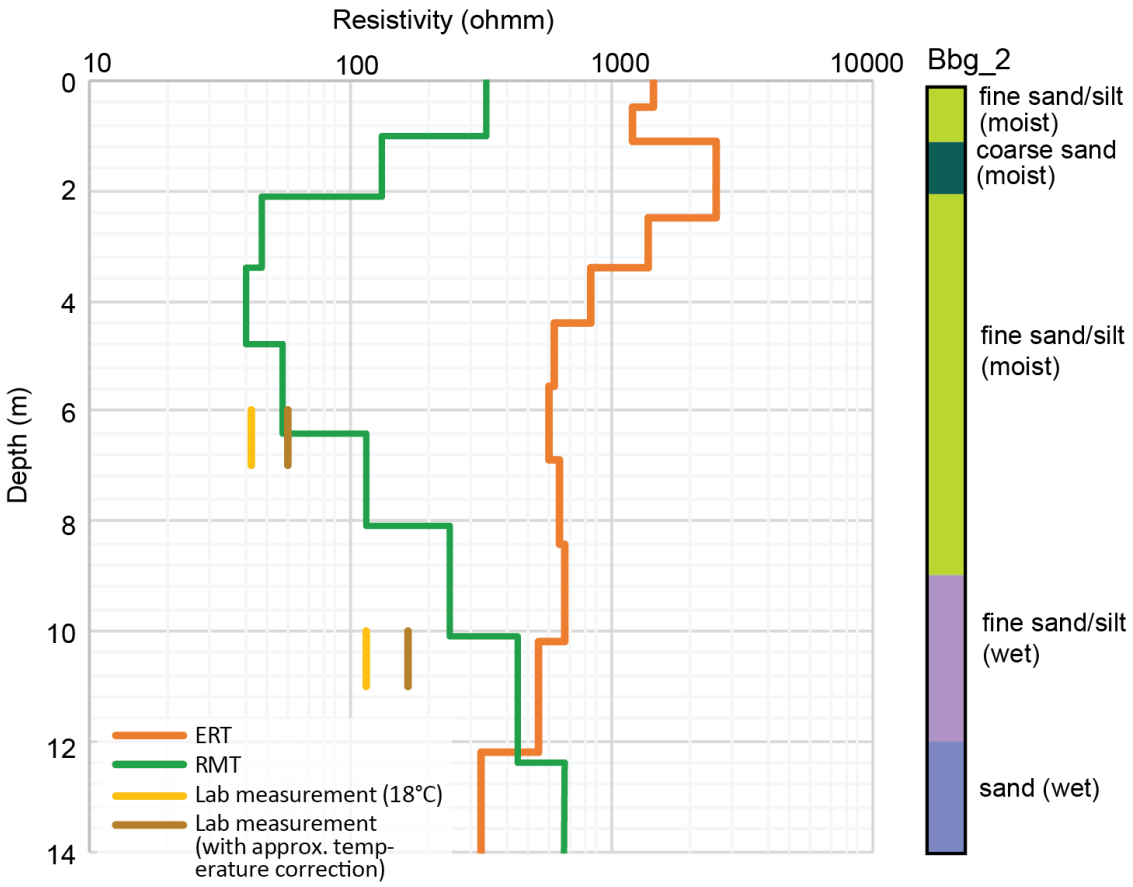

Figure 44. Comparison of ERT and RMT inversion results close to borehole Bbg_2. The results from laboratory measurements on the sample are shown with both uncorrected and corrected values for the temperature difference. The geological description of the borehole was observed during drilling.

Stollberg

At the Stollberg (also known as Gårdmyren) tailings dam five ERT-IP profiles and one RMT profile were acquired (Fig.45). The measurements took place in early May and the soil was still frozen down to at least one decimetre.

Later in 2022 SGU drilled four holes that aimed at reaching the bottom of the tailings. Detailed chemical analysis was conducted for every meter of the material taken from the boreholes. SIP was measured for two samples extracted from borehole BH2. Seven boreholes drilled in 2004 for other purposes (Envipro miljöteknik 2004) could also provide information.

At Stollberg the tailings take the form of a pile leaning against the flanks of a small valley, where the valley defines the northern and northwestern edges of the tailings deposit. It is contained on its other sides by dam walls whose structure is not known precisely but are probably made of blocks. The deposit is at most 18 m high. The material comes originally from the Stollberg mine field and was processed at the dressing plant located next to the tailings. It was deposited between 1949 and 1981.

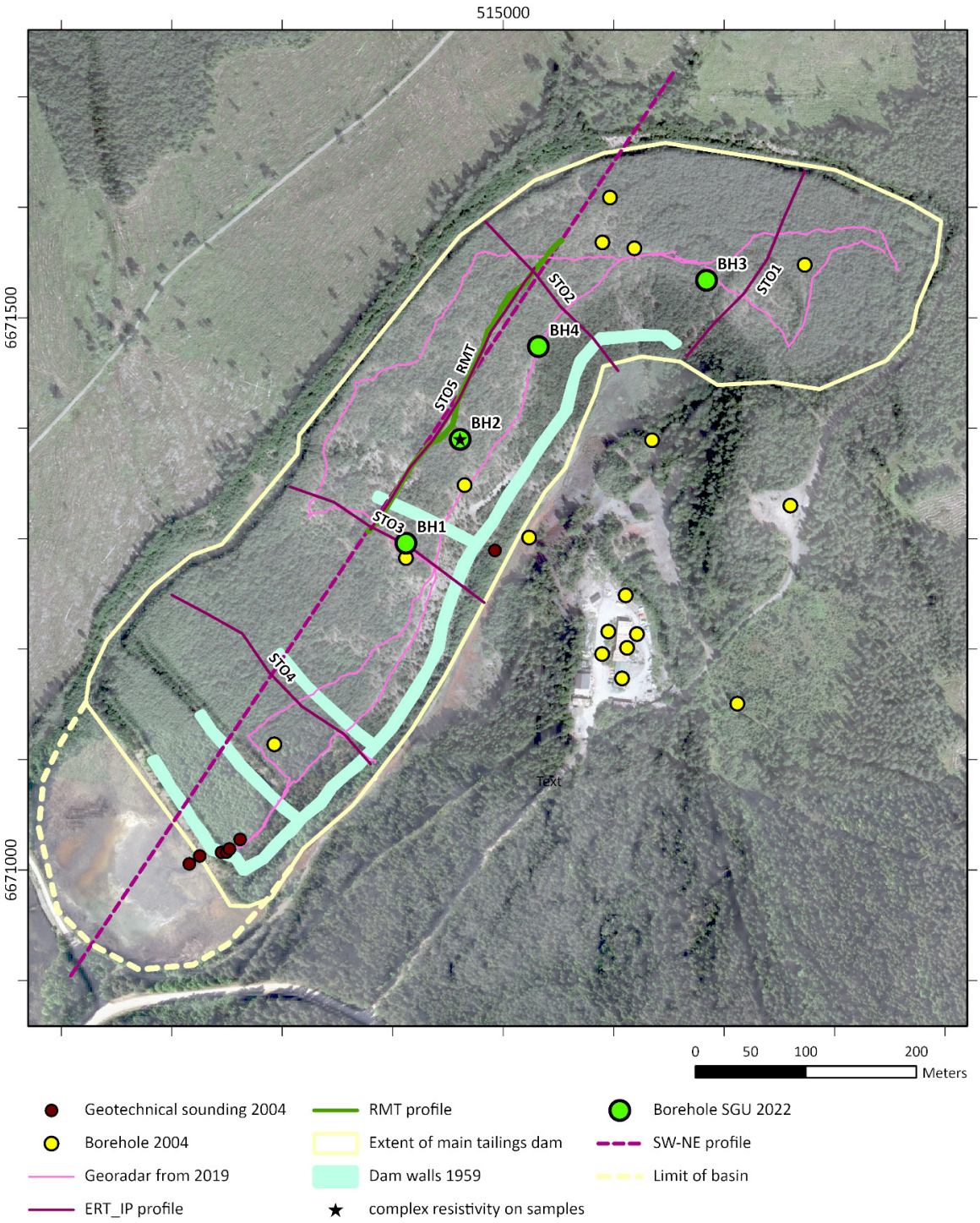

Figure 45. Map over the Stollberg tailings repository. The location of geophysical measurements and boreholes are shown. A high voltage power line is located immediately west of the area.

The tailings deposit is rich in arsenic, lead, zinc and cadmium and is subject to landslides. Hence this site poses a significant environmental risk. It has been the target of several detailed studies in the past (notably Envipro miljöteknik, 2004) and is actively under surveillance. From a resource point of view sampling and assessment is reported in (Hallberg and Reginiussen 2020) and (Casey et al. 2024). These studies show that the groundwater level is higher close to the northern and north-western flanks, but it generally lies relatively deep (below 12 m depth).

Because of the frost considerable efforts had to be made in the field to decrease the contact resistance between the electrodes and the ground. As a result of these efforts the resistance could be kept under or around 1000 ohmm for most of the electrodes, at least during testing at the beginning of each measurement. However, the frost and low surface temperature had a significant impact on the measurements and subsequent inversion results.

The quality of the ERT data was apparently good. Not many data points were removed and data residuals after the 2D inversion were low. Resistivity models from the 2D inversion of ERT data along profiles STO1 to STO4 are presented in Figure 46. In all the resistivity models the frozen ground can be observed clearly as a thin layer directly below the surface with relatively high resistivity (Fig. 46 and 47A). However, this resistive layer also appears to lead to a rapid decrease of the resolution with depth. The dam walls, constructed from blocks of resistive bedrock appear as high-resistive superficial structures (Fig. 47A). At a few meters depth one can see a limit between an upper more resistive layer and a lower more conductive layer (marked by dark blue dotted line in the models shown in Fig 46 and Fig. 47). This most probably corresponds to the groundwater level. The lowermost resistive layer is interpreted as the crystalline bedrock. This last layer appears discontinuous, but it is most probably due to loss of resolution at depth.

The RMT profile is 300 m long with a station spacing of 10 m and measured along the same profile as STO5 (Fig. 47). The signal quality was reasonably good, however, the transmitters at frequencies above 100 kHz had rather low signal to noise ratio. A 2D inversion of determinant RMT data produced the resistivity model shown in Figure 47B. In the RMT model the tailings appear as a relatively conductive layer, with resistivity between 20 and 150 ohmm. The groundwater level is not clearly apparent, even if the resistivity seems to be slightly higher in the upper part. A resistive formation is seen under the tailings that most probably corresponds to the bedrock. Because of lack of high frequency signal in the RMT band at this site, the RMT model shows less resolution at the shallower parts of the model. However, it has a deeper penetration and depth of investigation than the ERT data (Fig. 47A), which leads to a more continuous image of the bedrock.

A comparison was made between the RMT and ERT inverted soundings close to BH2 and the SIP results on the samples (Fig. 48). The high resistive frozen ground appears only on the ERT results, due to the reduced near-surface resolution of RMT as explained above. The loss of resolution for the ERT below 10 m is clearly apparent. An approximate temperature correction was applied to the laboratory measurements, using the equation (8). It was assumed that the temperature below 15 m depth was about 6°C which is the average air temperature in the area according to the Swedish meteorological Institute (SMHI). Since the measurements were taken in early spring and the soil was still frozen, we assumed that the temperature could be between 3 and 6 °C between 4 and 5 m depth. The estimated resistivities from inversion of RMT data yield values remarkably close to those for the laboratory measurements (Fig 48). One main reason is that the measurements of the electric field are not affected by the contact resistance and presence of the frozen material below the profile. Another reason is that the calculated apparent resistivities are made from complex impedance (see equation 24) which may lead to closer estimated resistivities to the SIP laboratory measurements.

► **Figure 46.** Inverted resistivity sections with boreholes and interpretation for ERT lines **A.** STO1. **B.** STO2 B. **C.** STO3.

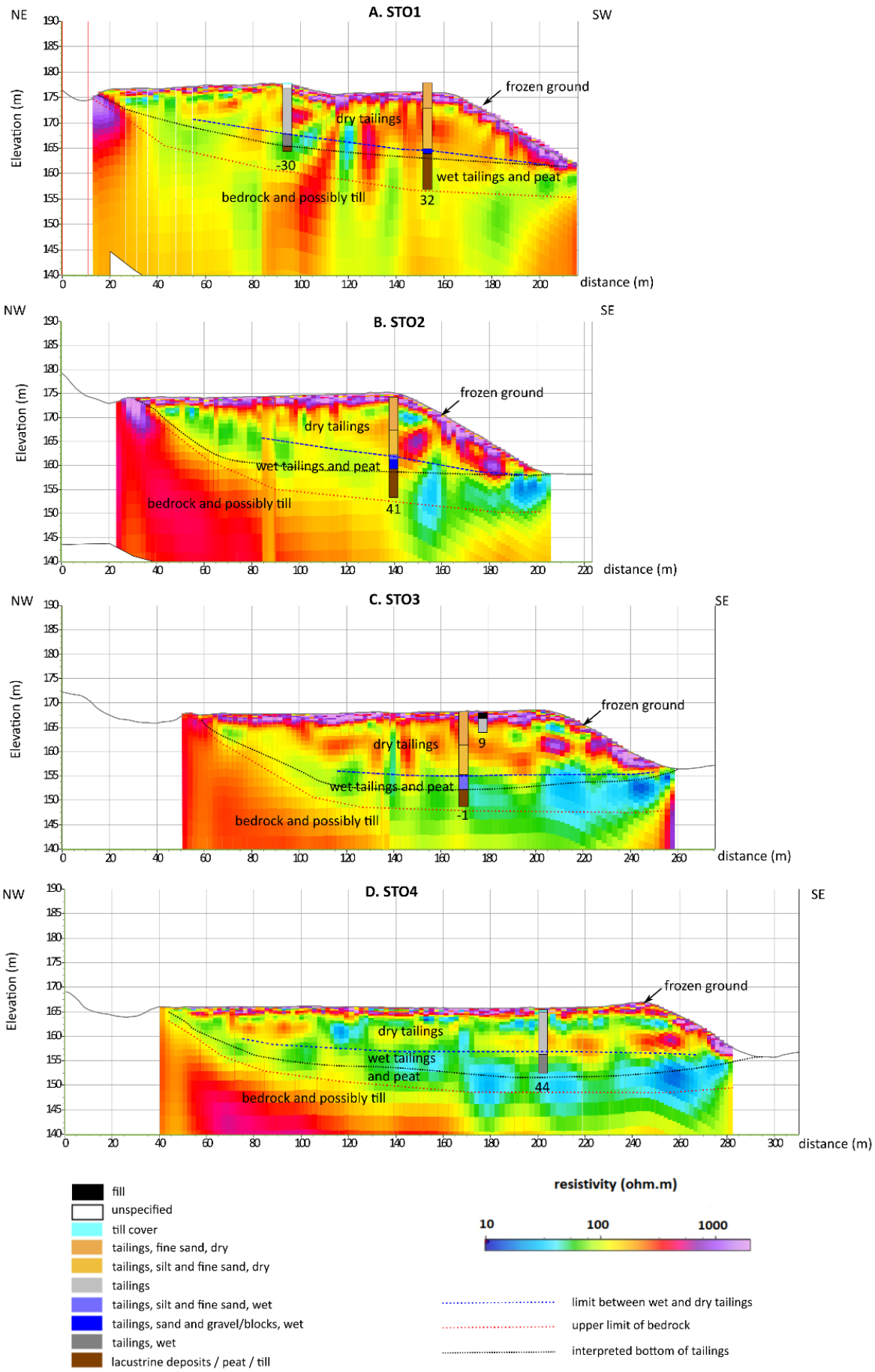
A. STO1
NE
SW
Elevation (m)
distance (m)
frozen ground
dry tailings
wet tailings and peat
bedrock and possibly till
-30
32
B. STO2
NW
SE
frozen ground
dry tailings
wet tailings and peat
bedrock and possibly till
41
C. STO3
9
-1
D. STO4
wet tailings
and peat
44
fill
unspecified
till cover
tailings, fine sand, dry
tailings, silt and fine sand, dry
tailings
tailings, silt and fine sand, wet
tailings, sand and gravel/blocks, wet
tailings, wet
lacustrine deposits / peat / till
resistivity (ohm.m)
10
100
1000
limit between wet and dry tailings
upper limit of bedrock
interpreted bottom of tailings

Boreholes were necessary to determine the depth to the different layers in the tailings deposit because the resistivity transitions on the inverted sections are relatively smooth. However, together with the borehole data the uncertainty of the interpreted depth of the base of the tailings was estimated to be of the order of several meters.

The IP data were noisy and difficult to use at Stollberg. The measured potentials are very small below the pseudo-depth of 6 m. In addition, the earlier parts of the decay curves (at least the first 10 ms) are affected by artefacts.

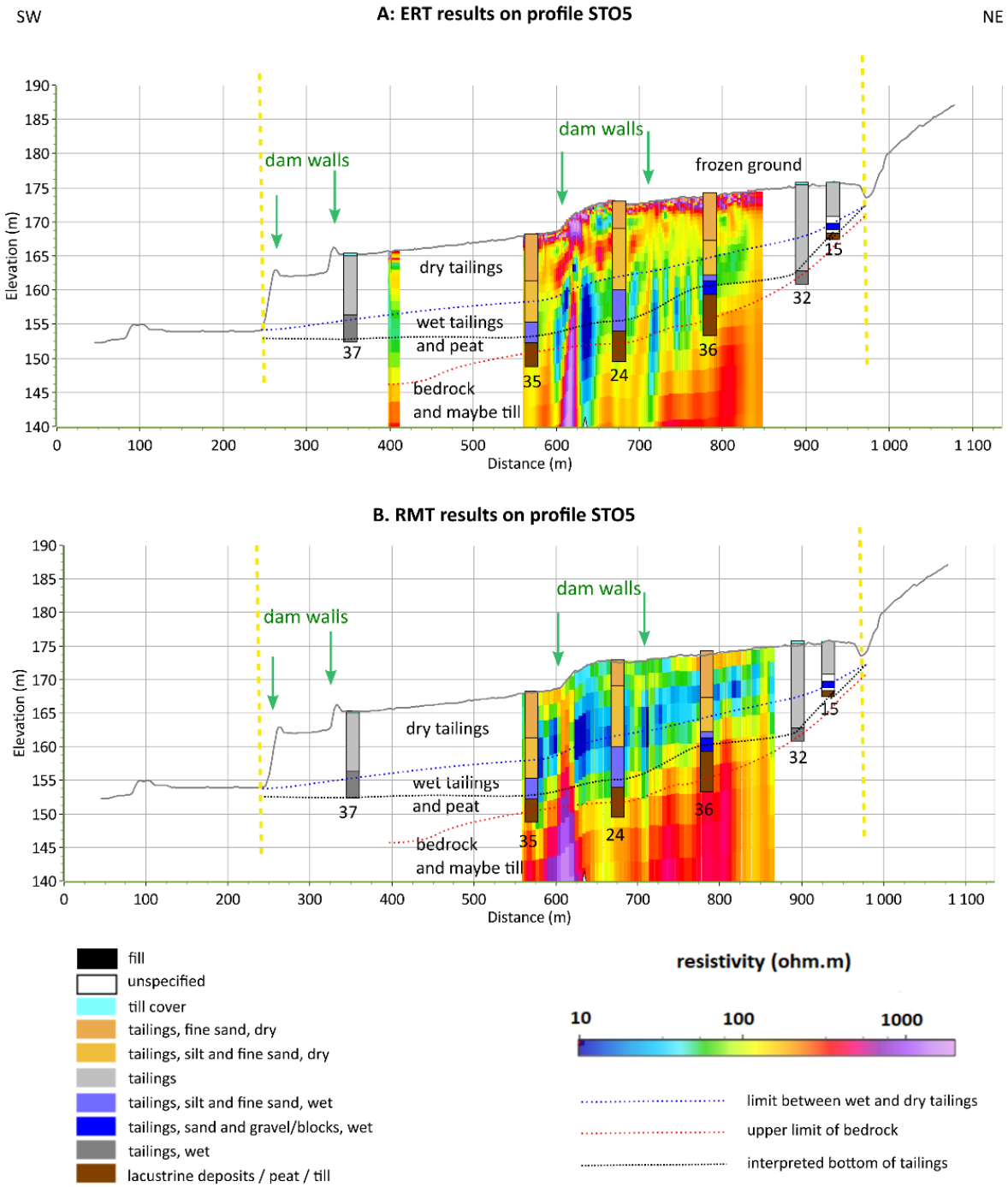

Figure 47. Resistivity models on a SW-NE profile crossing the whole repository with model from A. ERT and B. RMT. The boreholes and interpretation are presented on the models.

The SIP measurements yielded small chargeability and short time constants in the (Pelton) Cole-Cole modelling (see Fig 58, Table 5, and Appendix B). Values which were retrieved from the Debye decomposition of the laboratory results are not very different (see in appendix B). The peaks were observed a little above 6000 Hz (Appendix B, Fig. 2). The phase angles observed at 100 Hz are about 5 mrad. At 1000 Hz the observed phase shifts are 10 and 12 mrad. We have only two samples, but these measurements could explain why it was difficult to retrieve the chargeability of the tailings; the chargeability is small and the peak is at high frequency, therefore more difficult to retrieve, especially since early time-windows had to be removed. The increase of chargeability with depth measured on the samples (53mV/V for the sample between 4 and 5 m and 71 mV/V for the sample between 15 and 16 m) coincides with a slight increase in Fe content and a large increase in Pb and Zn content (see table 6). One should note that the Pb and Zn content are much lower in absolute value compared to the Fe content. At the Stollberg site an increase in Pb, Zn and Ag content was seen at depth in the boreholes (Casey et al. 2024), but also in other studies. It is reasonable to think that this leads to larger chargeability in the material, however, it is challenging to retrieve these variations from field measurements of TDIP at this site, at least with the technique used.

The radar profiles measured at Stollberg could not reach the base of the tailings or the groundwater table and they were not used in designing a 3-dimensional model of the site (Casey et al. 2024).

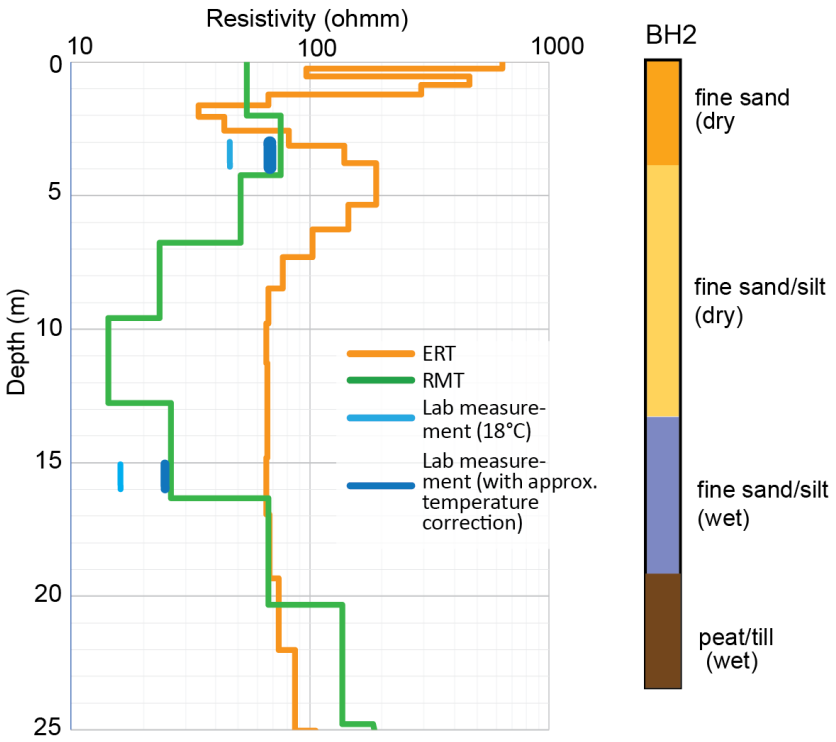

Figure 48. Comparison of ERT and RMT inversion results close to borehole BH2, results from laboratory SIP measurements and geological description of the borehole observed during drilling.

Riddarhyttefältet

The mining activities at Riddarhyttefältet were ongoing for several hundred years and consist of hundreds of abandoned mines. They were mined mainly for iron oxide and copper (Camitz et al. 2024). As part of this project, two tailings repositories, Källfallet and Bäckegruvan, were investigated with geophysical measurements and boreholes (see Fig. 1).

Källfallet

At Källfallet the tailings were deposited in the northwest area of lake Lien. Presently, the tailings lie within two separate tailings ponds (an eastern and western pond) separated by a small pine forest (Fig. 49).

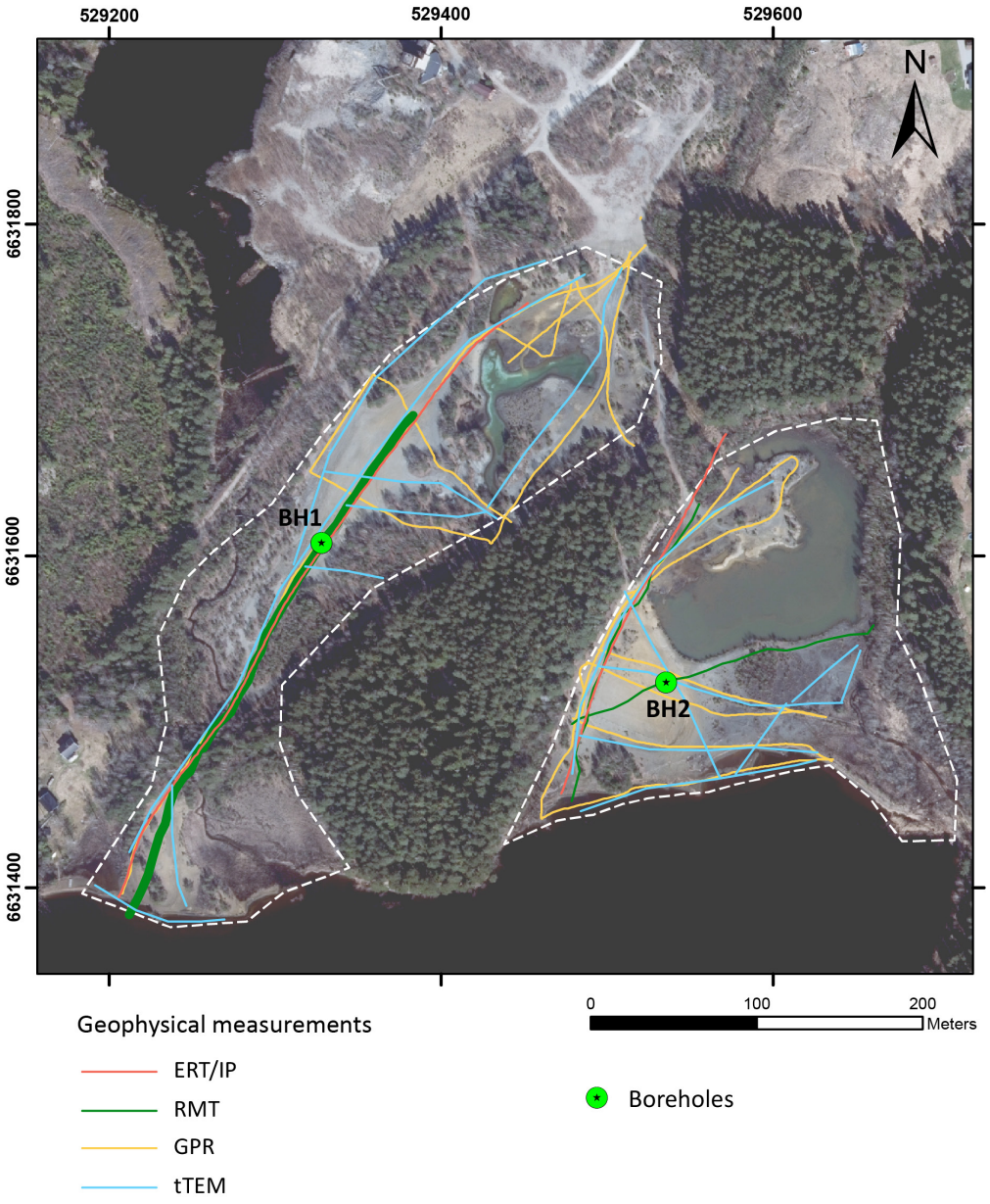

Figure 49. Orthophoto showing Källfallsgruvan tailing ponds. The dashed white lines represent the extent of the western and eastern tailing ponds. Ground geophysical measurements (lines with different colors) and boreholes (green dots) are shown on the map. The thick green line shows the location of the profile shown in Figure 50.

Geophysical measurements were conducted in the Källfallet tailings area during the spring and summer of 2021. The methods used include ERT-IP, tTEM, RMT, and GPR. The GPR and tTEM data were acquired relatively efficiently in a nearly continuous manner over the period of just half a day. Three profiles with ERT-IP using varying electrode spacing (2 and 5 m) and four RMT lines with 10 m station spacing were measured at Källfallet. Two boreholes were drilled down to the base of the tailings. In the western pond the borehole was drilled down to 7 m depth and in the eastern pond the well was drilled to 8 m depth, resulting in 21 samples of tailing material (see Fig. 49 for locations). No SIP samples were taken from this site. Chemical analysis results from surface samples and boreholes show a high iron content with an average value of 19% Fe_2O_3 and maximum value of 47% in one of the surface samples. Chemical analyses show also an elevated REE content (average 2388 ppm and max value 5989 ppm).

The IP data collected at Källfallet are of relatively low quality and are likely significantly affected by cultural noise. Consequently, no IP results could be used at this site. Figure 50 shows a comparison between the resistivity models from inversion of tTEM, ERT, RMT, and the measured GPR data. The observations in borehole (BH1) show good correlation with the resistivity models and the GPR data. The best correlation exists between the borehole observations and the RMT resistivity model. The sequence at the site, consisting of dry sand at the surface (high resistivity), underlain by wet sand (low resistivity) and finally till (very high resistivity) is resolved in the RMT model (Fig. 50C). Although the ERT and tTEM models show nearly the same resistivity trends, the boundaries in the RMT model coincide much better with the observed variations in the borehole. The GPR data seem to sharply resolve the till boundary at depth. However, the overlying boundaries (dry-wet sand) do not appear as sharply in the GPR cross-section. Approximately 60–120 m along the profile, where glaciofluvial deposits are reported in the SGU's quaternary map, a distinct high resistivity feature in the ERT models is resolved. In the same interval the GPR data reveal a rather sharp boundary overlying a higher reflectivity zone which may be caused by the variation in the underlying glaciofluvial deposits. At this location the RMT model shows a region of generally higher resistivities albeit less clearly defined than the ERT model. In the tTEM model only slightly higher resistivities can be observed at this location.

Figure 51A provides a more detailed comparison between the estimated resistivities from the tTEM, ERT, and RMT data inversions at the location of the borehole BH1. The measured iron oxide (Fe_2O_3) content and geological interpretation of the borehole during drilling are also shown. As mentioned earlier, the variations seen in the RMT model correlates best with the expected sequence observed in the boreholes. For example, the interval between 3 and 6 meters with wet fine-grained sand, silt and clay coincides with the lowest RMT resistivities (approximately 45 ohmm). The modelled ERT and tTEM resistivities do not show a distinct low resistivity feature at the same depth interval. One should also note that the RMT inversion cell size is coarser than the geological sampling interval.

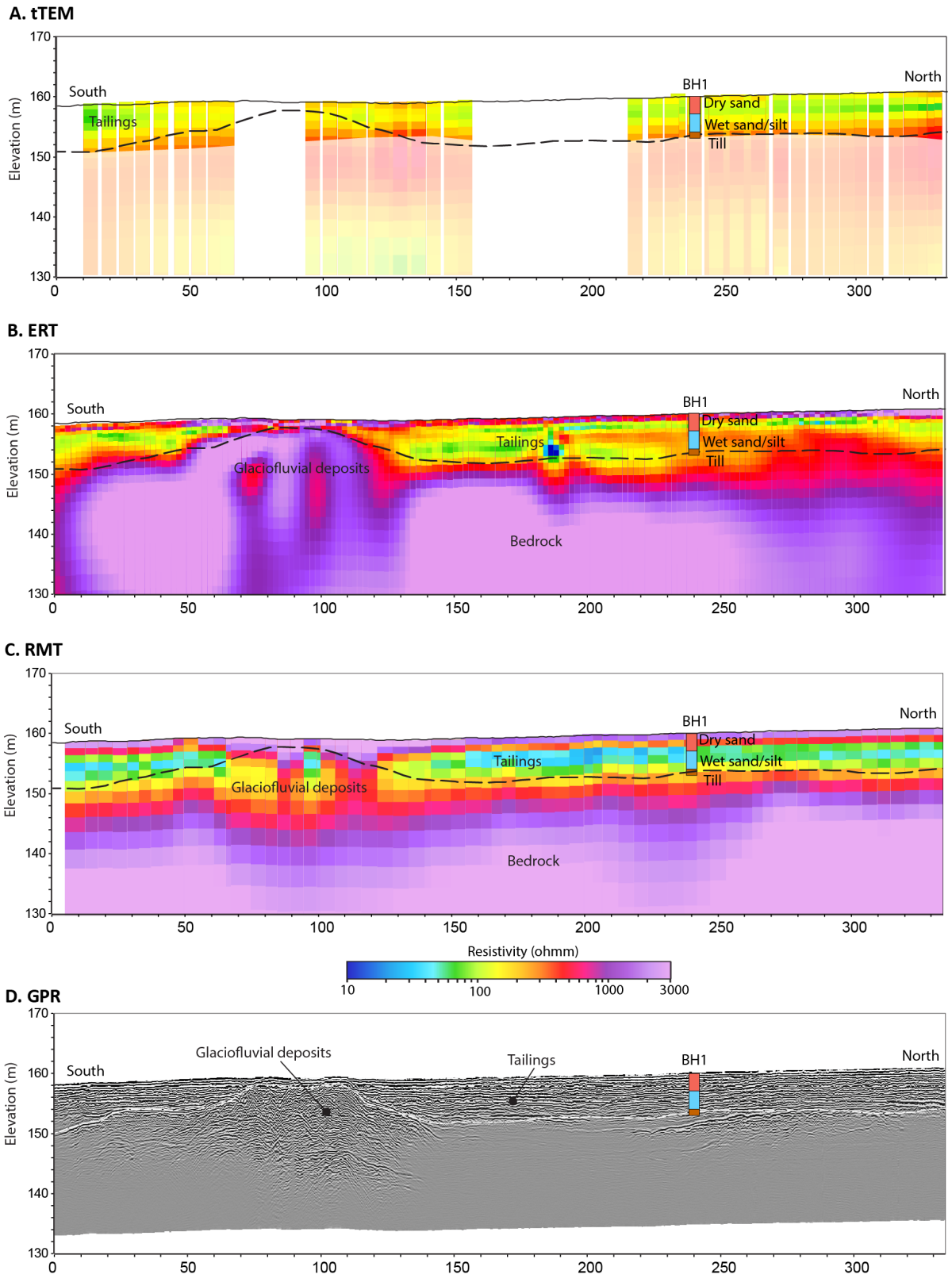

Figure 50. Profile located in the western tailing pond (Fig. 49). Resistivity models from three different methods; **A.** tTEM, **B.** ERT and **C.** RMT. **D.** Processed ground penetrating radar section (for 70 MHz source signal) recorded along the same profile as the resistivity models shown above. Borehole (BH1) with simplified geological description is shown on each section. The black dashed lines represent the interpreted base of the tailing.

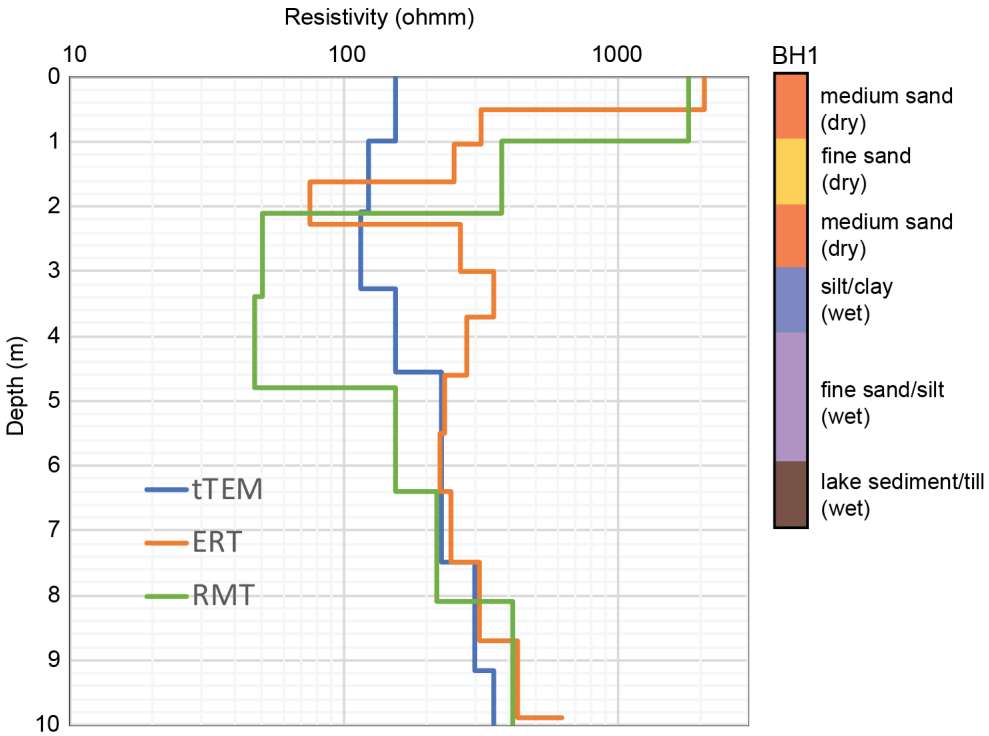

Figure 51. Resistivity models from the three different methods (tTEM, ERT and RMT) at the location of BH1 at Källfallet. The geological logs are presented for comparison.

Bäckegruvan

The tailings at Bäckegruvan were deposited within and around lake Skärsjön (Fig. 52) from as early as 1900 up until 1982 when the mining production ceased (Camitz et al. 2024). Between 1960 and 1963, the dressing plant was modified to improve the yield. The historical aerial photos from 1960 and 1975 show that the older material (before 1963) was mainly deposited in the south-western part of the tailings deposit while the younger material (after 1963) was deposited in the north-western part (Fig. 52). Today the northern part is impounded and covered with pine forest while the southern part is mostly open terrain and generally wet with the groundwater surface at the ground surface (Fig. 53). Analyses of surface samples from an earlier investigation showed high concentrations of metals including Fe, Cu, Co and REE in the tailings material (Hallberg & Reginiussen 2020).

The most extensive ground geophysical measurements within this project were performed at the Bäckegruvan tailings deposit. They include ERT-IP, GPR, RMT, and tTEM (Fig. 53). GPR and tTEM data acquisition covered a considerable part of the tailing pond and due to the terrain was acquired relatively efficiently (over about 4 hours). RMT measurements were performed along two profiles, and ten ERT-IP profiles were acquired. Unfortunately, similar problems were observed with the IP data at Bäckegruvan as at Källfallet (see previous section) where the data were of relatively low signal to noise ratio. As a result, no IP results will be shown in this report. The poor quality may be caused by inductive effects (EM-coupling), that are more significant when acquiring data with a conductive subsurface.

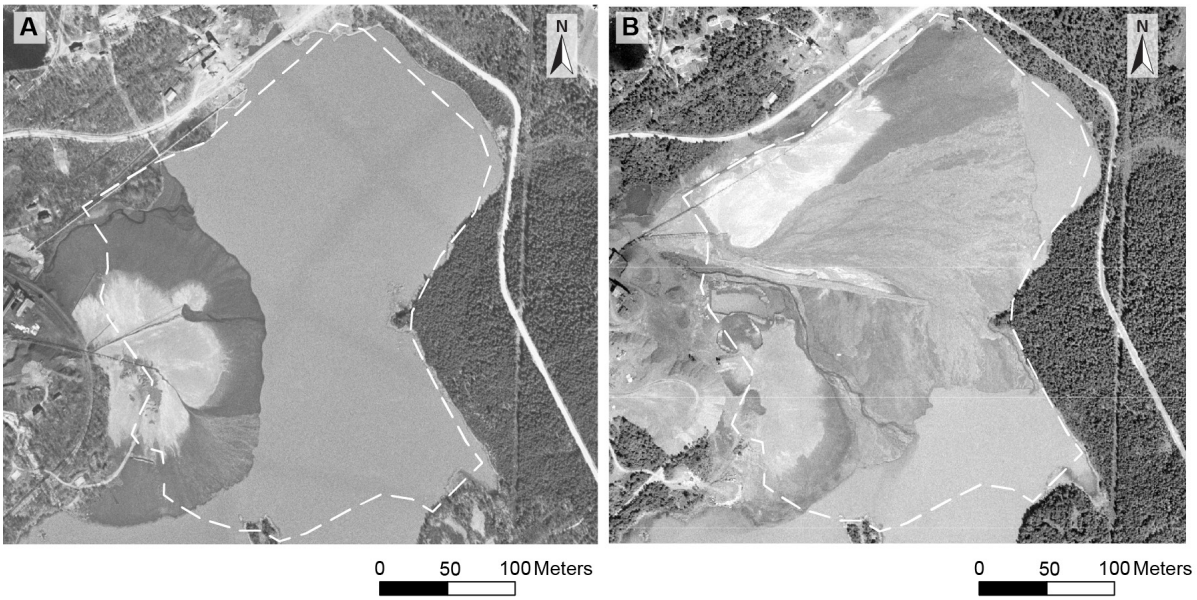

Figure 52. Aerial photos of the Bäckegruvan tailings deposit. The white dashed line shows the present-day extent of tailings deposit. **A.** Shows the tailings deposit in 1960. Here the extent of the material deposited prior to the upgrade of the processing plant, which occurred between 1960 and 1963, can be observed. **B.** Tailings deposit in 1975 where the material deposited prior to 1963 in the south-west and material after 1963 in the northern and eastern parts of the tailings deposit can be identified.

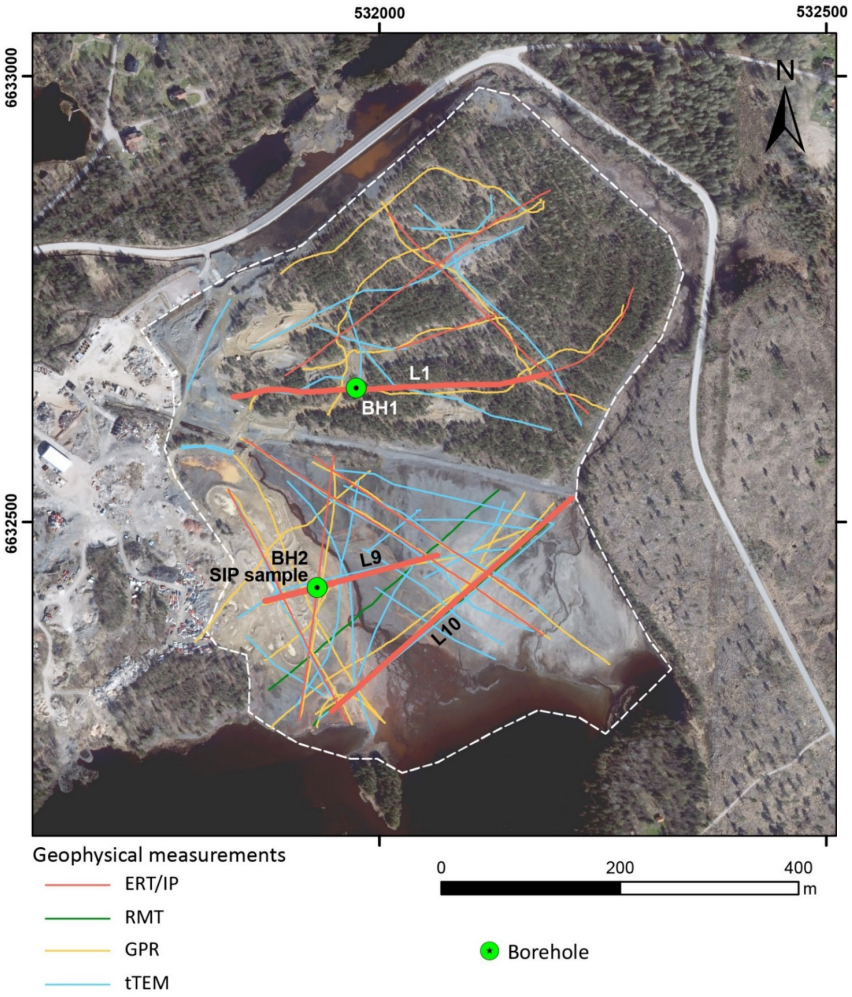

Figure 53. Location of ground geophysical measurements carried out at the Bäckegruvan tailing repository during the summer and fall of 2021. The location of ERT-IP, RMT, GPR, and tTEM profiles are shown with different colors on top of the orthophoto. The two bore-holes are marked with green symbols. Thicker lines labelled as L9 and L10 are those discussed in this report.

The resistivity models and geochemical data from surface samples were utilised to select locations for two boreholes which were drilled to investigate the tailings deposit at depth. Borehole BH1 was located in the northern part of the tailings deposit along profile L1. Borehole BH2 was located in the southern part along profile L9 (Fig. 53). Within BH2, two samples, one at 4–5 m depth and the other at 8–9 m depth were collected for SIP measurements (Table 4). Geophysical data along profile L9 and L10 located in the southern part of the tailings deposit were selected for presentation in this report. Both the ERT profiles are measured with a 2 m electrode separation.

Figure 54A–C show the resistivity models from the inversion of tTEM, ERT, and RMT data along profile L10, respectively. Figure 54D shows a processed GPR section along the same profile. The ERT and RMT resistivity models include very similar features. Specifically, both show similar variations in the upper layer, which generally has a lower resistivity, which is interpreted to correspond to the mine tailings. Both models also show a more resistive layer at depth, interpreted to correspond to the lake sediments and crystalline bedrock. In comparison, in the tTEM resistivity model (Fig. 54A) the bedrock at depth is poorly resolved, probably due to the lower penetration depth. Another explanation for the poor performance of the tTEM method could be the induced polarization effect in the TEM data as mentioned earlier in the "Methods" section.

Due to the 2 m electrode spacing used in the ERT measurements the ERT model demonstrates a considerably higher resolution in the shallower parts of the model compared to the tTEM and RMT models.

The GPR data (Fig. 54D) seem to be insensitive to deeper structures below approximately 5 m depth, where no strong reflectivity can be observed. This is probably due to the transition from the upper layer which has a relatively low resistivity (fine-grained silt) to more conductive fine-grained silt/clay at depth, where the signal is rapidly attenuated. This transition is also observed in the boreholes. However, between 80–120 m along the profile there is a good correlation between the resistivity models and the GPR data where a zone with higher resistivity and increased reflectivity can be seen. This zone coincides with the small stream (Fig. 53) and the increased resistivity and reflectivity may be caused by more sandy tailings at this location.

Based on the resistivity models, the base of the tailings is interpreted to undulate across the profile in all three models (54A–C). In addition, the material overlying the basement (interpreted to consist primarily of tailings) has lower resistivities in the southwestern part of the profile compared to the northeast. This transition in resistivities is interpreted to be coupled to the different phases of production of tailings, where the region of lower resistivities is associated with the older material deposited prior to 1963 and the higher resistivities are associated with the newer material deposited after 1963 (Figure 52). The change in resistivity of the tailings in this case is thought to be associated with the change in performance of the processing plant before and after upgrading.

The tTEM and ERT inversion results along profile L9 are presented in Figure 55 together with the geological observations from BH2. The resistivity models show similarities to the models along profile L10, where a low resistivity layer interpreted to be wet tailings overlies a more resistive layer interpreted to be lake sediments and the bedrock.

This interpretation is also supported by the borehole (BH2) which was drilled down to 14 m before reaching the lake sediments (Fig. 55). The resistivity variations within the tailings are also seen here where very low resistivities (<10 ohmm) are found in the western part of the profile and higher resistivities (30–70 ohmm) in the eastern part. These variations are interpreted to be due to variations in the composition and/or grain size between the older and younger tailings material.

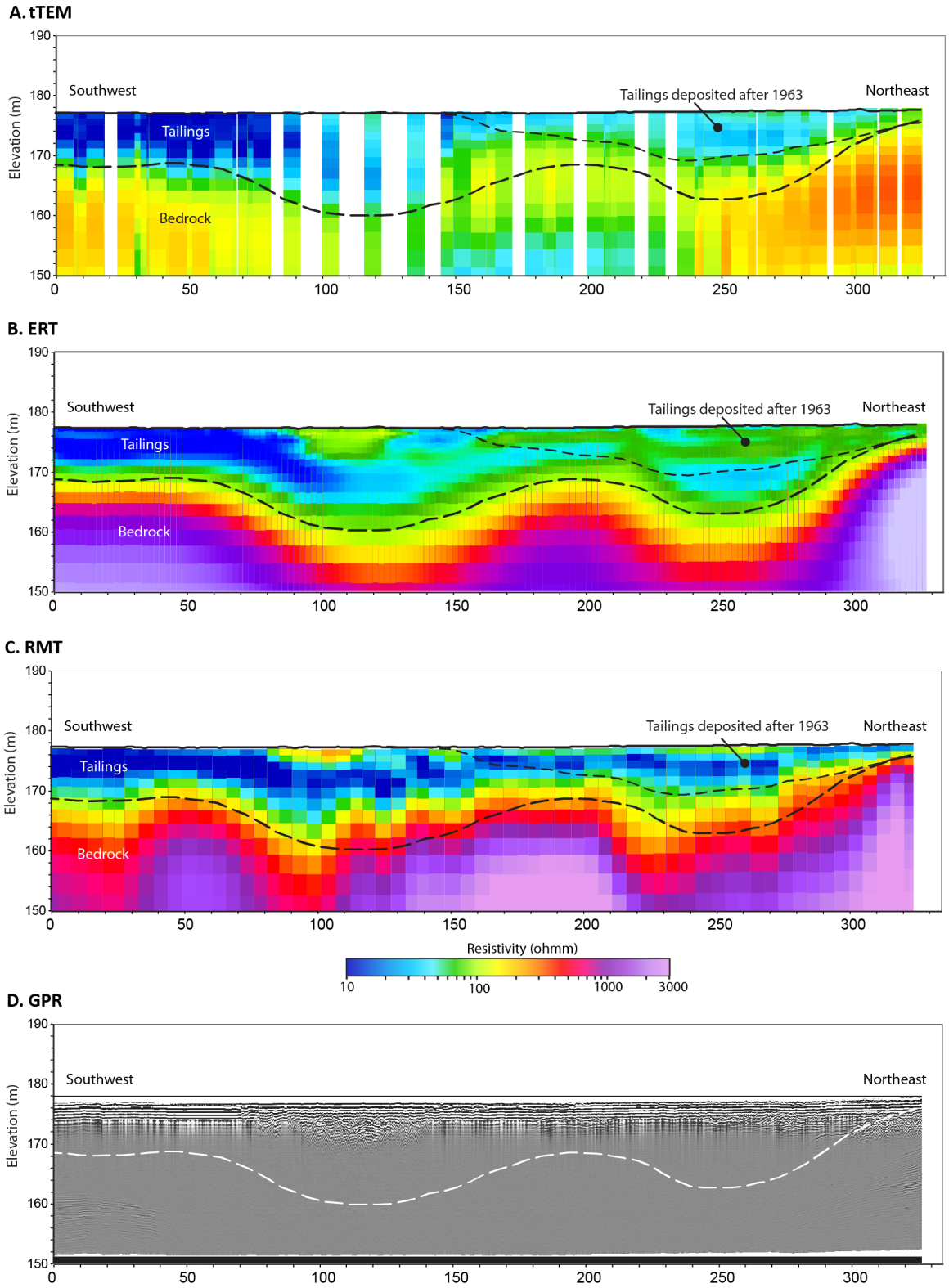

Figure 54. Resistivity model generated from **A.** tTEM, **B.** ERT, and **C.** RMT measurements along profile L10. **D.** Processed GPR data along the same profile. The deeper black dashed line represents the bottom of the tailings interpreted from resistivity the models and nearby boreholes. The uppermost thinner black dashed line marks the interpreted border between tailings deposited before and after 1963. See Figure 53 for the location of the profiles.

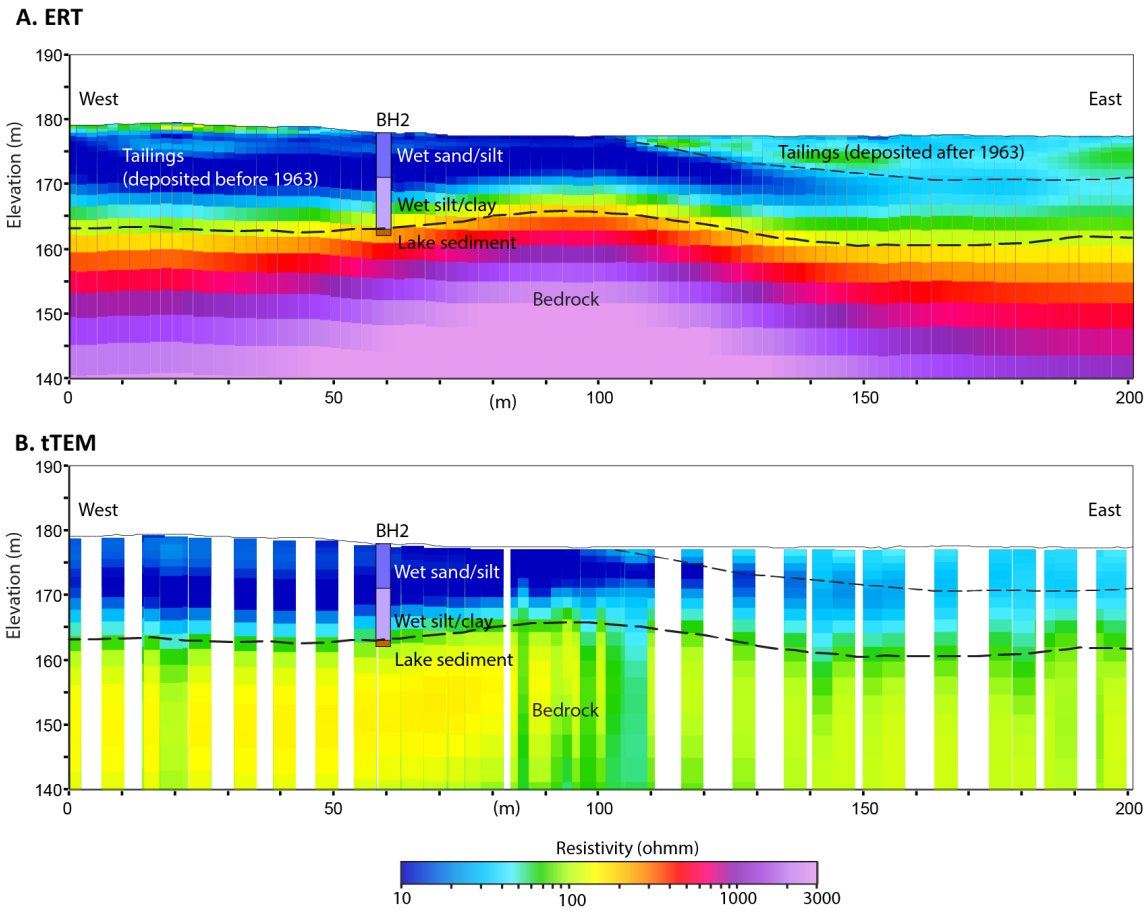

Figure 55. Resistivity model from **A.** ERT and **B.** tTEM measurements along profile L9. The lower black dashed line represents the base of the tailings interpreted from the resistivity models and nearby boreholes. The uppermost thinner black dashed line marks the interpreted border between older tailings deposited before 1963 and younger tailings deposited afterwards. See Figure 53 for the location of the profiles.

The resistivity models at the location of BH2 are compared are presented in detail in Figure 56, together with the borehole data. The ERT and tTEM model shows very similar patterns with an upper layer with resistivities of around 10–15 ohmm which extends to a depth of approximately 4 m. Below this the resistivity decreases to about 4–6 ohmm. Finally, at about 8 m depth the resistivities increase, probably due to the influence of the high resistive bedrock at the base of the sequence. This result is also in close agreement with the SIP laboratory measurements (see Fig. 58 and Appendix A) done on the samples collected at 4–5 m (14 ohmm) and 8–9 m (11 ohmm) depth (Fig. 56).

Visual observations of the tailings during drilling and sampling showed a decrease in grain size with depth; where sand was visible at the surface, followed by fine sand to silt transitioning to silt and clay at the base of the sequence. The sieving done on the SIP samples at 4–8 m depth and 8–9 m depth (Fig. 59) showed a similar pattern. The small change in resistivity seen in the upper part of the tailings may be caused by changes in the grain size were the increased silt and clay content causes the lower resistivity. The iron oxide content in the borehole is about 20% and is plotted in Figure 56.

The SIP laboratory measurements show a relatively high chargeability of 0.22 for the shallower sample B1 (see Fig. 58, Table 5 and Appendix A) but the maximum phase is reached at frequency outside the measurement range (> 10000 Hz) and far outside the frequency range for the field IP measurements. This may explain why the IP-data collected at this site was of poor quality.

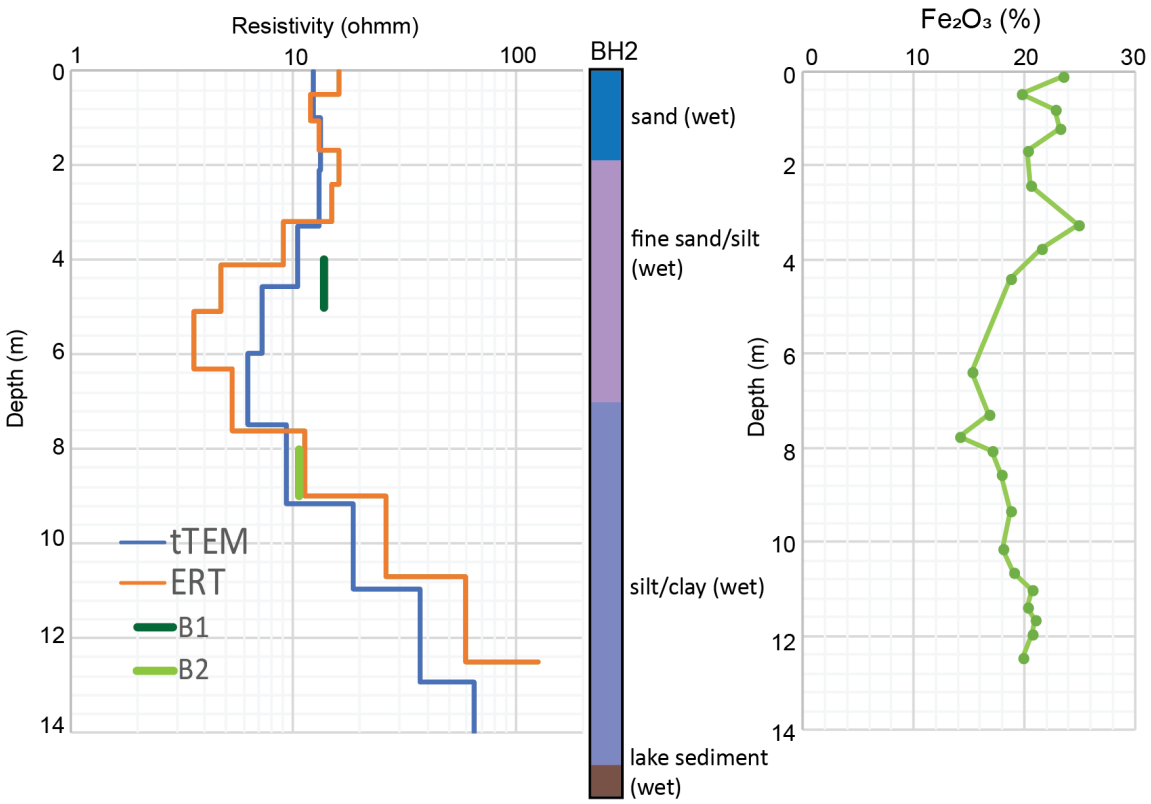

Figure 56. Resistivity models from two different methods (tTEM and ERT) at the location of BH2. The results from laboratory measurements on samples are shown for comparison. The geological description of the borehole is based on observations during drilling. See Figure 53 for the location of BH2.

The chemical analyses from both drilling and surface sampling showed that the highest concentrations in the selected elements (including Fe, Co, Cu, and REE) are found in the south-western part of the area where the tailings were deposited before 1963 (Fig. 50). The tTEM measurements have a very good coverage in the more open southern part of the area, where the older tailings were deposited. In Figure 57 the resistivity models from 0 to 5 m depths are interpolated to a grid covering the whole southern part of the tailing repository. It is evident that the western part has lower resistivity (10–20 ohmm) compared to the eastern part (40–60 ohmm) and that the low resistivity correlates with higher metal content (Fe_2O_3 and REE) in the surface samples which were analysed (Fig. 57).

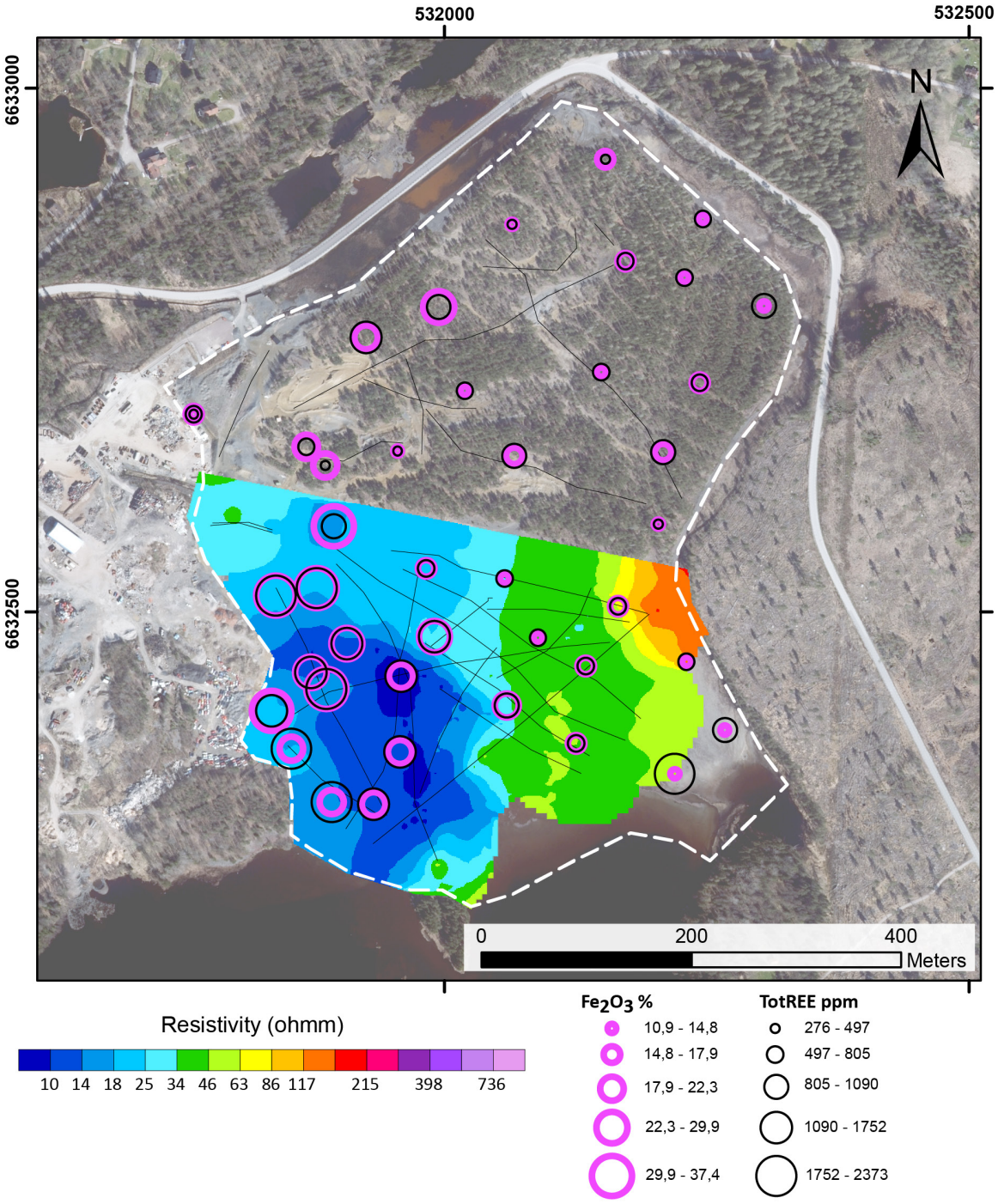

Figure 57. Interpolated tTEM resistivity models from 0–5 m depth at the Bäckegruvan tailing repository. Results from chemical analysis performed on surface samples are also shown.

Comparison of SIP laboratory data and borehole data

SIP measurements were conducted on the samples from five tailings deposits, two in 2021 (Bäckegruvan and Jan-Matsdammen) and three in 2022 (Blötberget, Yxsjöberg, and Stollberg). The final reports are attached in Appendix A and B and provide a detailed account of the laboratory measurements. The samples were placed in a four-point sample holder where two outer connections transmitted electrical current, and the two inner connections measured the potential difference. The frequency range for the measurements was 10 mHz to 10 kHz. The main motivation of the lab measurements was to study the IP response at different frequencies to observe if the results correlated with the existing standard models and to see how the response varied with different types of tailings material (i.e. with varying grain size, mineral content, etc). A comparison between the lab measurements and the models obtained with TDIP was also performed, to aid with interpretation and validation of the inversion results. Figure 58 is a compilation of results from the SIP measurements made on ten samples from the five selected sites (at each site two samples were taken from different depths). Table 5 contains the site specifications and information about the depth of the samples. Cole-Cole (CC) and Debye models could explain all the SIP measurements in the lab. Table 5 provides a summary of the estimated CC model parameters for the different samples.

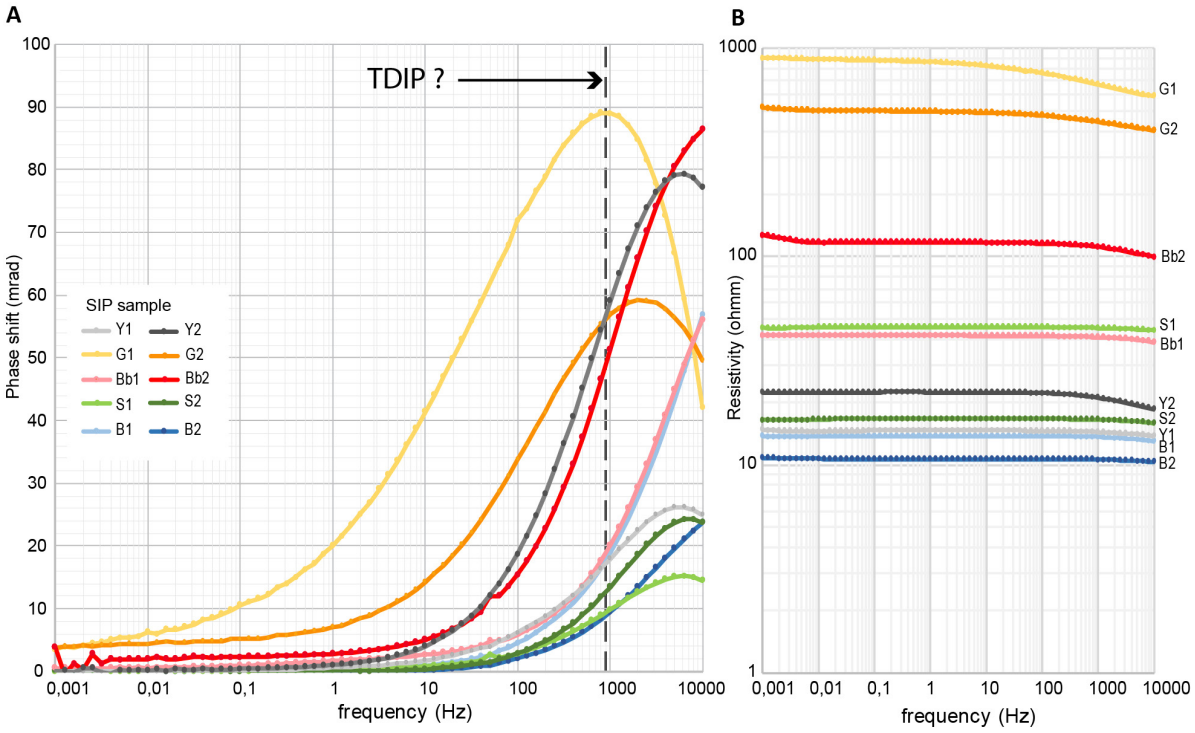

Figure 58. Results of SIP measurements made on ten samples from five tailing sites. **A.** Phase shift versus frequency. **B.** Resistivity versus frequency. The dashed grey line in A (labelled TDIP) is a very approximate estimate of the maximum resolvable frequency in the TDIP data collected in the field.

Table 6 contains results of the chemical analysis of CRMs, iron and base metals measured on the SIP samples shown in Table 5. Figure 59 shows iron content versus chargeability for the same samples. At most of the sites the same sample was used for the SIP and chemical analysis, where half of the material from a given sample was sent for chemical analysis, and the other half for laboratory SIP measurements. However, at two sites, Jan-Matsdammen and Bäckegruvan, the samples for the chemical analysis were taken from another borehole adjacent to the borehole sampled for SIP measurements. The grain size of the samples was also determined using a sieving procedure and the results are presented in Figure 60.

Tabell 5. Estimated Cole-Cole (CC) parameters using SIP measurements in the lab on the selected samples.

Sample ID	ρ_{cc} [Ωm]	m_{cc} [mV/V]	τ_{cc} [s]	C_{cc} [-]	Site name
Y1	14.6	96	2.80E-05	0.61	Yxsjöberg
Y2	22.4	258	3.90E-05	0.63	Yxsjöberg
G1	885.9	391	5.10E-04	0.43	Jan-Matsdammen
G2	501.4	269	9.60E-05	0.46	Jan-Matsdammen
Bb1	41.7	255	4.10E-06	0.59	Blötberget
Bb2	117.2	287	2.10E-05	0.60	Blötberget
S1	45.8	53	2.60E-05	0.64	Stollberg
S2	16.6	71	2.50E-05	0.74	Stollberg
B1	13.8	22	5.50E-06	0.65	Bäckegruvan
B2	10.7	76	1.10E-05	0.69	Bäckegruvan

Tabell 6. Chargeability and concentrations of CRM, iron and base metals in the SIP-samples

Sample	m_{cc}	Co ppm	Li ppm	P ppm	REE+Y ppm	Ti ppm	V ppm	W ppm	Fe_2O_3 %	Ni ppm	Cu ppm	Pb ppm	Zn ppm
Y1	0.096	30	4.6	100	131.94	530	29	680	19.95	14	460	5.9	209
Y2	0.258	37.9	7.1	130	157.09	650	39	633	23.4	7	397	4.5	183
G1	0.391	11	57.2	5.35	2127.49	900	450	20	20.36	21	9.3	8.1	48
G2	0.269	12	61.1	5.18	2362.58	990	302	18	16.35	20	14.8	6.8	54
Bb1	0.255	16	18	2.02	1840.63	1090	235	18.2	17.25	37	7	11.2	40
Bb2	0.287	10	18.4	1.86	1655.48	740	220	19.2	10.85	30	3.6	10.4	25
S1	0.053	<1	4.5	230	197.14	280	11	26.9	17.55	3	199.5	1730	3210
S2	0.071	1	4	220	171.44	330	11	29.2	17.75	3	171	3530	7200
B1	0.22	821	29.6	110	1504.06	590	7	51	19	7	438	4.1	26
B2	0.076	325	34.6	110	1141.57	580	7	64	17.99	5	330	3.8	34

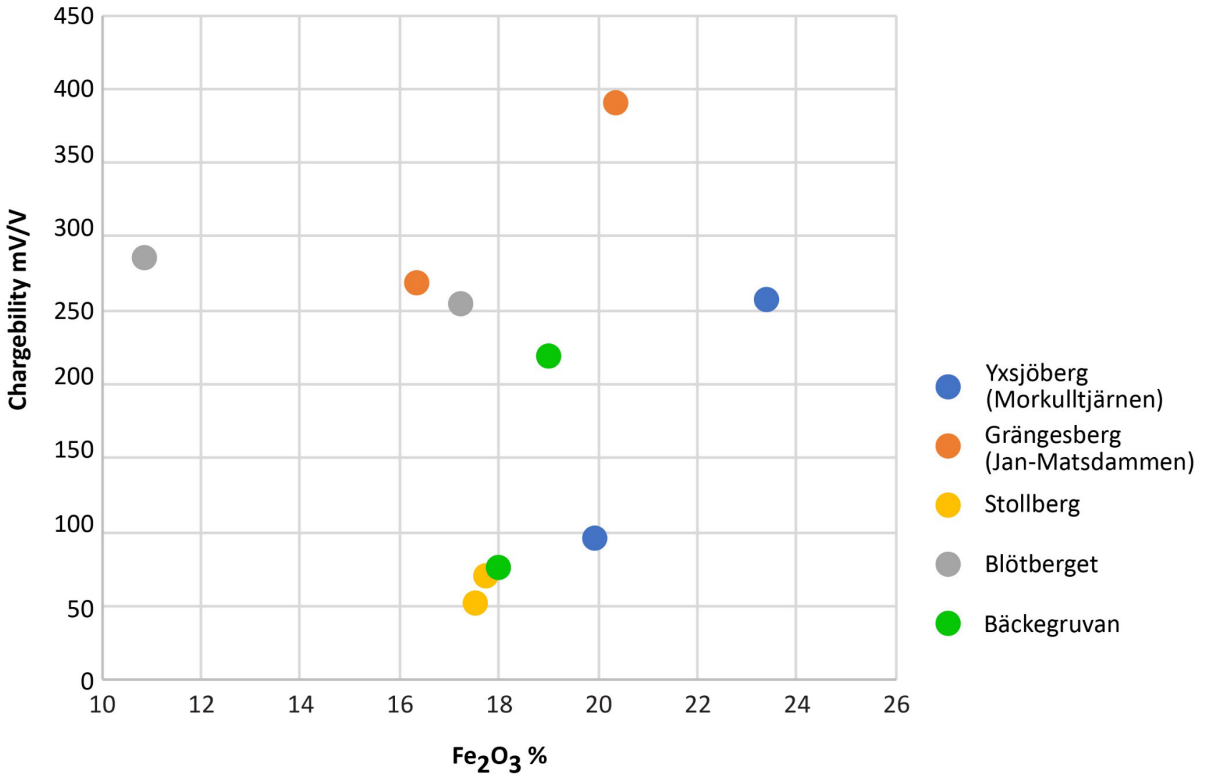

Figure 59. Chargeability obtained from lab measurements versus Fe_2O_3 content for the ten samples collected from the five different tailings sites.

The samples from Jan-Matsdammen (G1 & G2) show a distinct maximum phase peak at approximately 1000 Hz and 2000 Hz (Fig 58A). The samples from Jan-Matsdammen also exhibit the highest measured phase (Fig. 58A) and resistivity (Fig. 58B) compared to the samples from all other sites. One should note that the maximum phase for samples Y2 (Yxsjöberg) and Bb2 (Blötberget) show the same values, however, the maximums occur at considerably higher frequencies (>5000 Hz). These frequencies are beyond the maximum frequency that the TDIP measurements could resolve.

At Jan-Matsdammen the maximum phase is 90 mrad for the shallow sample (G1) and 60 mrad for the deeper one (G2). This correlates well to the iron content that is higher for G1 (20%) than for G2 (16%). Both samples consist of dry coarse sand that explains the high resistivity. One should also note that the largest grain size of all the samples belongs to G1 (60% above 200 µm) and G2 (70% above 200 µm). These samples also have the lowest frequency for maximum phase at 1 000 Hz (G1) and 2 000 Hz (G2) when compared to the other samples in the study areas. The modelled chargeability (m_{cc} in table 5) is also highest for the sample G1 (0.39) and third highest for G2 (0.269), which correlates with the measured iron contents.

The samples from Blötberget and Bäckegruvan show the largest maximum phase frequency above 10 000 Hz. This can be explained by the relatively fine-grained material in Bäckegruvan (mostly silt). However, this is not the case at Blötberget which has coarser material (especially Bb1).

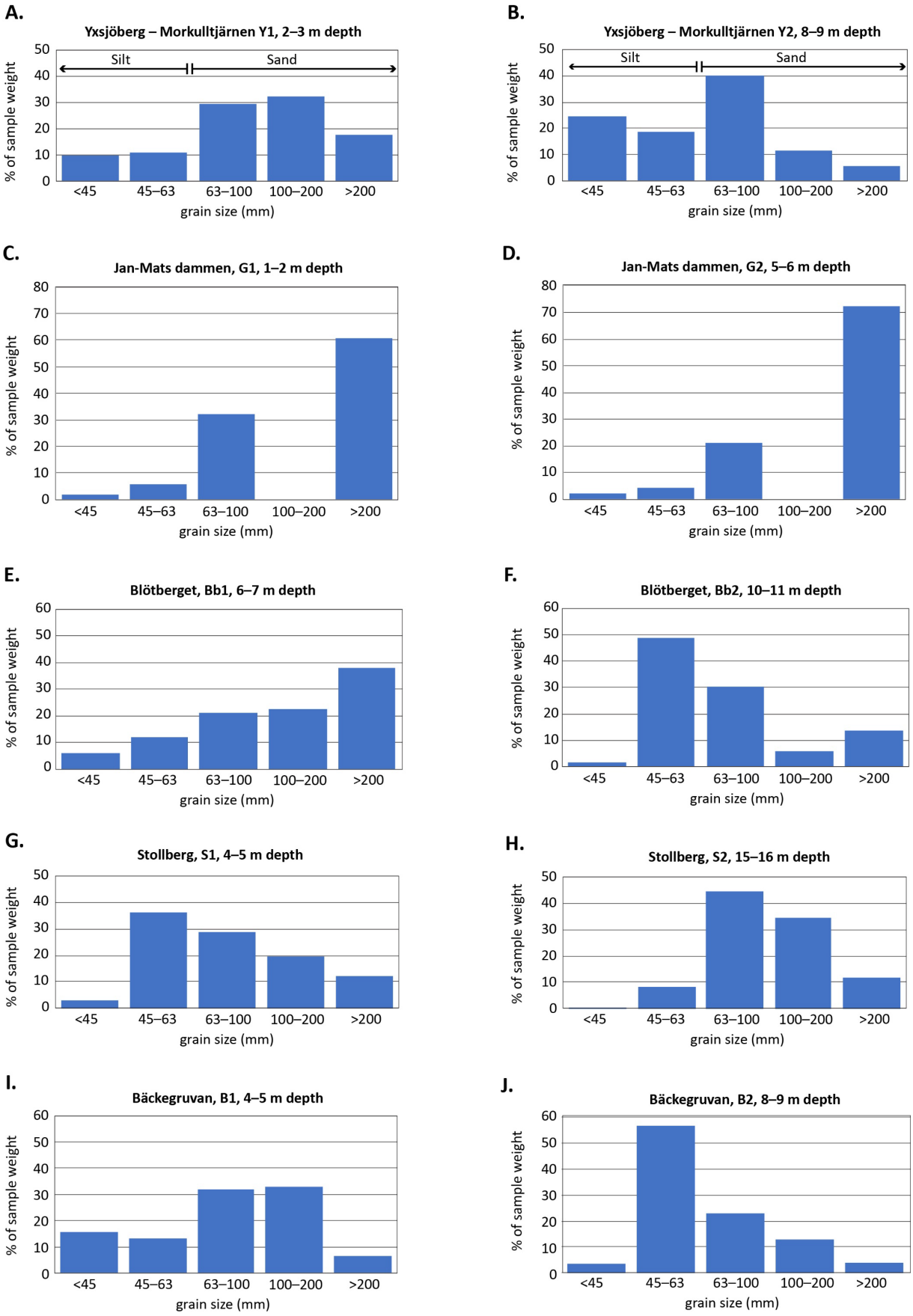

Figure 60. Results of grain size distribution measurements made on ten samples from the five tailings sites.

Discussion and conclusion

This study shows the results of investigation at eight tailing repositories using geoelectrical methods (ERT and IP), low-frequency electromagnetics (tTEM and RMT) and high-frequency electromagnetic methods (georadar). Over the eight sites there was significant variation in the physical and chemical characteristics of the tailings deposits (for example, variations in tailing composition, grain size, water content etc). Samples were taken from the surface and from within boreholes to investigate the chemical composition and grainsize of the tailings. Laboratory SIP analysis was also performed on ten samples collected at five of the tailings deposits.

When comparing the results from geophysical field measurements, laboratory, and borehole observations, it is important to consider the difference in scale over which the methods and analysis techniques operate. Specifically, the physical properties estimated from the field measurements represent a bulk value that reflect properties of a much larger volume compared to the observations made on the borehole samples. The inversion of geophysical data utilises various regularisations (e.g., vertical, and lateral smoothness) depending on the geological settings which in turn poses some limitations to the estimated parameters.

Moreover, the different signal to noise (S/N) conditions when measuring in the field compared to the laboratory-controlled environment may cause deviations of the estimated physical properties. For example, the laboratory SIP measurements have an equally good S/N for all the selected frequencies, whilst the signal for the TDIP measurements degrade at later times, corresponding to the low-frequency part of the spectrum. Lower resolution at depth for most of the field geophysical method is also a well-known issue.

Bearing in mind these limitations, the following sections summarises and discusses how the different methods and data could be combined and applied to the problem of characterisation of tailings deposits.

Extent and depth of the tailings

At all sites the resistivity models from the inversion of ERT, RMT and/or tTEM measurements, together with borehole information could be used to discriminate the tailings from their more resistive surroundings. At least two of the geophysical methods were used at every site and this turned out to be a successful strategy.

The resistivity models obtained from the ERT, tTEM and RMT measurements typically gave consistent patterns, even if the absolute values retrieved after inversion were not the same. The differences between the models are most likely due to the differences in resolution and depth of investigation for the different methods. The ERT measurements with 2 m electrode spacing gave models with the highest resolution in the near surface while the RMT models gave the greatest depth penetration.

In cases where the sequence consists primarily of water saturated tailings with low resistivity (< 100 ohmm), the base of the tailings was clearly identified with all three methods (for example at the Morkulltjärnen, Källfallet and Bäckegruvan tailings sites). In cases where there was a relatively thick sequence of highly resistive material close to the surface the ERT method had relatively low depth penetration and the base of the tailings could not be identified. This was most likely due to the poor conditions for current injection. This was the case at the Svandammen and Jan-Matsdammen where a relatively thick layer of dry sand was present or at Stollberg and Blötberget where dry sand was present which was frozen at the surface. In the cases where the near surface was resistive the RMT method gave the most reliable and consistent model of the deeper structures.

The transition from wet tailings (typically low resistivity) to lake sediments and bedrock (typically high resistivity) is rather smooth for all methods, as can be expected due to the poorer resolution with depth (and the smoothing regularisation used). Here, information from the borehole is crucial to make a more accurate interpretation of the bottom of the tailings.

Composition of the tailings

The resistivity variation within the tailing material seems to be primarily affected by changes in the water saturation and grain size (which in turn affects the effective porosity). Within this study dry sand typically showed high resistivities above 1000 ohmm while water saturated sand typically showed resistivities between 100 and 1000 ohmm. With an increased silt and clay content the water saturated tailings show resistivities below 100 ohmm.

At Hötjärnen the resistivity models obtained from both ERT and RMT measurements show three different layers that can be linked to metal content and grain size (Fig. 40). The ERT model measured with 2 m electrode spacing show the highest resolution at this site, where a thin upper layer with low resistivities (100 ohmm) is resolved. This upper interval coincides with a sand layer with increased iron content. At 14 m depth a shift in grain size occurs from sand to more fine-grained clay-rich material. This transition is also evident in the resistivity model where the resistivities change from approximately 400 ohmm to 50 ohmm. A very prominent increase in the concentration of REEs and P_2O_5 occurs at the same level. Hence, at this site it appears to be the case that high Fe-content is related to coarser grain sizes, whereas higher concentrations of REEs are associated with the finer grained clay-rich material, which in turn is associated with a lower resistivity. Therefore, in this case the results from the ERT measurements can be used to directly map and identify the layer with higher concentrations of REEs.

Bäckegruvan is another example were a variation in metal content correlates with variations in resistivity. Here we see a lateral change in resistivity in the wet sand that coincides with changes in Fe and REE content from surface samples (Fig. 57). In the southwestern part of the area lower resistivities are observed (<20 ohmm), which are associated with older tailings material with a higher concentration of metals. In the northeastern part of the area higher resistivities are observed (40–70 ohmm) corresponding to younger tailings material with lower concentrations of metals.

Comparison between field and lab resistivity measurements

At five sites the complex resistivity was measured in the lab using samples collected from boreholes (two samples at each site). This enabled a comparison between the resistivities measured in the laboratory with the resistivity models from inversions of the ERT, RMT and tTEM data. The comparisons are shown in the Figures 22, 36, 44, 48 and 56. Some of the field measurements were done in the early spring and therefore temperature corrections have been applied to the laboratory samples to simulate the field conditions. They lead to significant difference between measured lab values and estimated in-situ values. The corrections remain however approximate since we do not know the exact temperature, nor the exact correction coefficient.

The lab measurements were fitted very nicely with the Cole-Cole model there a clear MPA was constructed for all the samples taken at two depths in each borehole. The models revealed an excellent correlation between the changes observed in the grain size and MPA response. This means that the tailings with larger grain size showed lower MPA frequency (or conversely longer relaxation times). This is a classical behaviour to report.

At Morkulltjärnen and Bäckegruvan (Fig. 22 and Fig. 56) there is good agreement between the lab measurement and the resistivities inferred from ERT, RMT and tTEM measurements. Bearing in mind of course the difference in the scale and the discretization and smoothing inherent in the inversion process. At these sites the tailings are primarily water saturated with low resistivities (< 100 ohmm), as mentioned above.

At Jan-Matsdammen, Blötberget and Stollberg (Figs. 36, 44 and 48) high resistive material (dry sand and/or frozen ground) is present in the upper part of the tailings. In these sites the agreement between the lab measurement and the resistivity retrieved from the ERT-measurements is poor. The modelled resistivity generally shows much higher values compared to lab measurements. In contrast, the resistivity models retrieved from RMT show a good agreement with the lab measurements and more consistent results at two of the sites (Blötberget and Stollberg). At Jan-Matsdammen the RMT data were disturbed by cultural noise and could not be used.

tTEM were also measured at Jan-Matsdammen but not shown in Fig. 36. As mentioned previously, the resistivity models from Jan-Matsdammen showed unreliable results, due to the significant IP-effect in the collected data.

SIP laboratory measurements and TDIP measurements

The SIP laboratory measurements on the samples showed that for all ten samples the complex resistivity can be fitted to CC and Debye models. There are also noticeable variations in the amplitude and the spectrum of the phase shift observed for the different tailings. Samples from Jan-Matsdammen, Blötberget, Yxjöberg and Bäckegruvan showed chargeability over 200mV/V and phase shifts of over 50 mrad. The Fe concentrations in the samples are high (10–20%) in comparison with the other metals. No clear correlation can be seen between the Fe-content and chargeability among the ten samples as a group (Fig. 59). However, on inspection of the pairs of samples taken from the individual deposits, it can be observed that for four of the five tailings the chargeability increases with increased Fe content.

Jan-Matsdammen is the site where the TDIP measurements provided the best results, with good-quality measurements and a reasonable data fit. This provided a good basis to compare the inversion results with both the SIP measurements in the lab as well as the grain size analysis and mineral content data collected in nearby boreholes. The comparison shows interesting correlations where the high maximum phases in the SIP data correlated well with those in the MPA inversion models. The increase in chargeability was also well correlated with the increase in the metallic mineral contents such as Fe_2O_3 (Figs. 32 and 32). Models of decay constant show a fairly good correlation with the variations in the grain size distribution from the sieving data (Fig. 35).

The measured SIP data at the different sites showed an interesting correlation with the maximum phase and the grain sizes determined with different methods (Figs. 58 and 60). For example, the samples in Jan-Matsdammen have a maximum phase that occurs at frequencies that are far lower (larger grains) than those for the Bäckegruvan site (smaller grains). The results indicate that grain size and mineralogical composition (and consequently chemical composition) exert the main controls on the complex resistivity spectra.

Processing of IP decay curves is demanding in terms of time and all the data could not be processed or inverted. In many sites different regularisations and input inversions parameters resulted in very different models. There was not sufficient time to test the influence of inversion settings either. However, some general observations can be made. It has been difficult to retrieve induced polarization and SIP parameters (respectively chargeability, tau and c) from the field data for several reasons. In several cases the signal levels measured from a certain focus depth were

very low and the data were very noisy. It was then difficult to invert them in a satisfactory manner. The frequency range from the field ERT-IP data is probably limited and made it more difficult to retrieve the complex resistivity spectrum from ERT-IP field data when the peak is beyond 1000 Hz.

The IP measurements collected showed very strong negative decays and signs of high noise and even EM coupling. The question of best processing of negative decays is presently an active research topic. Hence, it is likely that considerable improvements of the estimated Cole-Cole models could be achieved in the future.

Future work

In this study the resistivity models estimated from the inversion of geoelectrical and low-frequency EM data together with borehole data were used to successfully characterise the geometry and structure of tailings deposits. A few improvements to the approach and methodology are suggested below.

To reduce the uncertainty in the interpretation and subsequent modelling one could also acquire refraction seismic data, which are sensitive to the acoustic properties of the subsurface. One would anticipate refracted events associated with the interface between the bedrock and overlying soft sediments, as well as potentially stratifications within the tailings deposit.

Induced polarization can potentially help to discriminate between tailings and their surroundings, as well as variations in the composition of the tailings deposits. Using the ERT-IP time-domain technique it would be advantageous to increase the signal-to-noise ratio of the measurements. One could for instance use more powerful transmitters to generate higher signal levels. Since nearly all deposits of mine tailings are located close to power lines and sometimes railways it is important to check the effectiveness of the background corrections. Testing the influence of the inversion settings, especially the choice of starting model, on the obtained IP inversion results is also important. With the aim of increasing the frequency range obtained and to improve the reliability of the results.

Alternatively, if one has an idea of the key frequency range for the target, one could use frequency-domain field IP measurements on a selected set of frequencies to discriminate between materials. However, a downside to this approach is that measurement over a large range of frequencies in the field can take a long time.

There are indications that a modified processing and inversion flow of tTEM measurements could potentially retrieve complex resistivity spectra with high frequency peak, but this is not yet confirmed. One can also think that ERT-IP and tTEM measurements can complement each other in attempting to recover the full frequency range.

One could also perform a joint inversion of geoelectrical and low-frequency electromagnetic data to take advantage of the different resolution and depth of investigation of the methods. This could possibly lead to a better definition of the resistivity contrasts at depth and a more accurate recovery of the resistivity of the different formations.

Finally, further investigation is needed to understand what parameters influences the induced polarization response of tailings. Measuring the spectral induced polarization response of a greater number of samples with known chemical and mineralogical composition and grain size distribution, under controlled water saturation and temperature could be very informative.

Acknowledgments

This report contains the contributions from a number of individuals. Without their dedication and knowledge, the collection of data which form the basis for all the analysis carried out would not have been possible. We would like to thank our colleagues at SGU: Johan Söderman, Sverker Olsson, Mats Thörnelöf, Robert Berggren and Jan Wittke for their commitment and high spirits in sometimes challenging field conditions. We would also like to thank the extra employees Kaveh Homagoon and Afaf Said Mohd Abu Hassan for their appreciated contribution in the field.

Torleif Dahlin from Engineering Geology, Lund University (LTH) shared precious advice about modern field procedures. He kindly provided an instrument protocol, tested LTH in-house processing on a profile and advised on some of the effects observed in the collected data.

Tina Martin, also at LTH, performed all laboratory-based SIP measurements and shared her experience and knowledge during numerous discussions and correspondence. Her help is warmly acknowledged.

The Hydrogeophysics group at Aarhus university in Denmark did all the tTEM) measurements as well as processing and inversion of the data. Presently, the inversion of tTEM data in the presence of significant induced polarization is a challenging task that requires innovation. We would like to acknowledge Pradip Kumar Maurya, Muhammad Rizwan Asif, Line Meldgaard Madsen and Jesper Bjergsted Pedersen who made extensive tests to assess and improve the inversion result in these conditions, where they shared their preliminary results and reflections with us.

Gianluca Fiandaca at Università degli Studi di Milano in Italy kindly accepted to attend a meeting where he shared his expertise on the processing and inversion of IP data with us.

Personnel from Aarhus GeoSoftware were always prompt in answering our questions, finding solutions and updating the software for our needs.

We thank Lee Slater from Rutgers University Newark, New Jersey, USA for his encouragement at the beginning of the study.

Finally, we thank Daniel Sopher for taking the time to review our manuscript and providing constructive feedback to improve it.

References

Archie, G. E., 1942: The electrical resistivity log as an aid in determining some reservoir characteristics. *Transactions of the AIME*, *146*(01), 54–62.

Auken, E., Christiansen, A.V., Jacobsen, B.H., Foged, N., & Sørensen, K.I., 2005: Piecewise 1D Laterally Constrained Inversion of resistivity data. *Geophysical Prospecting*, *53*, 497–506. doi: 10.1111/j.1365-2478.2005.00486.x.

Auken, E., Christiansen, A.V., Westergaard, J.A., Kirkegaard, C., Foged, N., & Viezzoli, A., 2009: An integrated processing scheme for high-resolution airborne electromagnetic surveys, the SkyTEM system. *Exploration Geophysics 40*, 184–192.

Auken, E., Foged, N., Larsen, J.J., Lassen, K.V.T., Maurya, P. K., Dath, S.M., & Eiskjær, T.T., 2019: tTEM – a Towed transient electromagnetic system for detailed 3D imaging of the top 70 m of the Subsurface. *Geophysics 84 (1)*, E13-E22. doi: 10.1190/geo2018-0355.1.

Bastani, M., 2001: EnviroMT - A new controlled source/radio magnetotelluric system. Ph.D. thesis, *Acta Universitatis Upsaliensis*, Uppsala Dissertations from the Faculty of Science and Technology 32.

Bastani, M., & Pedersen, L.B., 2001: Estimation of magnetotelluric transfer functions from radio transmitters. *Geophysics 66*, 1038–1051, doi: 10.1190/1.1487051.

Bastani, M., A. Savvaidis, L. B. Pedersen, & T. Kalscheuer, 2011: CSRMT measurements in the frequency range of 1–250 kHz to map a normal fault in the Volvi basin, Greece. *Journal of Applied Geophysics 75*, 180–195. doi: 10.1016/j.jappgeo.2011.07.001.

Bastani, M., Hübert., J., Kalscheuer, T., Pedersen, L.B., Godio, A. & Bernard, J. 2012: 2D joint inversion of RMT and ERT data versus individual 3D inversion of full tensor RMT data: An example from Trecate site in Italy. *Geophysics* 77, WB233-WB243. doi: /10.1190/geo2011-0525.1.

Bastani, M., Persson, L., Beiki, M. & Harinen, R., 2013: A radio magnetotelluric study to evaluate the extents of a limestone quarry in Estonia. *Geophysical Prospecting* 61, 678–687. doi: /10.1111/j.1365-2478.2012.01101.x

Bastani, M., Persson, L., Mehta, S. & Malehmir, A., 2015: Boat-towed radio-magnetotellurics – A new technique and case study from the city of Stockholm. *Geophysics* 80, B193-B10. doi: /10.1190/geo2014-0527.1.

Bérubé C., 2024: Machine learning of complex conductivity anisotropy, *7th International IP workshop*, Lund, S1_07.

Binley, A., Slater, L., 2020: Resistivity and Induced Polarization, theory and applications to the near-surface Earth, Cambridge University Press.

Bücker, M., Orozco, A. F., & Kemna, A., 2018: Electrochemical polarization around metallic particles – Part 1: The role of diffuse-layer and volume-diffusion relaxation. *Geophysics*, *83*(4), E203-E217.

Campbell, D.L. and Fitterman, D.V., 2000: Geoelectrical Methods for Investigating Mine Dumps. In: *Proceedings of the 5th International Conference on Acid Rock Drainage* (ICARD), Vol. 2, Denver, 21–24 May 2000, Society for Mining, Metallurgy, and Exploration, Inc., Littleton, 1513–1523

Casey, P. Brolin, C. Persson, L. Sopher D. Leroux, V. & Persson, S., 2024: Characterisation of mining waste in central and western Bergslagen, Sweden. *SGU-rapport 2024:02*, Sveriges geologiska undersökning.

Camitz, J. Rauséus, G, Jönberger, J. Persson, L. Sopher, D & Bastani, M., 2024: Characterisation of mining waste in central and southern Bergslagen, Sweden. *SGU-rapport 2024:03*, Sveriges geologiska undersökning.

Christiansen, A. V., & Auken, E., 2012: A global measure for depth of investigation. *Geophysics, 77*, WB171-WB177.

Coperey, A., Revil, A., Abdulsamad, F., Stutz, B., Duvillard, P.-A., & Ravanel, L., 2019: Low-frequency induced polarization of porous media undergoing freezing: preliminary observations and modeling. *Journal of Geophysicsl Research: Solid Earth* (124), 4523–4544.

Dahlin, T., & Loke, M. H., 2015: Negative apparent chargeability in time-domain induced polarisation data. *Journal of Applied Geophysics*, *123*, 322–332.

Dahlin, T., & Leroux, V., 2012: Improvement in time-domain induced polarization data quality with multi-electrode systems by separating current and potential cables. *Near Surface Geophysics*, *10*(6), 545–565.

Dahlin, T., & Zhou, B., 2006: Multiple-gradient array measurements for multichannel 2D resistivity imaging. *Near Surface Geophysics*, 113–123.

Dahlin, T., & Zhou, B., 2004: A numerical comparison of 2D resistivity imaging with 10 electrode arrays. *Geophysical Prospecting, 52*, 379–398.

Dahlin, T., Leroux, V., & Nissen, J., 2002: Measuring techniques in induced polarisation imaging. *Journal of Applied Geophysics, 50*, 279–298.

Eadie, T., Legault, J., Plastow, G., Prikhodko, A., & Tishin, P., 2018: VTEM ET: An improved helicopter time-domain EM system for near surface applications. *ASEG Extended Abstracts*, doi: 10.1071/ASEG2018abW9_3H

Fiandaca, G., Olsson, P. I., Maurya, P. K., Kühl, A., Bording, T., Dahlin, T., & Auken, E., 2022: Heterodox transients in time-domain-induced polarization. *Geophysics*, *87*(1), E35-E47.

Fiandaca, G., Madsen, L. M., & Maurya, P. K., 2018: Re-parameterisations of the Cole-Cole model for improved spectral inversion of induced polarization data. *Near Surface Geophysics, 16*, 385–399.

Fiandaca, G., Ramm, J., Binley, A., Gazoty, A., Christiansen, A. V., & Auken, E., 2013: Resolving spectral information from time domain induced polarization data through 2-D inversion. *Geophysical Journal International*, *192*(2), 631–646.

Envipro miljöteknik., 2004: Efterbehandling av sandmagasin i Stollbergsområdet, huvudstudie – Effekter av äldre silver, bly och zinkbrytning i Smedjebackens kommun. Linköping.

Gagnon, J.L., 2024: Integration of rock anisotropy in the GEMTIP model, *7th International IP workshop*, Lund, S1_10.

Ghorbani, A., Camerlynck, C. & Florsch, N., 2009: CR1Dinv: A Matlab program to invert 1D spectral induced polarization data for the Cole–Cole model including electromagnetic effects: 2009, *Computers & Geosciences* 35(2), 255–266.

Günther, T., & Martin, T., 2016: Spectral two-dimensional inversion of frequency-domain induced polarization data from a mining slag heap. *Journal of Applied Geophysics*, 135, 436–448, doi: /10.1016/j.jappgeo.2016.01.008.

Goldman, M.M., & Fitterman, D. V., 1987: Direct time-domain calculation of the transient response for a rectangular loop over a two-layer medium, *Geophysics 52*, 997–1006, doi: /10.1190/1.1442735

GRANGEX, 2023: *GRANGEX Apatit. Tekniska rapporter.* <https://grangesbergexploration.se/verksamheter/apatitprojektet/apatit-tekniska-rapporter/> Last accessed Januari 20, 2023.

Hallberg, A. & Reginiussen, H., 2018: Slutrapportering av regeringsuppdrag: Kartläggning av innovationskritiska metaller och mineral. *Regeringsrapport 2018:05,* Sveriges geologiska undersökning, 90 s.

Hallberg, A. & Reginiussen, H., 2020: Critical raw materials in ores, waste rock and tailings in Bergslagen. *SGU–rapport 2020:38*, Sveriges geologiska undersökning, 60 s.

Hupfer, S., Martin, T., Weller, A., Günther, T., Kuhn, K., Djotsa Nguimeya Ngninnjio, V., & Noell, U., 2016: Polarization effects of unconsolidated sulphide-sand mixtures. *Journal of Applied Geophysics, 135*, 456–4654.

HydroGeophysics Group, 2022: tTEM mapping Bergslagen. *HydroGeophysics Group – Aarhus University. Report number 0405202*, 31 pp.

Hällström, L.P.B., Alakangas, L. & Martinsson, O., 2018: Geochemical characterization of W, Cu and F skarn tailings at Yxsjöberg, Sweden. *Journal of Geochemical Exploration 194*, 266–279.

Ingeman-Nielsen, T., Baumgartner, F., 2006: CR1Dmod: A Matlab program to model 1D complex resistivity effects in electrical and electromagnetic surveys. *Computers & Geosciences*, *32*(9), 1411–1419.

Isunza Manrique, I., Caterina, D., Dumont, M., Mignon B., Masse A., Kessouri P., & Nguyen, F., 2022: Characterization of past metallurgical residues using geophysical imaging: A case study of Duferco site (Belgium). *Capri, Italy: 6th symposium on circular economy and urban mining, sum 2020-UROWASTE SRL*. <https://hdl.handle.net/2268/293065> Last accessed November 25, 2024.

Keller, G.V., & Frischknecht, F.C., 1966: Electrical methods in geophysical prospecting.

Kemna, A., Binley, A., Cassiani, G., Niederleithinger, E., Revil, A., Slater, L., Williams, K.H., Flores Orozco, A, Haegel, F.-H., Hördt A., Kruschwitz S., Leroux, V., Titov, K., & Zimmermann, E., 2012: An overview of the spectral induced polarization method for near-surface applications. *Near Surface Geophysics*, *10*(6), 453–468.

Kemna, A., 2000: *Tomographic inversion of complex resistivity – Theory and Application*. Der Andere Verlag, Osnabrück, Germany

Kratzer, T. & Macnae, J., 2012: Induced polarization in airborne EM. *Geophysics 77,* E317-E327, doi: 10.1190/geo2011-0492.1.

Lesmes, D. P., & Frye, K. M., 2001: The influence of pore fluid chemistry on the complex conductivity and induced-polarization responses of Berea sandstone. *Journal of Geophysical Research*, 106(B3), pp. 4079–4090.

Lévy, L., Maurya, P. K., Byrdina, S., Vandemeulebrouck, J., Sigmundsson, F., Árnason, K., Ricci, T., Deldicque, D., Roger, M., Gilbert, B. & Labazuy, P., 2019: Electrical resistivity tomography and time-domain induced polarization field investigations of geothermal areas at Krafla, Iceland: comparison to borehole and laboratory frequency-domain electrical observations. *Geophysical Journal International*, *218*(3), 1469–1489.

Macnae, J., 2016: Quantifying Airborne Induced Polarization effects in helicopter time domain electromagnetics: *Journal of Applied Geophysics 135*, 495–502, doi: /10.1016/j.jappgeo.2015.10.016

Madsen, L. M., Asif, M. R., Maurya, P. K., Kühl, A. K., Domenzain, D., Jensen, C., Martin T., Bastani M. & Persson, L., 2023: Comparison of tTEM-IP and ERT-IP: cases from mine tailing sites in Sweden. In: *NSG2023 29th European Meeting of Environmental and Engineering Geophysics* (Vol. 2023, No. 1, pp. 1–5). European Association of Geoscientists & Engineers.

Madsen, L. M., Fiandaca, G., Auken, E., & Christiansen, A. V., 2017: Time-domain induced polarization – an analysis of Cole–Cole parameter resolution and correlation using Markov Chain Monte Carlo inversion. *Geophysical Journal International*, *211*(3), 1341–1353.

Maierhofer, T., Hauck, C., Hilbich, C., Kemna, A., & Flores-Orozco, A., 2022: Spectral induced polarisation imaging to investigate an ice-rich mountain permafrost site in Switzerland. *The Cryosphere*, *16*(5), 1903–1925.

Martin, T., Günther, T., Weller, A., & Kuhn, K., 2021: Classification of slag material by spectral induced polarization laboratory and field measurements. *Journal of Applied Geophysics*, *194*, 104439.

Martin, T., Günther, T., Flores Orozco, A., & Dahlin, T., 2020: Evaluation of spectral induced polarization field measurements in time and frequency domain. *Journal of Applied Geophysics* (180), 104–141.

Martínez, J., Mendoza, R., Rey, J., Sandoval, S., & Hidalgo, M.C., 2021: Characterization of Tailings Dams by Electrical Geophysical Methods (ERT, IP): Federico Mine (La Carolina, Southeastern Spain). Minerals 2021, 11, 145. doi: /10.3390/min11020145

Maurya, P. K., Fiandaca, G., Christiansen, A. V., & Auken, E., 2018: Field-scale comparison of frequency- and time-domain spectral induced polarization. *Geophysical Journal International, 214*, 1441–1466.

Nabighian, M.N., & Macnae, J.C., 1991: Time Domain Electromagnetic Prospecting Methods. In: Nabighian, M.N. (Ed.): *Investigations in Geophysics No 3. Electromagnetic Methods in Applied Geophysics*. Society of Exploration Geophysicists, Oklahoma, 427–514. doi: /10.1190/1.9781560802686.ch6

Nguyen, F., Ghose, R., Isunza Manrique, I., Robert, T., & Dumont, G., 2018: Managing past landfills for future site development: A review of the contribution of geophysical methods. In: *Proceedings of the 4th International Symposium on Enhanced Landfill Mining,* 27–36. <https://hdl.handle.net/2268/225435> Last accessed November 25, 2024.

Nordsiek, S., & Weller, A., 2008: A new approach to fitting induced polarization spectra. *Geophysics, 73*(6).

Olsson, P.-I., Dahlin, T., Fiandaca, G., & Auken, E., 2015: Measuring time-domain spectral induced polarization in the on-time: decreasing acquisition time and increasing signal-to-noise ratio. *Journal of Applied Geophysics* (123), 316–321.

Olsson, P.-I., Fiandaca, G., Larsen, J. J., Dahlin, T., & Auken, E., 2016: Doubling the spectrum of time-domain induced polarization by harmonic de-noising, drift correction, spike removal, tapered gating and data uncertainty estimation. *Geophysical Journal International* (207), 774–784.

Palacky, G., 1987: Resistivity Characteristics of Geological Targets. In: Nabighian, M. (Ed): *Electromagnetic Methods in Applied Geophysics-Theory*. Society of Exploration Geophysicists Tulsa, 53–129. doi: 10.1190/1.9781560802631.ch3

Palo, M., 2021: Evaluation of the applicability of geophysical methods when characterizing mine waste in Yxsjöberg, Sweden. Luleå University of Technology. Retrieved from <http://urn.kb.se/resolve?urn=urn:nbn:se:ltu:diva-82837>

Parasnis, D.S., 1997: *Principles of Applied Geophysics*. 5th Edition, Chapman and Hall, London.

Pedersen, L.B., & Engels, M., 2005: Routine 2D inversion of magnetotelluric data using the determinant of the impedance tensor. *Geophysics 70* (2), G33–G41, doi: 10.1190/1.1897032.

Pedersen, L.B., Bastani, M., & Dynesius, L., 2006: Some characteristics of the electromagnetic field from radio transmitters in Europe: *Geophysics 71*, G279–G284, doi:10.1190/1.2349222

Pelton, W. H., Ward, S. H., Hallof, P. G., Sill, W. R., & Nelson, P. H., 1978: Mineral discrimination and removal of inductive coupling with multifrequency IP. *Geophysics, 43*(3), 588–609.

Persson, L., 2001: *Plane Wave Electromagnetic Measurements for Imaging Fracture Zones*. PhD thesis. Acta Universitatis Upsaliensis, Uppsala Dissertations from the Faculty of Science and Technology 30.

SIP measurements on four sandy tailing samples

Tina Martin

REPORT 2022-01

Engineering geology
Faculty of Engineering
Lund university

SIP MEASUREMENTS ON FOUR SANDY TAILING SAMPLES

Report for order 2021-27068/2MW

LUND UNIVERSITY

LTH
FACULTY OF ENGINEERING

Lund, 2022-01-20

Tina Martin
tina.martin@tg.lth.se

Summary

Spectral induced polarisation (SIP) was measured on four samples in their original water saturation condition. The results showed resistivities between 10 Ωm (Bäckegruvan samples) and 1000 Ωm (Grängesberg samples). The phase shift was quite high for the Grängesberg samples (up to -90 mrad) with a maximum at a frequency of approximately 1000 Hz. Lower values (approximately -5 mrad) were measured at low frequencies. The Bäckegruvan samples show almost no phase effects at the entire low frequency range until up to around 30 Hz but increased at higher frequencies. That increase is due to polarisation processes at higher frequencies (> 10 kHz) but partly also due to electromagnetic high frequency effects. The differences in resistivities between all samples is probably mainly related to the different water saturation conditions while the high phase values might be linked to metallic particles left in the tailings.

Introduction

The four samples were taken from the two mining dumps Bäckegruvan and Grängesberg (Jan Mats Dammen) and delivered some days later via mail. Each sample was stored in two plastic bags, wrapped in each other. They arrived at 2021-11-16 and the package was soaked at the bottom due to leakage from two of the samples (Bäckegruvan). But all four samples were in a good condition and could be measured.

Method & Measurements

Spectral Induced Polarisation

Spectral induced polarisation is a geoelectrical method which measures the resistivity and the phase shift between the injected current and the potential voltage signal. The resulting impedance Z^* (means the complex voltage-to-current ratio) is measured and transformed into a complex electrical resistivity that results from a multiplication of the impedance by a geometrical factor, which depends on the geometry of the sample and the measuring cell,

$$\rho^* = KZ^* = K\frac{U^*}{I^*}, \qquad (1)$$

where ρ^* is the resistivity in Ωm, K is the geometrical factor in m, U^* is the voltage in V, and I^* is the current in A. All values marked by asterisks are complex values.

The complex resistivity can be also expressed by the absolute value, $|\rho^*|$, and the phase, ϕ,

$$\rho^* = |\rho^*|\exp(i\phi), \qquad (2)$$

or, alternatively, as the real, ρ', and imaginary, ρ'', values,

$$\rho^* = |\rho^*|\exp(i\phi), \qquad (3)$$

with i=√(-1) being the imaginary unit, and

$$\tan(\phi) = \frac{\rho''}{\rho'}, \qquad (4) \qquad \text{and } |\rho^*| = \sqrt{\rho'^2 + \rho''^2}. \qquad (5)$$

While $|\rho^*|$ [Ωm] and phase ϕ [mrad] are the measurement quantities, the real component of the complex resistivity (ρ') represent the ohmic conduction which means primarily the conductivity of the fluid within a geological sample. The imaginary part (ρ'') represents the much smaller polarization part that can give information about (e.g.) grain/pore size properties. By application of the electrical field at different frequencies it is also called spectral induced polarisation (SIP).

Samples and measurements

Due to practical reasons, the samples were re-named to B1 and B2 for the two Bäckegruvan samples and G1 and G2 for the two Grängesberg samples (see also Table 1). The Bäckegruvan samples appeared as very fine grained and of black colour. The Grängesberg samples were coarser grained, dark grey coloured and interspersed with shiny (metallic?) particles.

Approximately 160 g from each sample was taken and filled homogenously into the sample holder. The condition of the samples was either highly water saturated (Bäckegruvan samples, see B1 and B2 samples in Figure 1) or medium water saturated. In any case, the original saturation was used, and no additional fluid was added.

Table 1: Table of the investigated samples.

Name	Sample name SGU	Location
B1	PCY210252: 4-5m intervall	Bäckegruvan (Prio 3 Nedre delen)
B2	PCY210256: 8-9m intervall	Bäckegruvan (Prio 3 Nedre delen)
G1	PCY210293: 1-2m intervall	Grängesberg: Jan Mats Dammen (PRIO 1 JMD_3)
G2	PCY210294: 5-6m intervall	Grängesberg: Jan Mats Dammen (PRIO 1 JMD_3)

A four-point sample holder was used as described in Kruschwitz (2008) (Figure 2a). The two outer connection plugs were used for the electrical current transmission and the two inner plugs (blue taps in Figure 2a) for the potential measurement. The sample holder was then connected to the PSIP instrument (Ontash & Ermac, see Figure 2b). The measurements were carried out at 71 frequencies in a range between 1 mHz and 10 kHz. This measurement took (with the used settings) approximately 3.5 h for each sample. All samples were repeated at least three times with varying settings and frequency ranges.

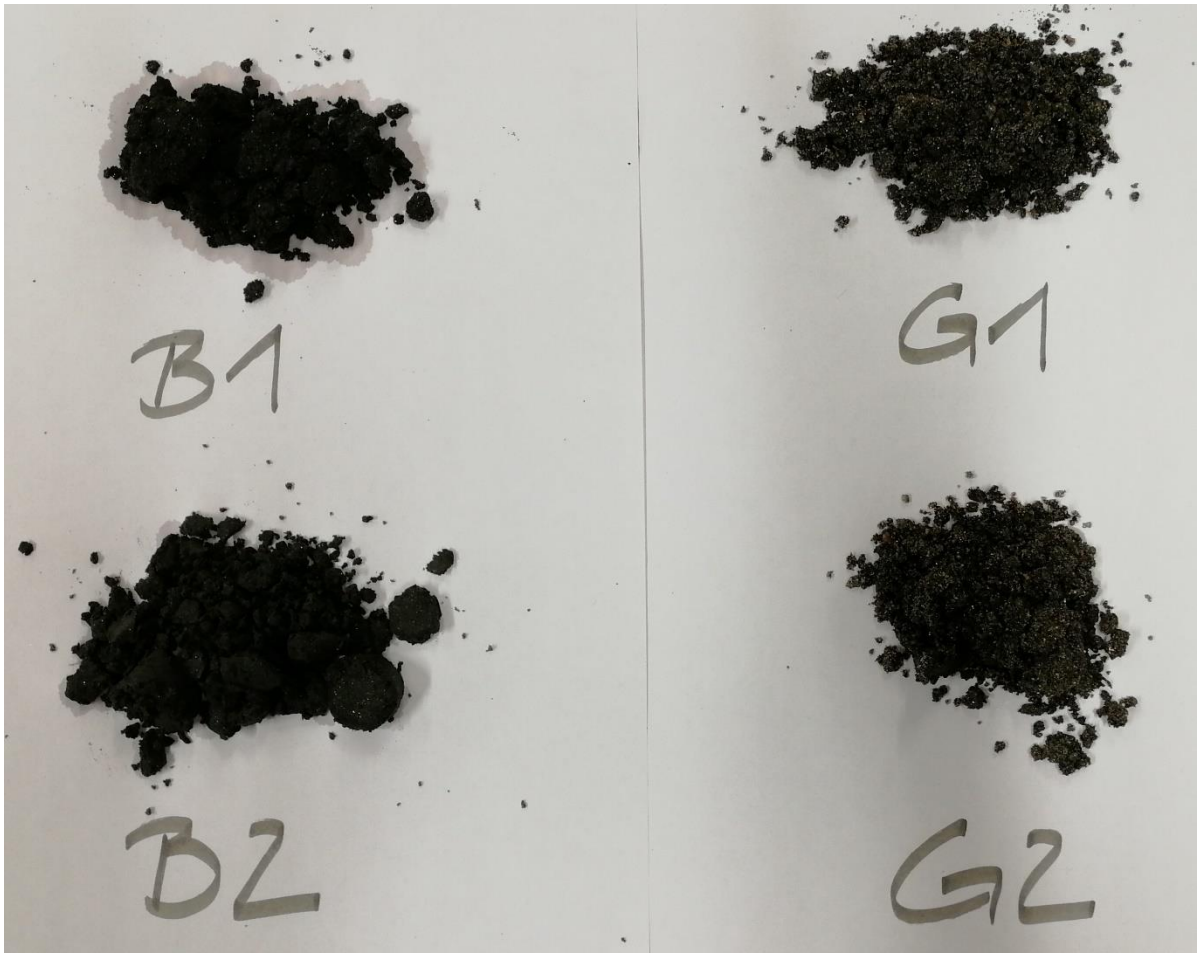

Figure 1: Photo of the measured samples. Samples B1 and B2 arrived highly saturated whereas G1 and G2 were only medium water saturated.

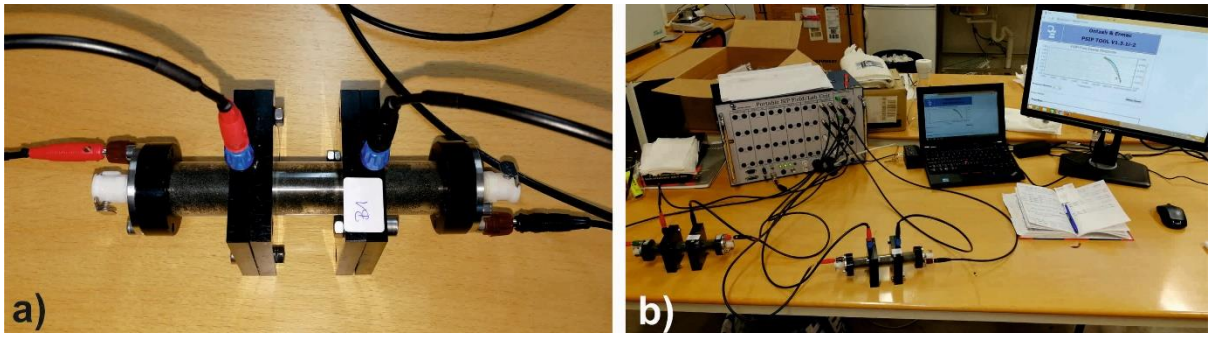

Figure 2: Photo of the used sample holder and the PSIP instrument.

Results & Discussion

Figure 3 shows the measurement results for the four samples for the resistivity (a) and the phase (b). The data quality was very good, only for the higher resistive samples (G1, G2) the frequency at 50 Hz was interfered and therefore removed.

The two Grängesberg samples G1 and G2 showed much higher resistivities (500 – 1000 Ωm) compared with the Bäckegruvan samples (10 – 14 Ωm). In phase (Figure 3b), high phase

effects at high frequencies could be observed for all samples. The phase maximum for the sample G1 and G2 is still within the frequency range and shows maximum values between -60 and - 90 mrad. At low frequencies, the Grängesberg samples do also show slightly higher phases of around -5 mrad. The maxima of the Bäckegruvan samples are at frequencies higher 10 kHz. At these frequencies, electromagnetic coupling effects cannot be ruled out and do also affect the data. For low frequencies no phase shift could be observed.

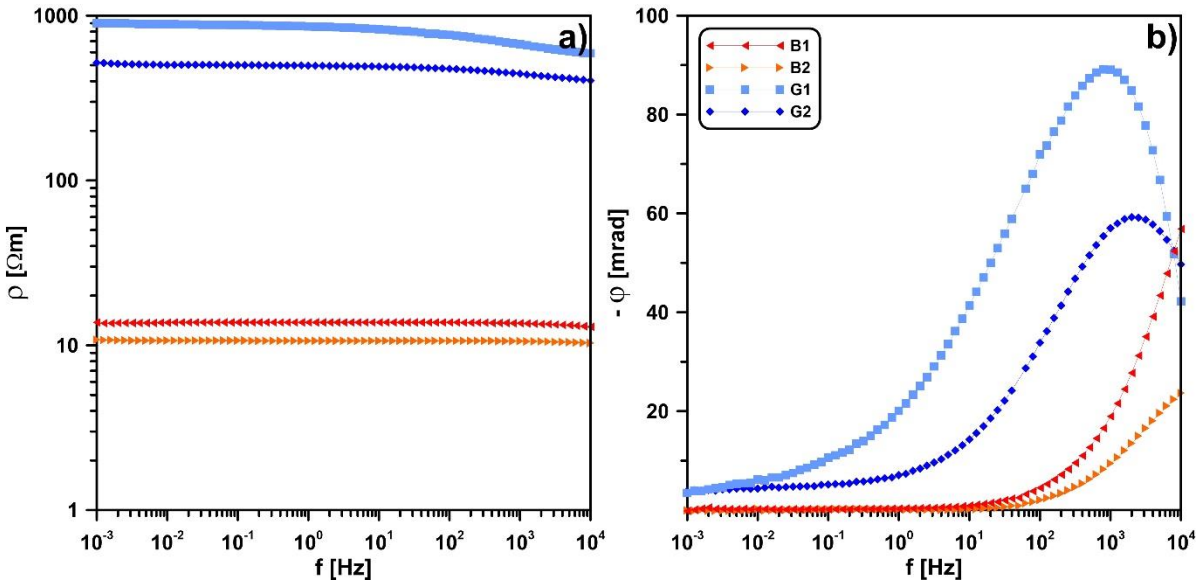

Figure 3: SIP results for the four investigated samples. a) resistivity, b) phase. Blue: samples from Grängesberg, red/orange: from Bäckegruvan.

The four representative spectra were then fitted to a Cole-Cole and Debye model with the SIPSpectrum class in pyGIMLi (https://www.pygimli.org/index.html). The fitting worked very well for all samples (see attachment). Only sample G1 showed slight discrepancies for the Cole-Cole model.

The Cole-Cole parameter after Pelton et al. (1978) and the Debye decomposition parameter after Nordsiek and Weller (2008) can be found in Table 2. Here, ρ_{CC} is the DC resistivity [Ωm], m_{CC} the chargeability [-], τ_{CC} the relaxation constant [s] and c the so-called Cole-Cole exponent. In the Debye decomposition, m_{DD} is the total chargeability [-] and τ_{DD} the mean relaxation time [s]. The results differ depending on the dump. The samples from Bäckegruvan show lower DC resistivities, lower chargeabilities and smaller relaxation times compared with the Grängesberg samples.

Table 2: Table of the Cole-Cole (CC) and Deby decomposition (DD) fitting parameter.

Sample	ρ_{CC} [Ωm]	m_{CC} [-]	τ_{CC} [s]	c_{CC} [-]	m_{DD} [-]	τ_{DD} [s]
B1	13.8	0.22	5.50E-06	0.65	0.131	2.50E-05
B2	10.7	0.076	1.10E-05	0.69	0.057	3.60E-05
G1	885.9	0.391	5.10E-04	0.43	0.355	2.10E-03
G2	501.4	0.269	9.60E-05	0.46	0.225	3.30E-04

In general, the samples between the two dumps are different. The resistivity is lower for B1 and B2 than for G1 and G2. According to available information from SGU, the fluid conductivity at the Bäckegruvan dump was around 175 μS/cm (approximately 57 Ωm) and at Grängesberg 280 μS/cm (approximately 36 Ωm). That means that the differences in resistivity seems to be mainly caused by the different saturation since the samples B1 and B2 were much more saturated.

It is known from literature that the grain size has an influence on the frequency of the phase maximum (e.g., Hupfer et al. 2016). With a decrease in grain size the phase maximum appears at higher frequencies. That can be one of the reasons why the phase maximum for the fine-grained material from Bäckegruvan cannot be observed. It is also known (e.g., Pelton et al. 1978, Hupfer et al. 2016) that with increasing mineral content the phase and the chargeability (m) increases. Based on that, the Grängesberg samples seems to have higher polarisable material (minerals?) left in the tailings. It would be interesting to correlate these findings with the mineralogical and chemical results (if available).

Conclusion

The measurements of the samples worked very well, and a good data quality could be achieved. The samples showed different resistivity based on the different saturation conditions and fluid conductivities. A generally high polarisation effect at high frequencies could be observed for all samples. According to the existing literature can that be linked to mineral residues left in the tailings. The phase maximum for the very fine-grained material (B1 and B2) could not be clearly detected in the investigated frequency range since it is outside the frequency range of the instrument (> 10 kHz). The correlation of the SIP results with mineralogical and geochemical findings is recommended and might be useful for the further interpretation of the tailing dumps.

References

Hupfer, S., Martin, T., Weller, A., Kuhn, K., Günther, T., Djotsa, V. & Noell, U., 2016. Polarization effects of unconsolidated sulphide-sand-mixtures, Journal of Applied Geophysics, http://dx.doi.org/10.1016/j.jappgeo.2015.12.003

Kruschwitz, S., 2007, Assessment of the complex resistivity behavior of salt affected building materials, PhD thesis, TU Berlin, Germany.

Nordsiek, S. & Weller, A., 2008. A new approach to fitting induced-polarization spectra, Geophysics, 73(6), 235–245.

Pelton, W.H., Ward, S.H., Hallof, P.G., Sill, W.R. & Nelson, P.H., 1978. Mineral discrimination and removal of inductive coupling with multifrequency IP. Geophysics, 43, 588–609.

Appendix

4 pages with fitting parameters for samples B1, B2, G1 and G2.

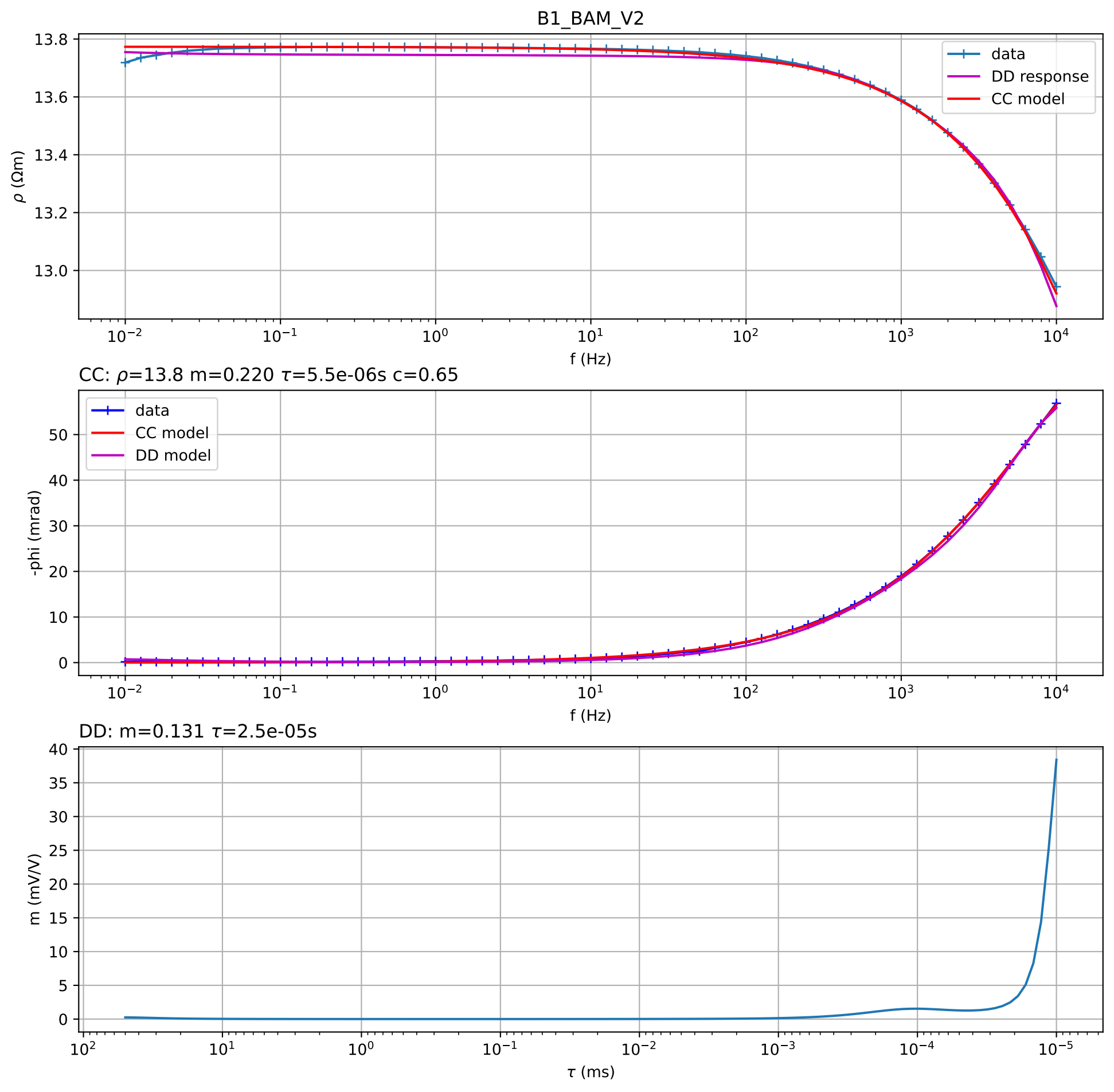
B1_BAM_V2
data
DD response
CC model
ρ (Ωm)
f (Hz)
CC: ρ=13.8 m=0.220 τ=5.5e-06s c=0.65
data
CC model
DD model
-phi (mrad)
f (Hz)
DD: m=0.131 τ=2.5e-05s
m (mV/V)
τ (ms)

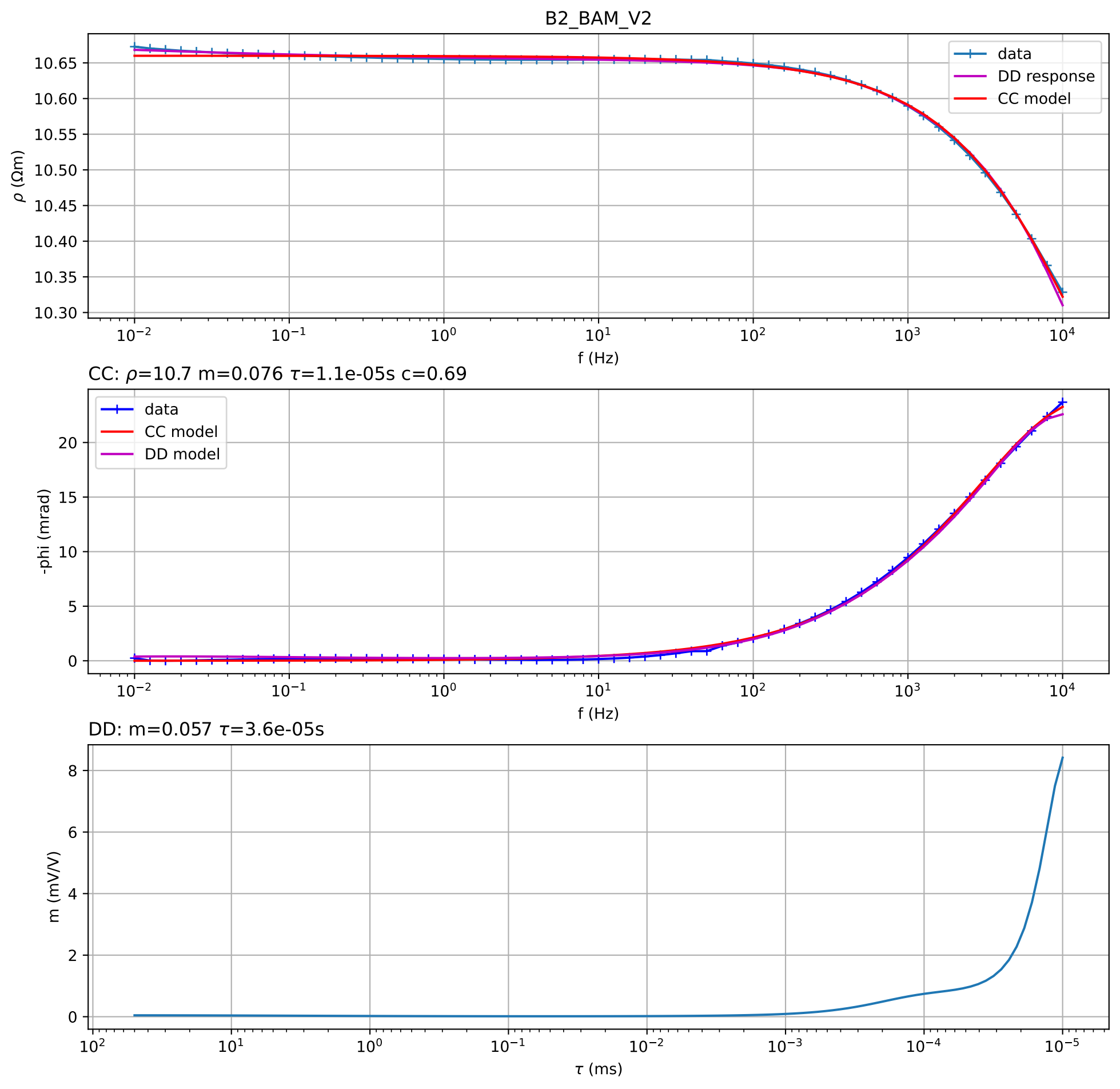
B2_BAM_V2
data
DD response
CC model
ρ (Ωm)
f (Hz)
CC: ρ=10.7 m=0.076 τ=1.1e-05s c=0.69
data
CC model
DD model
-phi (mrad)
f (Hz)
DD: m=0.057 τ=3.6e-05s
m (mV/V)
τ (ms)

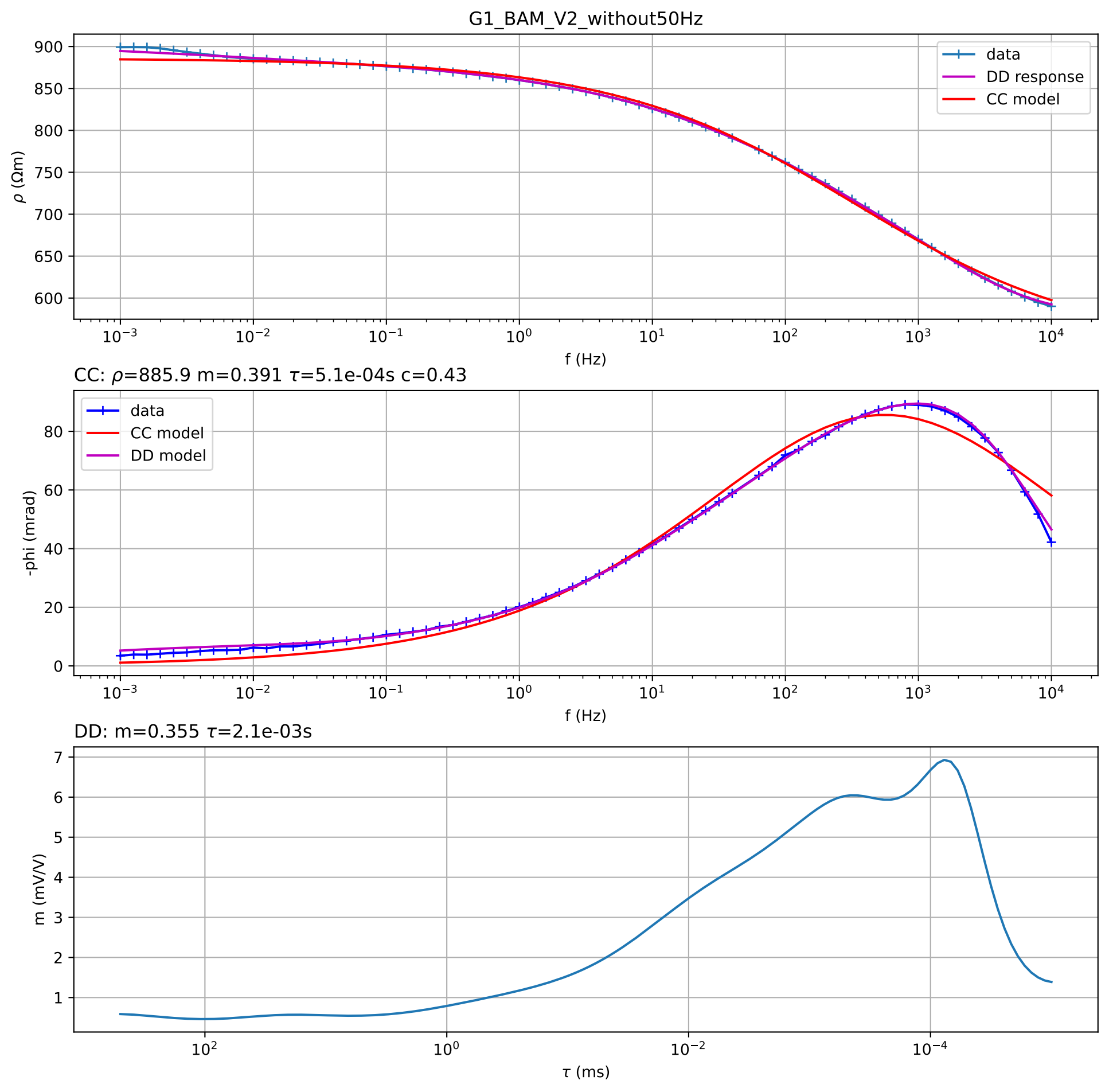
G1_BAM_V2_without50Hz
data
DD response
CC model
ρ (Ωm)
f (Hz)
CC: ρ=885.9 m=0.391 τ=5.1e-04s c=0.43
data
CC model
DD model
-phi (mrad)
f (Hz)
DD: m=0.355 τ=2.1e-03s
m (mV/V)
τ (ms)

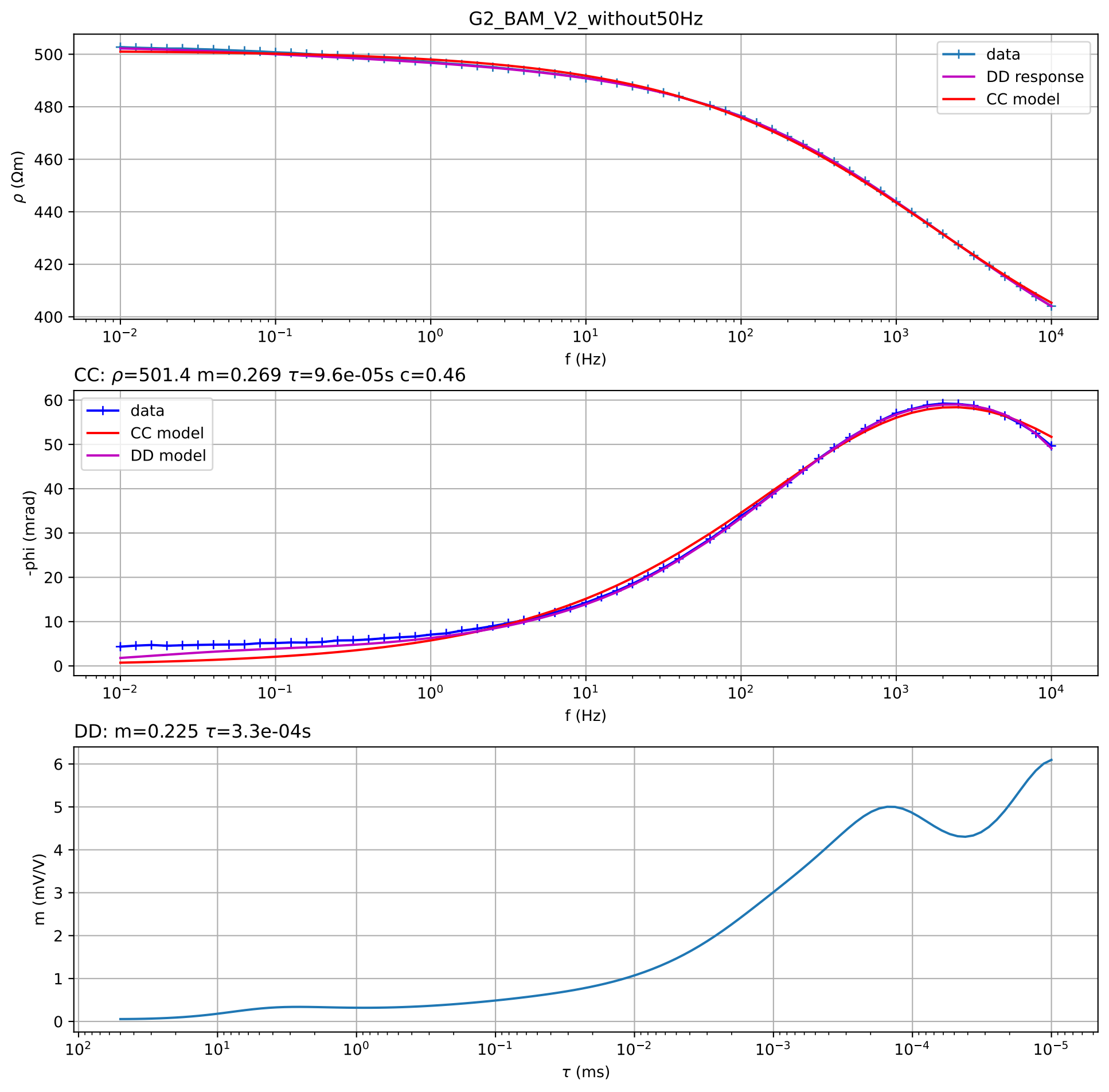
G2_BAM_V2_without50Hz
data
DD response
CC model
ρ (Ωm)
f (Hz)
CC: ρ=501.4 m=0.269 τ=9.6e-05s c=0.46
data
CC model
DD model
-phi (mrad)
f (Hz)
DD: m=0.225 τ=3.3e-04s
m (mV/V)
τ (ms)

SIP measurements on six sandy tailing samples

Tina Martin

REPORT 2022-08

Engineering Geology
Faculty of Engineering
Lund University

SIP MEASUREMENTS ON SIX SANDY TAILING SAMPLES

Report for order 2022-27068/2MW

LUND UNIVERSITY

LTH
FACULTY OF ENGINEERING

Lund, 2022-08-10

Tina Martin
tina.martin@tg.lth.se

Summary

Spectral induced polarisation (SIP) was measured on six samples in their original water saturation condition. The results showed resistivities between 13 Ωm (Yxsjöberg samples) and 130 Ωm (Blötberget samples). The phase shift varied for the different samples but was between -86 mrad (Blötberget) and -15 mrad (Stollberget) at high frequencies. All six samples showed their phase shift maximum at very high frequencies (> 5 kHz). At lower frequencies (< 1 Hz) the phase shift was close to zero. The differences in resistivities between all samples is probably mainly related to the different water saturation conditions while the high phase values might be linked to different metallic particle concentrations left in the tailings.

Introduction

The six samples were taken from the three different mining dumps: Blötberget (Bb), Yxsjöberg (Y) and Stollberget (S). The samples arrived at LTH on 2022-06-07 via regular mail. Each sample was stored in three plastic bags, wrapped in each other. All samples were in different saturated conditions. Some of them have leaked into the bag so the excess water has been removed.

Method & Measurements

Spectral Induced Polarisation

Spectral induced polarisation is a geoelectrical method which measures the resistivity and the phase shift between the injected current and the potential voltage signal. The resulting impedance Z^* (means the complex voltage-to-current ratio) is measured and transformed into a complex electrical resistivity that results from a multiplication of the impedance by a geometrical factor, which depends on the geometry of the sample and the measuring cell,

$$\rho^* = KZ^* = K\frac{U^*}{I^*}, \qquad (1)$$

where ρ^* is the resistivity in Ωm, K is the geometrical factor in m, U^* is the voltage in Volt, and I^* is the current in Ampere. All values marked by asterisks are complex values.

The complex resistivity can be also expressed by the absolute value, $|\rho^*|$, and the phase, ϕ,

$$\rho^* = |\rho^*|\exp(i\phi), \qquad (2)$$

or, alternatively, as the real, ρ', and imaginary, ρ'', values,

$$\rho^* = \rho' + i\rho'' \qquad (3)$$

with i=√(-1) being the imaginary unit, and

$$\tan(\phi) = \frac{\rho''}{\rho'}, \qquad (4) \qquad \text{and } |\rho^*| = \sqrt{\rho'^2 + \rho''^2}. \qquad (5)$$

While $|\rho^*|$ [Ωm] and phase ϕ [mrad] are the measurement quantities, the real component of the complex resistivity (ρ') represent the ohmic conduction which means primarily the conductivity of the fluid within a geological sample. The imaginary part (ρ'') represents the much smaller polarisation part that can give information about (e.g.) grain/pore size properties. Both quantities can be also described in real ($\sigma' = 1/\rho'$) and imaginary part of conductivity ($\sigma'' = 1/\rho''$). By application of the electrical field at different frequencies it is also called spectral induced polarisation (SIP).

Samples and measurements

Due to practical reasons, the samples were re-named to Bb1 and Bb2 for the two Blötberget samples, Y1 and Y2 for the two Yxsjöberg samples and S1 and S2 for the two Stollberget samples (see also Table 1). Most of the samples were in very wet conditions only samples S1 and Y2 appeared drier. In general, all samples were very fine-grained.

Between 158 g and 188 g from each sample was taken and filled homogenously into the sample holder. The original saturation was used, and no additional fluid was added.

Table 1: Table of the investigated samples.

Name	Sample name SGU	Location
Bb1	PCY220017A: 6-7m intervall	Blötberget
Bb2	PCY220021A: 10-11m intervall	Blötberget
Y1	PCY220125A: 2-3m intervall	Yxsjöberg
Y2	PCY220131A: 8-9m intervall	Yxsjöberg
S1	PCY220184A: 4-5m intervall	Stollberget
S2	PCY220195A: 15-16m intervall	Stollberget

A four-point sample holder was used as described in Kruschwitz (2008) (Figure 1a). The two outer connection plugs were used for the electrical current transmission and the two inner plugs (blue taps in Figure 1a) for the potential measurement. The sample holder was then connected to the PSIP instrument (Ontash & Ermac, see Figure 1b). The measurements were carried out at 71 frequencies in a range between 1 mHz and 10 kHz. This measurement took (with the used settings) approximately 3.5 h for each sample. All samples were repeated at least three times with varying settings and frequency ranges.

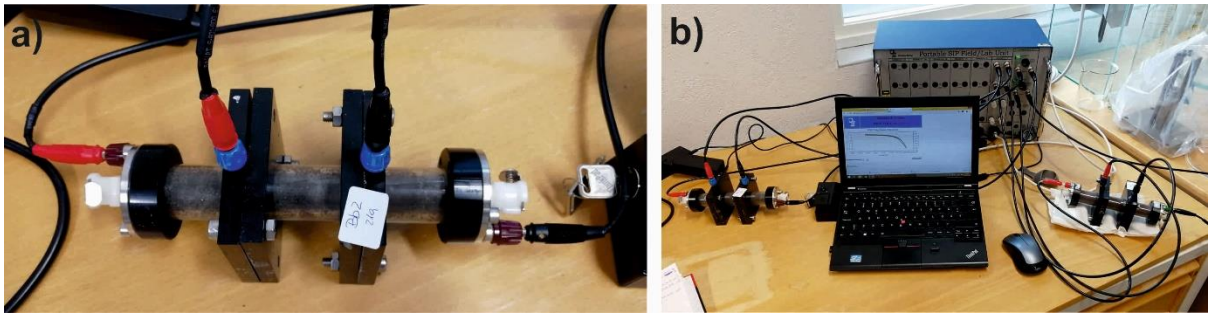

Figure 1: Photos of the used sample holder and the PSIP instrument.

Results & Discussion

Figure 2 shows the measurement results of the six samples for the resistivity (a), the phase shift (b), the real part of conductivity (c) and the imaginary part of conductivity (d). The data quality was very good, only occasionally interference occurred at the 50 Hz.

In resistivity and real part of conductivity the samples show a mixed behaviour which can be related to the saturation of the samples. Whereas the Blötberget samples show higher resistivities (sample Bb2 up to 130 Ωm) the lowest resistivities can be found for the Yxsjöberg sample Y1 (13 Ωm). In phase shift (Figure 2b) all phase effects occurred at high frequencies, starting around 1 Hz. For the four samples S1, S2, Y1 and Y2 the phase maximum could still be observed in the investigated frequency range (at 5 resp. 6 kHz). But the maxima for the samples Bb1 and Bb2 are outside of the investigated frequency range. The magnitude of the phase shift varies between -15 mrad (S1) and -86 mrad (Bb2). Whereas the magnitude of the phase shift is also affected by the resistivity magnitude (eq. 4), the imaginary conductivity (d) shows the pure polarisation part. Here can be noticed that the order of polarisation effects changes for the different samples. In general, the samples from Yxsjöberg have the highest polarisation effect. Since the phase and imaginary conductivity are around zero for low frequencies for all samples, a close-up figure is presented in the appendix showing the imaginary part also in logarithmic scale (Figure 3).

Usually, electromagnetic coupling effects interfere with the IP measurements at very high frequencies and can therefore not be ruled out. But since four of the samples show a peak within the investigated frequency range, only for the Blötberget samples the IP effect cannot be observed clearly.

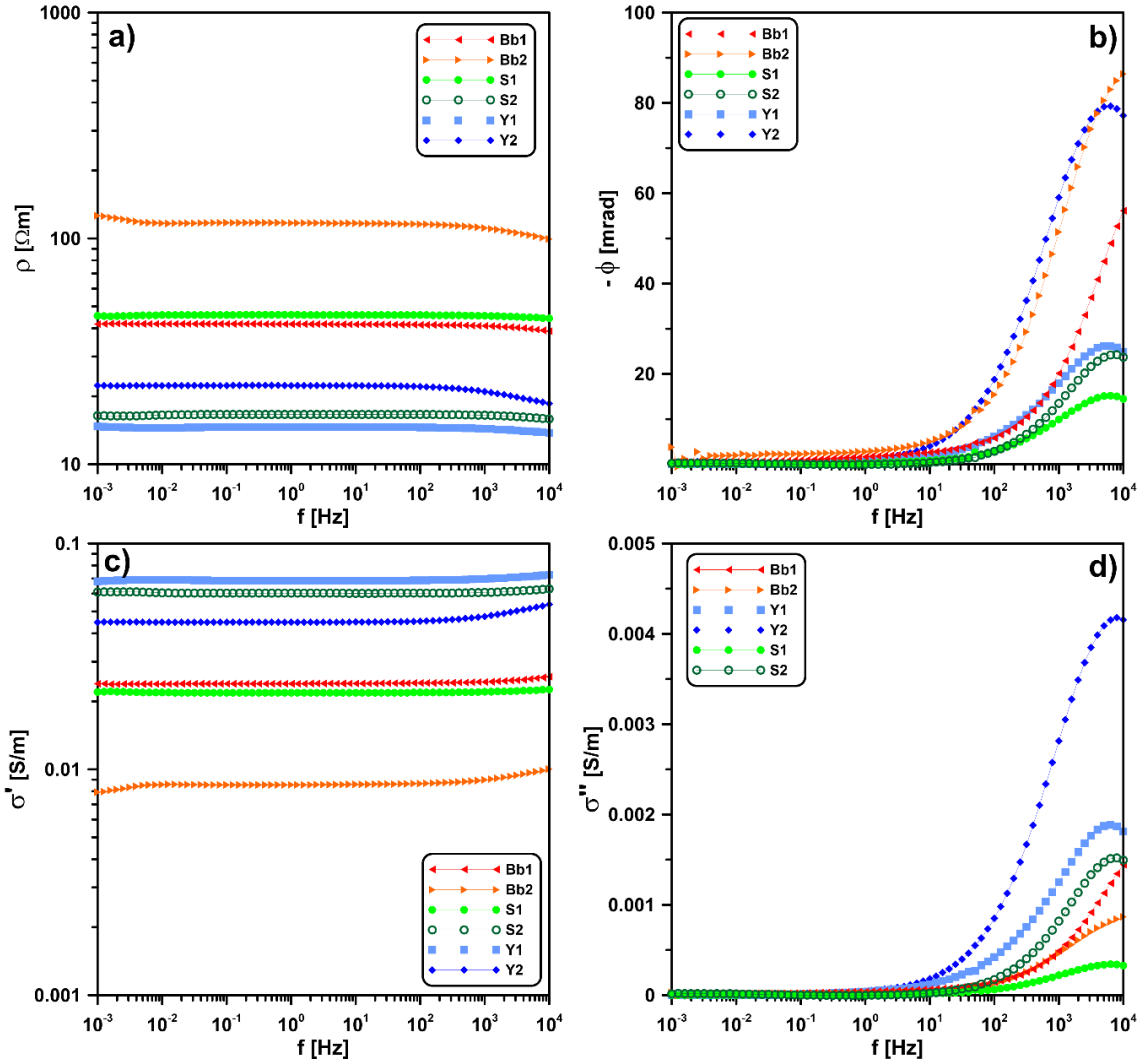

Figure 2: SIP results for the six investigated samples. a) resistivity, b) phase, c) real part of conductivity, d) imaginary part of conductivity. Blue: samples from Yxsjöberg, red/orange: from Blötberget, green: from Stollberget.

The six representative spectra were then fitted to a Cole-Cole and Debye model with the SIPSpectrum class in pyGIMLi (https://www.pygimli.org/index.html). The low frequency range (< 0.1 Hz) was cut off for the fitting. In general, the fitting worked very well for all samples (see attachment).

The Cole-Cole parameter after Pelton et al. (1978) and the Debye decomposition parameter after Nordsiek and Weller (2008) can be found in Table 2. Here, ρ_{CC} is the DC resistivity [Ωm], m_{CC} the chargeability [-], τ_{CC} the relaxation constant [s] and c the so-called Cole-Cole exponent. In the Debye decomposition, m_{DD} is the total chargeability [-] and τ_{DD} the mean relaxation time [s]. The results differ depending on the dump. As probably the resistivity is mainly affected by the saturation, the chargeability values are at highest for the Blötberget samples and Y2.

Table 2: Table of the Cole-Cole (CC) and Deby decomposition (DD) fitting parameter.

Sample	ρ_{CC} [Ωm]	m_{CC} [-]	τ_{CC} [s]	c_{CC} [-]	m_{DD} [-]	τ_{DD} [s]
Bb1	41.7	0.255	4.10E-06	0.59	0.135	3.40E-05
Bb2	117.2	0.287	2.10E-05	0.60	0.232	5.10E-05
Y1	14.6	0.096	2.80E-05	0.61	0.077	5.70E-05
Y2	22.4	0.258	3.90E-05	0.63	0.225	6.40E-05
S1	45.8	0.053	2.60E-05	0.64	0.044	5.30E-05
S2	16.6	0.071	2.50E-05	0.74	0.063	3.60E-05

It is known from literature that the grain size has an influence on the frequency of the phase maximum (e.g., Hupfer et al. 2016). With a decrease in grain size the phase maximum appears at higher frequencies. That can be one of the reasons why the phase maximum for the very fine-grained material from Blötberget cannot be observed within the frequency range. It is also known (e.g., Pelton et al. 1978, Hupfer et al. 2016) that with increasing mineral content the phase and the chargeability (m) increases. Based on that, the Blötberget samples as well as the Yxsjöberg sample Y2 seems to have higher polarisable material (minerals?) left in the tailings. It would be interesting to correlate these findings with the mineralogical and chemical results.

Conclusion

The measurements of the samples worked very well, and a good data quality could be achieved. The samples showed different resistivity mainly based on the different saturation conditions. A polarisation effect at high frequencies could be observed for all samples. According to the existing literature that can be linked to fine-grained mineral residues left in the tailings. The phase maximum for the Blötberget samples could not be clearly detected in the investigated frequency range since it is outside the frequency range of the instrument (> 10 kHz). It is recommended to investigate possible correlation of the SIP results with mineralogical and geochemical findings, as it might be useful for the further interpretation of the tailing dumps.

References

Hupfer, S., Martin, T., Weller, A., Kuhn, K., Günther, T., Djotsa, V. & Noell, U., 2016. Polarization effects of unconsolidated sulphide-sand-mixtures, Journal of Applied Geophysics, http://dx.doi.org/10.1016/j.jappgeo.2015.12.003

Kruschwitz, S., 2007, Assessment of the complex resistivity behavior of salt affected building materials, PhD thesis, TU Berlin, Germany.

Nordsiek, S. & Weller, A., 2008. A new approach to fitting induced-polarization spectra, Geophysics, 73(6), 235–245.

Pelton, W.H., Ward, S.H., Hallof, P.G., Sill, W.R. & Nelson, P.H., 1978. Mineral discrimination and removal of inductive coupling with multifrequency IP. Geophysics, 43, 588–609.

Appendix

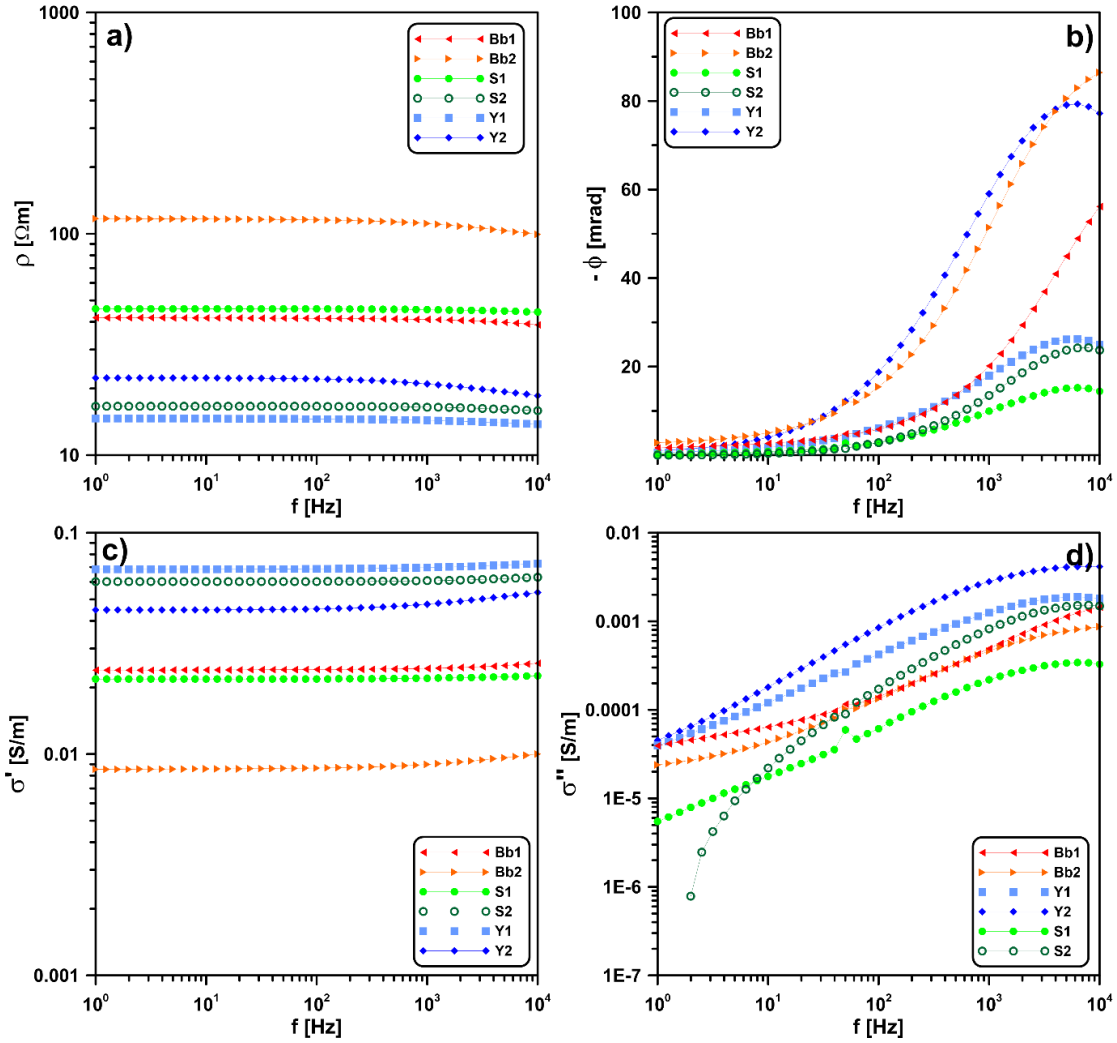

Figure 3: Close-up of the SIP results for the six investigated samples within a shorter frequency range (1 Hz – 10 kHz). a) resistivity, b) phase, c) real part of conductivity, d) imaginary part of conductivity (now in log scale). Blue: samples from Yxsjöberg, red/orange: from Blötberget, green: from Stollberget.

Below 6 pages with fitting parameters for all samples.

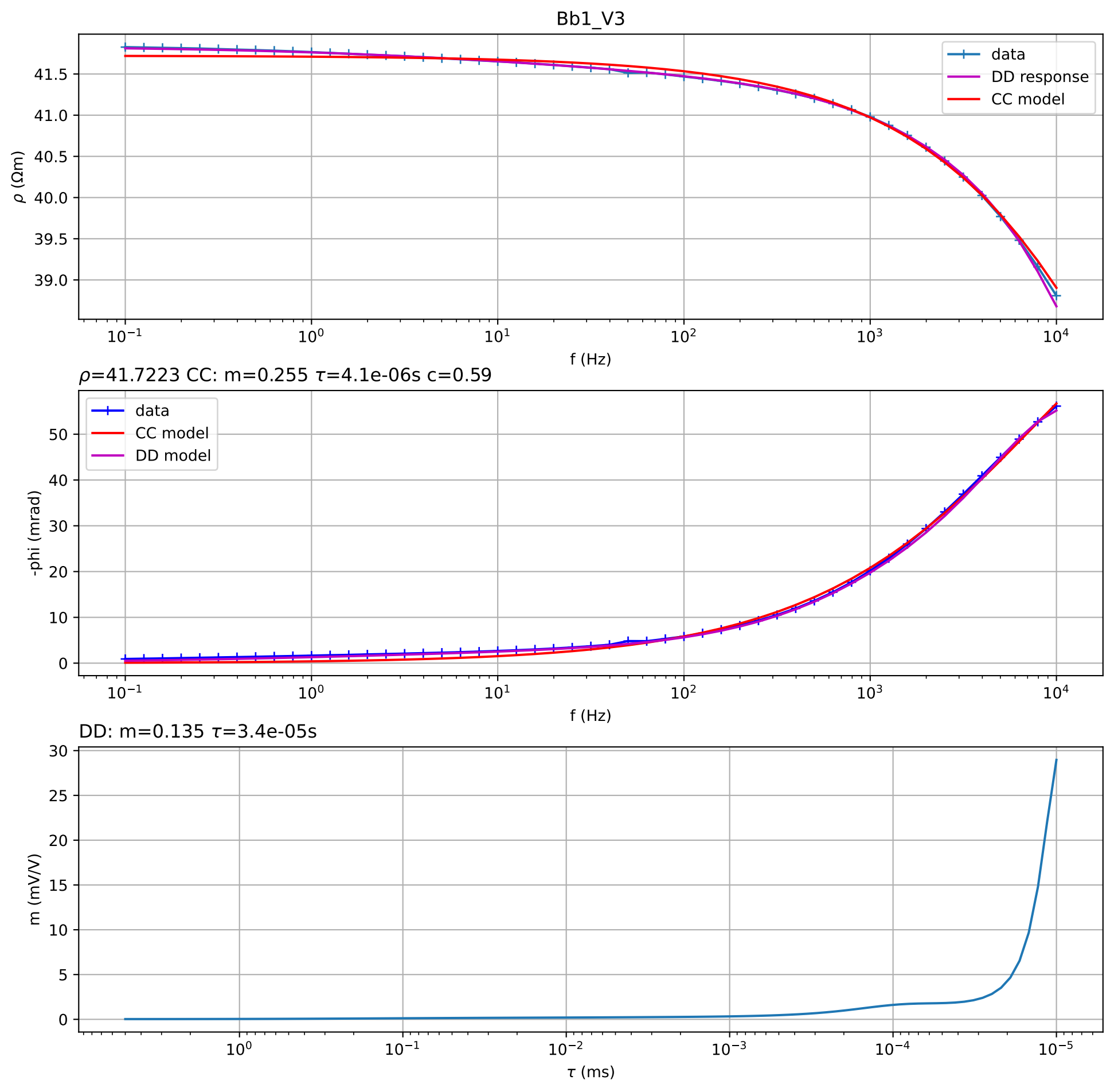
Bb1_V3
data
DD response
CC model
ρ (Ωm)
f (Hz)
ρ=41.7223 CC: m=0.255 τ=4.1e-06s c=0.59
data
CC model
DD model
-phi (mrad)
f (Hz)
DD: m=0.135 τ=3.4e-05s
m (mV/V)
τ (ms)

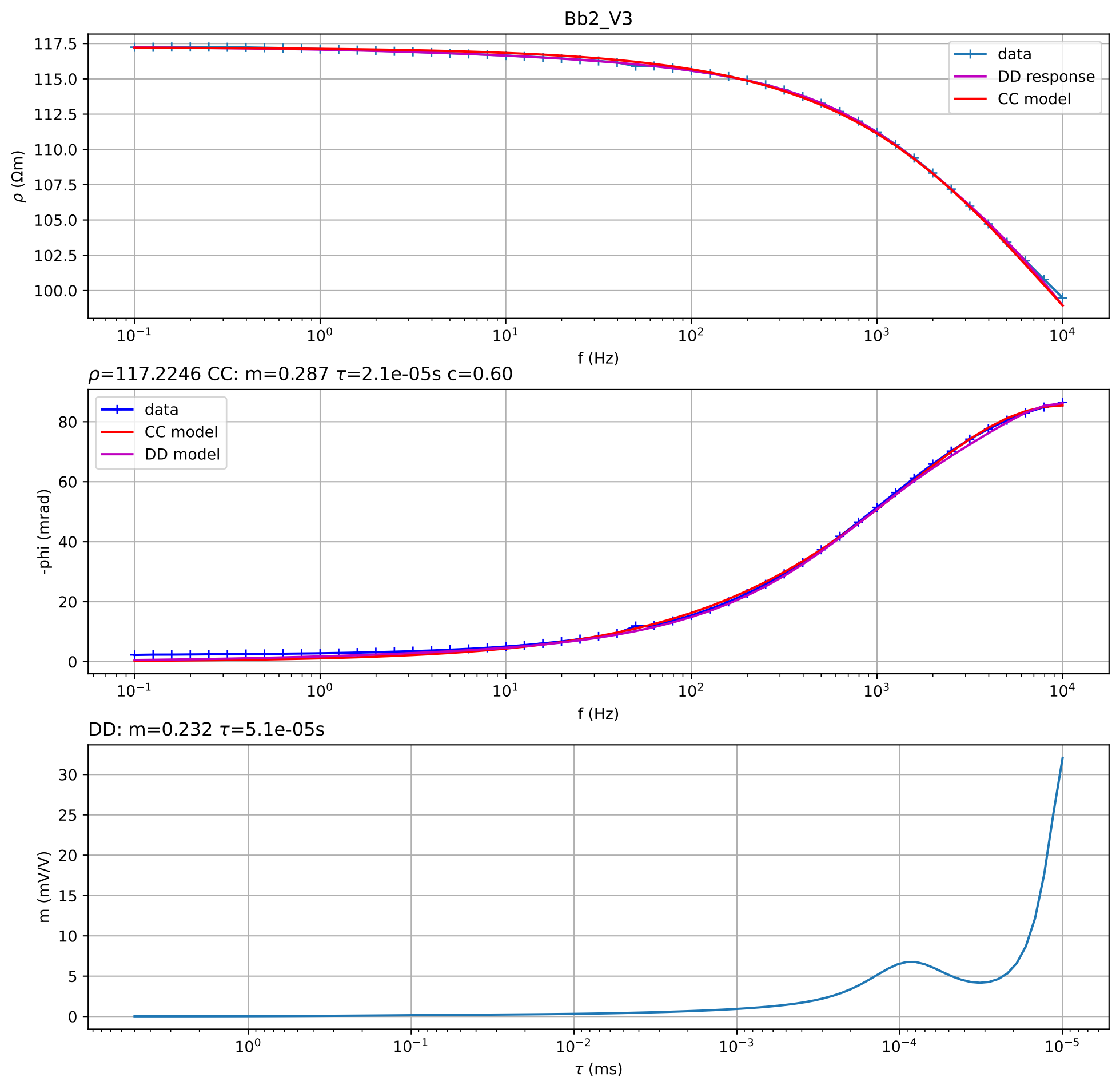
Bb2_V3
data
DD response
CC model
ρ (Ωm)
f (Hz)
ρ=117.2246 CC: m=0.287 τ=2.1e-05s c=0.60
data
CC model
DD model
-phi (mrad)
f (Hz)
DD: m=0.232 τ=5.1e-05s
m (mV/V)
τ (ms)

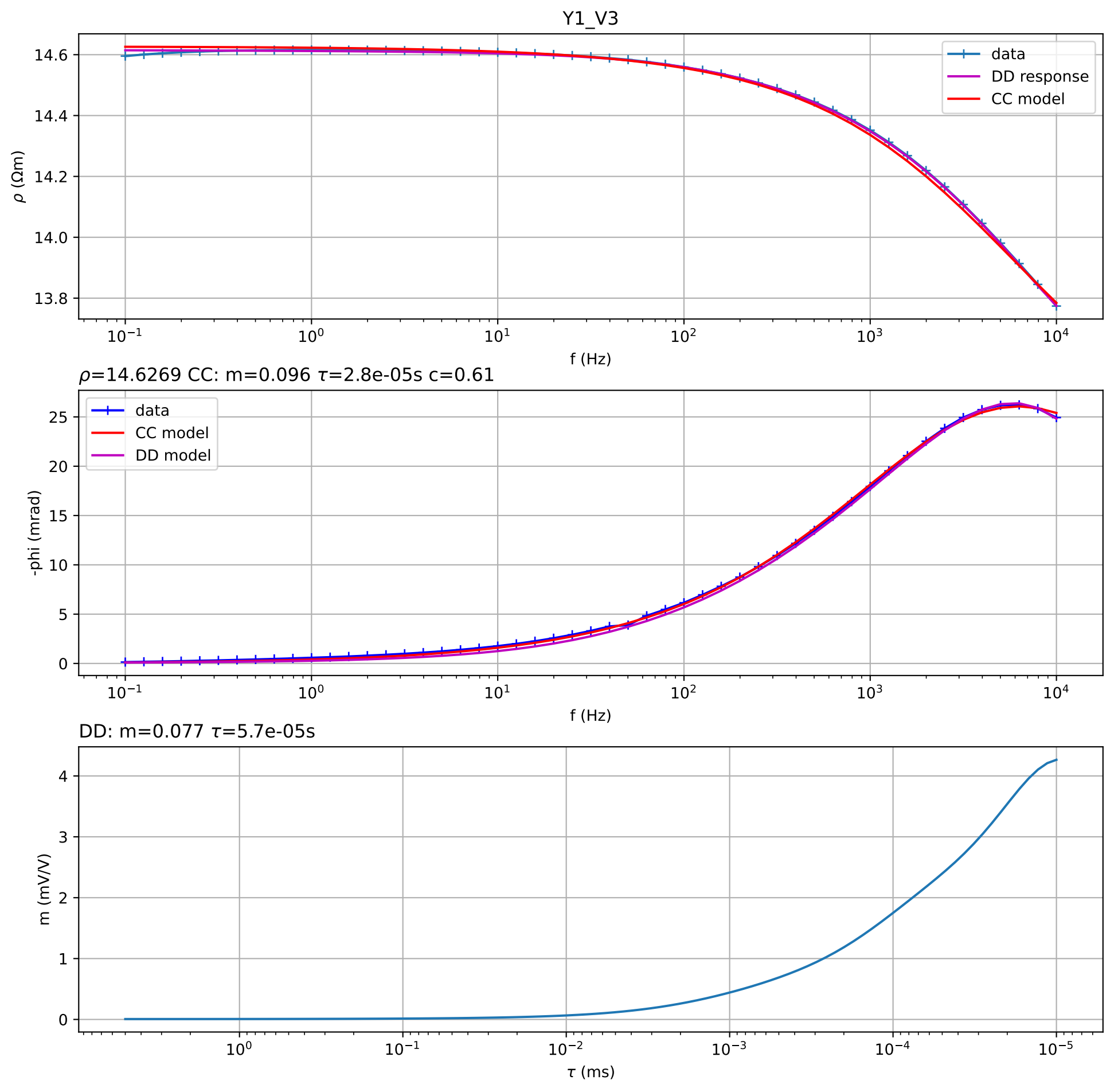
Y1_V3
data
DD response
CC model
ρ (Ωm)
f (Hz)
ρ=14.6269 CC: m=0.096 τ=2.8e-05s c=0.61
data
CC model
DD model
-phi (mrad)
f (Hz)
DD: m=0.077 τ=5.7e-05s
m (mV/V)
τ (ms)

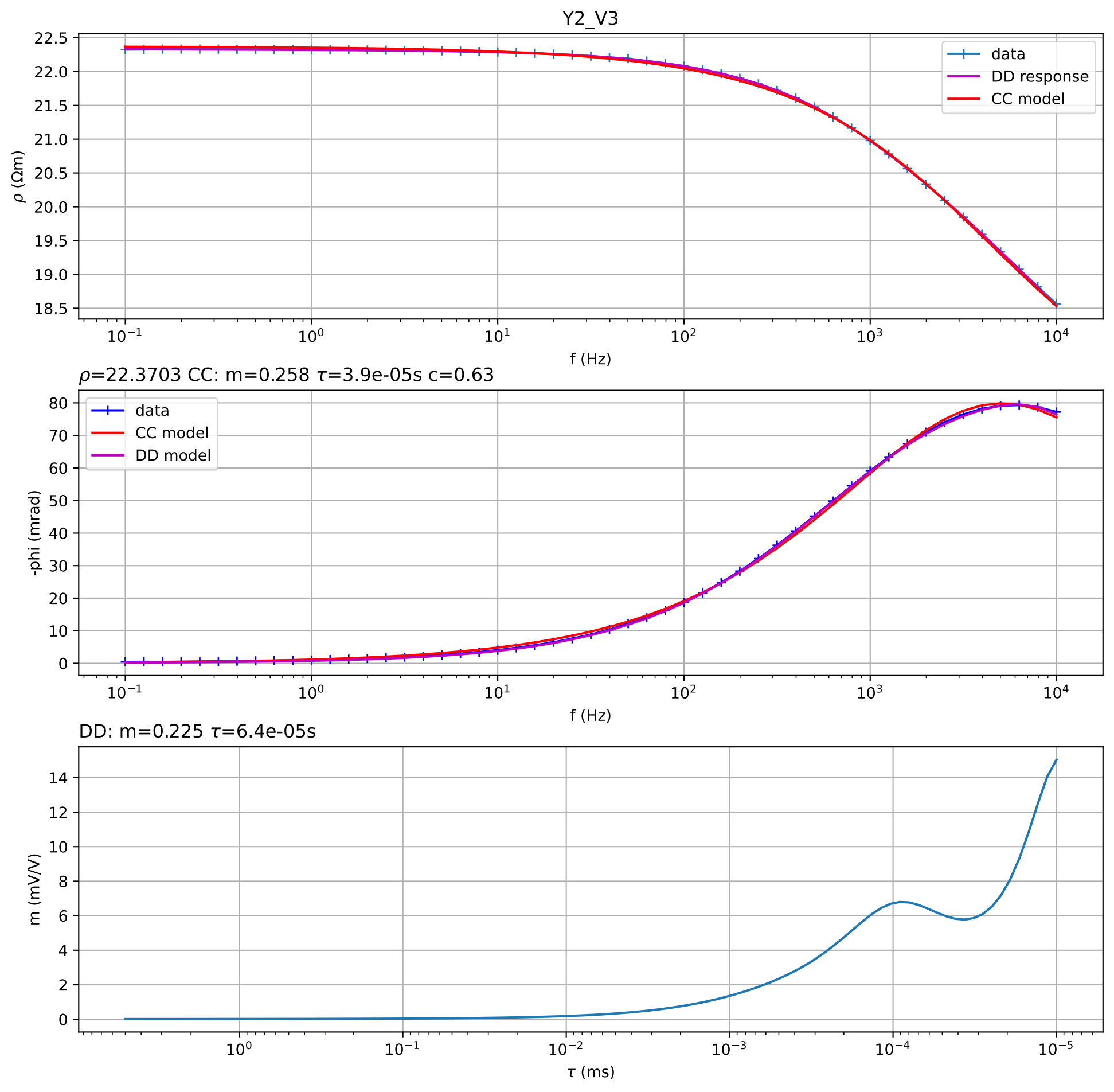
Y2_V3
data
DD response
CC model
ρ (Ωm)
f (Hz)
ρ=22.3703 CC: m=0.258 τ=3.9e-05s c=0.63
data
CC model
DD model
-phi (mrad)
f (Hz)
DD: m=0.225 τ=6.4e-05s
m (mV/V)
τ (ms)

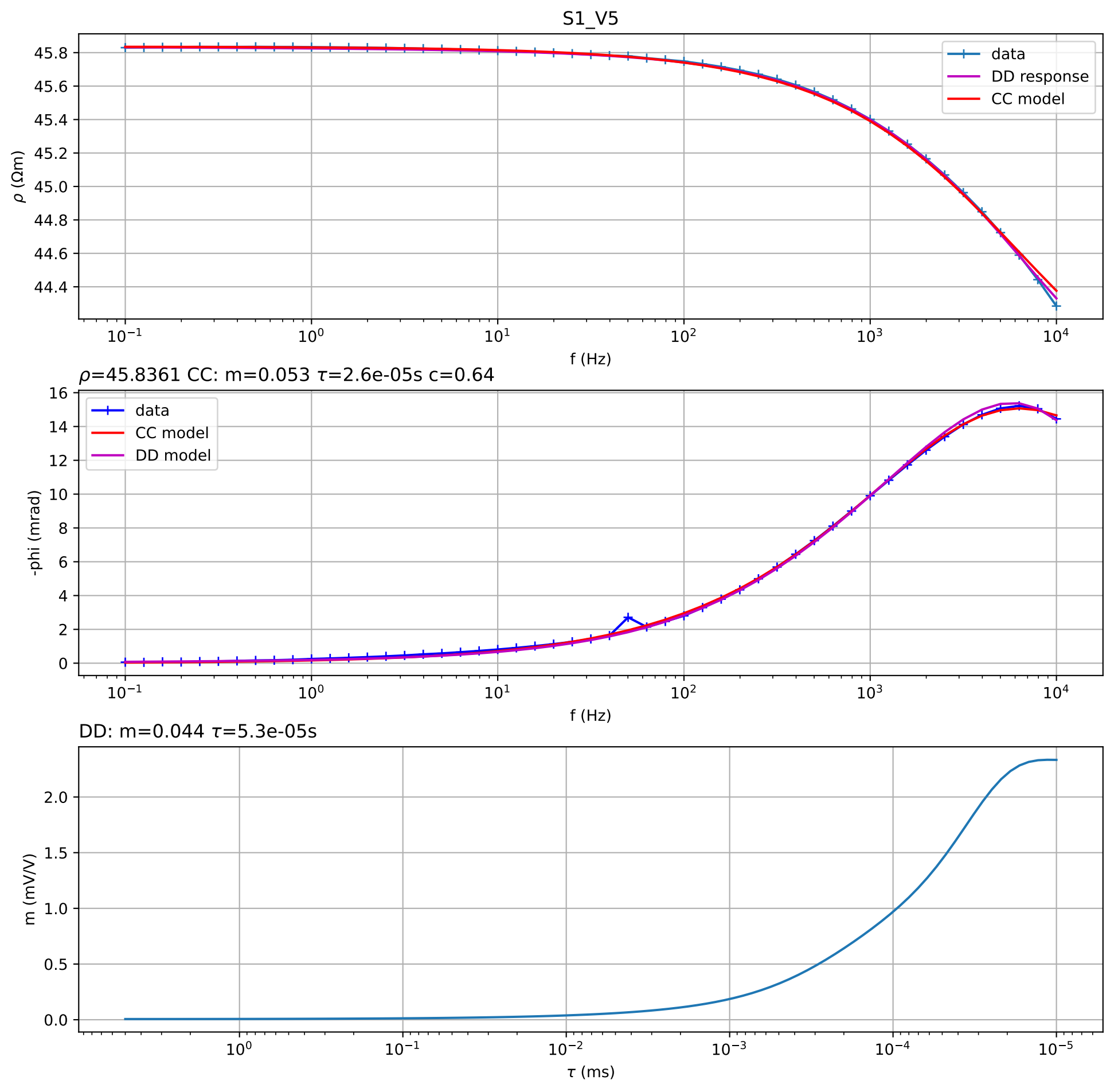
S1_V5
data
DD response
CC model
ρ (Ωm)
f (Hz)
ρ=45.8361 CC: m=0.053 τ=2.6e-05s c=0.64
data
CC model
DD model
-phi (mrad)
f (Hz)
DD: m=0.044 τ=5.3e-05s
m (mV/V)
τ (ms)

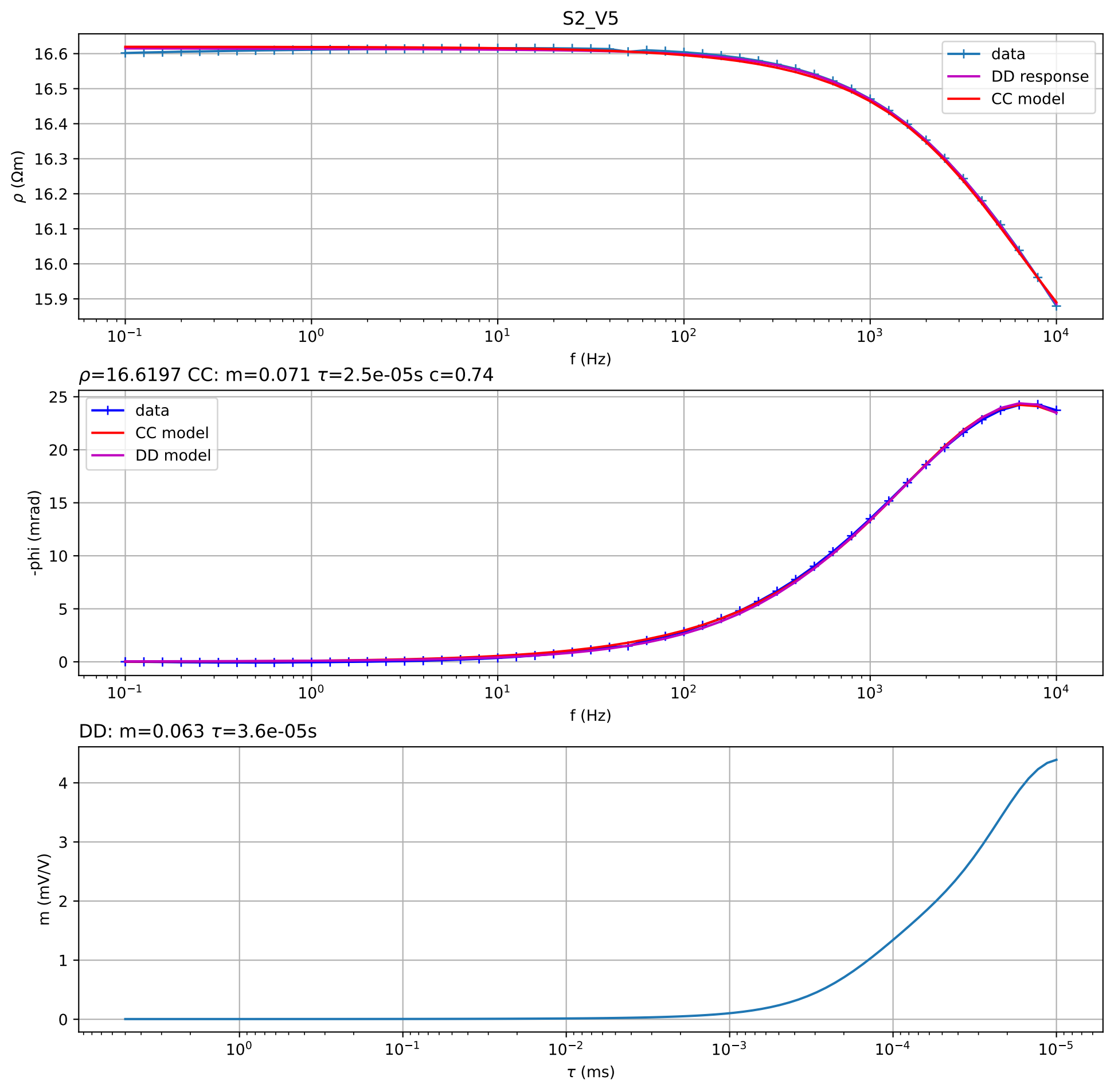
S2_V5
data
DD response
CC model
ρ (Ωm)
f (Hz)
ρ=16.6197 CC: m=0.071 τ=2.5e-05s c=0.74
data
CC model
DD model
-phi (mrad)
f (Hz)
DD: m=0.063 τ=3.6e-05s
m (mV/V)
τ (ms)